



National Library  
of Canada

Bibliothèque nationale  
du Canada

Acquisitions and  
Bibliographic Services Branch

Direction des acquisitions et  
des services bibliographiques

395 Wellington Street  
Ottawa, Ontario  
K1A 0N4

395, rue Wellington  
Ottawa (Ontario)  
K1A 0N4

*Your file* *Votre référence*

*Our file* *Notre référence*

## NOTICE

## AVIS

The quality of this microform is heavily dependent upon the quality of the original thesis submitted for microfilming. Every effort has been made to ensure the highest quality of reproduction possible.

La qualité de cette microforme dépend grandement de la qualité de la thèse soumise au microfilmage. Nous avons tout fait pour assurer une qualité supérieure de reproduction.

If pages are missing, contact the university which granted the degree.

Si il manque des pages, veuillez communiquer avec l'université qui a conféré le grade.

Some pages may have indistinct print especially if the original pages were typed with a poor typewriter ribbon or if the university sent us an inferior photocopy.

La qualité d'impression de certaines pages peut laisser à désirer, surtout si les pages originales ont été dactylographiées à l'aide d'un ruban usé ou si l'université nous a fait parvenir une photocopie de qualité inférieure.

Reproduction in full or in part of this microform is governed by the Canadian Copyright Act, R.S.C. 1970, c. C-30, and subsequent amendments.

La reproduction, même partielle, de cette microforme est soumise à la Loi canadienne sur le droit d'auteur, SRC 1970, c. C-30, et ses amendements subséquents.

Canada

UNIVERSITY OF ALBERTA

**ADAPTIVE LINEARIZATION OF POWER AMPLIFIERS FOR DIGITAL  
CELLULAR RADIO**

By



**Yvonne Jacqueline den Otter**

A thesis submitted to the Faculty of Graduate Studies and Research in partial fulfillment of the requirements for the degree of **MASTER OF SCIENCE**.

DEPARTMENT OF ELECTRICAL ENGINEERING

EDMONTON, ALBERTA

FALL 1992

The author has granted an irrevocable non-exclusive licence allowing the National Library of Canada to reproduce, loan, distribute or sell copies of his/her thesis by any means and in any form or format, making this thesis available to interested persons.

The author retains ownership of the copyright in his/her thesis. Neither the thesis nor substantial extracts from it may be printed or otherwise reproduced without his/her permission.

L'auteur a accordé une licence irrévocable et non exclusive permettant à la Bibliothèque nationale du Canada de reproduire, prêter, distribuer ou vendre des copies de sa thèse de quelque manière et sous quelque forme que ce soit pour mettre des exemplaires de cette thèse à la disposition des personnes intéressées.

L'auteur conserve la propriété du droit d'auteur qui protège sa thèse. Ni la thèse ni des extraits substantiels de celle-ci ne doivent être imprimés ou autrement reproduits sans son autorisation.

ISBN 0-315-77285-9

UNIVERSITY OF ALBERTA

RELEASE FORM

NAME OF AUTHOR: **Yvonne Jacqueline den Otter**

TITLE OF THESIS: **Adaptive Linearization of Power Amplifiers for Digital Cellular Radio**

DEGREE: **Master of Science**

YEAR THIS DEGREE GRANTED: **Fall 1992**

Permission is hereby granted to the University of Alberta Library to reproduce single copies of this thesis and to lend or sell such copies for private, scholarly or scientific research purposes only.

The author reserves all other publication and other rights in association with the copyright in the thesis, and except as hereinbefore provided neither the thesis nor any substantial portion thereof may be printed or otherwise reproduced in any material form whatever without the author's prior written permission.



Yvonne J. den Otter

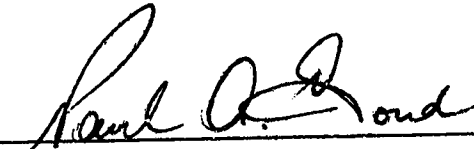
#106 11660-79 Avenue  
Edmonton, Alberta  
T6G 0P7


DATE: 16 July 1992

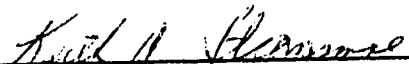
UNIVERSITY OF ALBERTA


FACULTY OF GRADUATE STUDIES AND RESEARCH

The undersigned certify that they have read, and recommend to the Faculty of Graduate Studies and Research for acceptance, a thesis entitled **ADAPTIVE LINEARIZATION OF POWER AMPLIFIERS FOR DIGITAL CELLULAR RADIO** submitted by **Yvonne Jacqueline den Otter** in partial fulfillment of the requirements for the degree of **Master of Science**.

  
\_\_\_\_\_  
Dr. P. A. Goud, Co-Supervisor

  
\_\_\_\_\_  
Dr. C. G. Englefield, Co-Supervisor

  
\_\_\_\_\_  
Dr. K. A. Stromsmoe, Internal Examiner

  
\_\_\_\_\_  
Dr. J. Tartar, External Examiner

DATE: 92.04.07

***To Craig,  
For encouraging me.***

## Abstract

This thesis investigates and compares two adaptive predistortion systems used to linearize the RF power amplifier in a digital cellular radio transmitter. In order to increase the capacity of cellular radio systems, spectrally efficient linear modulation techniques are being considered. The recommended modulation method,  $\pi/4$  DQPSK, is spectrally efficient, but has significant RF envelope fluctuation. As a result, this modulation scheme requires highly linear RF power amplifiers if the transmitter output signal is to have the low out-of-band power necessary to minimize adjacent channel interference. However, acceptably linear power amplifiers have a lower dc-to-ac conversion efficiency than less linear power amplifiers. Nonlinear power amplifiers exhibit amplitude-to-amplitude distortion (AM-AM) and amplitude-to-phase distortion (AM-PM). To reduce these distortion effects, amplifier linearization techniques are used.

In this thesis, computer simulation is used to compare the performance of two prominent linearization techniques, namely: Cartesian coordinate negative feedback and complex gain predistortion. The simulation models for the digital cellular transmitter include a random data source, a  $\pi/4$  DQPSK modulator, and a square-root raised cosine pulse shaping filter. Two different nonlinear RF power amplifiers, namely a class AB and a single-ended class B amplifier, were evaluated. The amplifier model parameters were obtained from measurements of their AM-AM and AM-PM characteristics. Models were also developed for the complex gain predistorter and for the Cartesian coordinate negative feedback linearizer. In addition, models to simulate the equivalent distortion provided by non-ideal quadrature modulators and the demodulator are included. The out-of-band power and the intermodulation distortion product power levels are used to compare the effectiveness of the two adaptive predistortion techniques.

The recommended digital cellular system has a channel bandwidth of 30 kHz. Using a  $\pi/4$  DQPSK signal, the simulations show that the nonlinear amplifiers increase the normalized out-of-band power to approximately -40 dB (relative to the center of the main channel) in the adjacent channel (channel 1) centered 30 kHz away from the transmitter channel. In the next 30 kHz channel (adjacent channel 2), centered 60 kHz away, the relative out-of-band power is -45 dB. Next, 90 kHz (adjacent channel 3) away, the relative out-of-band power is -55 dB. The Cartesian system reduces the out-of-band power by approximately 22 dB in each channel. The complex gain system reduces the out-of-band power approximately 30 dB in channel 1, 22 dB in channel 2, and 10 dB in channel 3. Using two-tone tests, the  $IM_3$  and  $IM_5$  for the uncompensated class AB amplifier were found to be -28.6 dB and -36.3 dB, respectively. The complex gain system reduces  $IM_3$  and  $IM_5$  by approximately 35 dB and the Cartesian feedback system reduces  $IM_3$  and  $IM_5$  by approximately 20 dB.

When the effects of a non-ideal quadrature modulator are included, the Cartesian feedback system reduces the spurious tones caused by a two-tone test signal by 20 dB, while the complex gain predistorter reduces them by less than 5 dB. Neither system can reduce the effects of demodulation distortion. These results indicate that further research is needed in controlling modulator and demodulator distortion before these predistortion linearization techniques can be usefully employed in the proposed digital cellular telephone network.



## **Acknowledgments**

I would like to express my sincere thanks to my supervisors, Dr. Paul Goud and Dr. Colin Englefield, for their interest, advice, and encouragement throughout the course of this work.

NovAtel Communications Ltd., especially Dr. Andrew Wright, provided valuable input to this project.

Financial and technical support were provided by Telecommunications Research Laboratories. Thanks to Dr. Mike MacGregor for the computing environment support at TR Labs. In addition, thanks to the research staff and graduate students at TR Labs for their help and support. I would also like to thank Rohit Sharma and Richard Tse for their help and many stimulating discussions.

Finally, I thank my husband, Craig Senych, and my family and friends, for their support and encouragement throughout the completion of this project.

# Table of Contents

<b>1. Introduction</b> .....	<b>1</b>
1.1 Digital Cellular Mobile Radio .....	1
1.2 Digital Transmitter .....	2
1.2.1 Speech Encoder .....	2
1.2.2 Modulator .....	3
1.2.3 Power Amplifier .....	4
1.3 Adaptive Predistortion .....	4
1.4 Thesis Outline .....	5
<b>2. Amplifier Distortion and Linearization Techniques</b> .....	<b>7</b>
2.1 Amplifier Distortion .....	7
2.1.1 AM-AM Distortion .....	8
2.1.2 AM-PM Distortion .....	9
2.2 Evaluation of Amplifier Nonlinearities .....	9
2.2.1 Intermodulation Distortion .....	9
2.2.2 Out-of-Band Power .....	11
2.3 Amplifier Linearization Techniques .....	12
2.3.1 Feedforward Correction .....	13
2.3.2 LINC .....	14
2.3.3 Adaptive Predistortion .....	16
2.3.3.1 Mapping Predistortion .....	18
2.3.3.2 Complex Gain Predistortion .....	20
2.3.4 Cartesian Coordinate Negative Feedback .....	25
2.4 Summary .....	28
2.5 Simulation Plan .....	29
<b>3. Computer Simulation Models</b> .....	<b>31</b>
3.1 The BOSS Environment .....	31
3.2 System Model .....	32
3.2.1 Random Data Generator .....	34
3.2.2 Phase Modulator .....	35
3.2.2.1 $\pi/4$ DQPSK Modulation .....	35
3.2.2.2 Simulation Model .....	36
3.2.3 Pulse Shaping Filter .....	38
3.3 Nonlinear Power Amplifier .....	41
3.3.1 Complex Gain Predistorter .....	45
3.3.2 Address Block and Lookup Table .....	47
3.3.3 Error and Update Blocks .....	47
3.4 Cartesian Coordinate Negative Feedback .....	49
3.5 Modulator and Demodulator Errors .....	51
3.5.1 Complex Envelope Modulator and Demodulator Distortion .....	53
3.6 Measurement of Power Spectra .....	59
3.7 Summary .....	64

<b>4. Results</b> .....	<b>66</b>
4.1 Simulation Outline .....	66
4.2 RF Power Amplifier Characteristics.....	66
4.2.1 Class AB Amplifier.....	67
4.2.2 Class B Amplifier .....	70
4.2.3 Amplifier Distortion Comparison.....	72
4.3 Complex Gain Predistortion .....	72
4.3.1 Sampling Rate.....	73
4.3.2 Table Size .....	75
4.3.3 Power Level .....	77
4.3.4 Amplifiers. ....	79
4.3.5 Performance Analysis .....	81
4.3.6 Complex Gain System Summary .....	82
4.4 Cartesian Coordinate Negative Feedback .....	84
4.4.1 Loop Gain .....	85
4.4.2 Input Power Level .....	87
4.4.3 Amplifier .....	89
4.4.4 Performance Evaluation .....	91
4.4.5 Cartesian Coordinate Negative Feedback Summary .....	92
4.5 Comparison of the Complex Gain and the Cartesian Systems .....	94
4.6 Modulation/Demodulation Distortion .....	96
4.6.1 Basic Transmitter. ....	96
4.6.2 Complex Gain System.....	101
4.6.3 Cartesian Coordinate Feedback System. ....	104
4.6.4 Modulation and Demodulation Distortion Summary .....	108
4.7 Summary of Results. ....	108
 <b>5. Summary And Conclusions</b> .....	 <b>110</b>
5.1 Simulation Models. ....	110
5.2 Summary of Results. ....	113
5.3 Implementation Feasibility. ....	114
5.4 Recommendations .....	115
 <b>References</b> .....	 <b>116</b>
 <b>Appendix A</b> .....	 <b>120</b>
 <b>Appendix B</b> .....	 <b>126</b>
 <b>Appendix C</b> .....	 <b>128</b>

## Table of Figures

Figure 1.1	Block Diagram of a Digital Transmitter .....	3
Figure 2.1	Output Power Characteristic. ....	7
Figure 2.2	Types of Amplifier Distortion (a) Nonlinear Amplitude (Envelope) Distortion (b) Nonlinear Phase Distortion. ....	8
Figure 2.3	Harmonic and Intermodulation Spectra for a Nonlinear Power Amplifier (a) Input Spectra (b) Output Spectra .....	11
Figure 2.4	Allowed Transmitted Power in Adjacent Channels .....	12
Figure 2.5	Feedforward Correction [6] .....	13
Figure 2.6	LINC Transmitter .....	15
Figure 2.7	Adaptive Predistortion .....	17
Figure 2.8	Mapping Predistortion.. .....	19
Figure 2.9	Complex Gain Predistorter .....	21
Figure 2.10	Cartesian Coordinate Negative Feedback System .....	26
Figure 2.11	Basic Feedback Amplifier.. .....	27
Figure 3.1	Block Diagram of a $\pi/4$ DQPSK Transmitter .....	33
Figure 3.2	BOSS Simulation Model: $\pi/4$ DQPSK Transmitter .....	33
Figure 3.3	Modulation Constellations: (a), (b) QPSK Constellation, (c) $\pi/4$ DQPSK Constellation .....	36
Figure 3.4	Signal Converter. ....	37
Figure 3.5	Frequency Response of Square Root Raised Cosine Filter .....	39
Figure 3.6	Impulse Response of Square Root Raised Cosine Filter. ....	40
Figure 3.7	Constellation of Square Root Raised Cosine Filter .....	40
Figure 3.8	Implementation of Nonlinear Amplifier in BOSS (AM-AM and AM-PM Conversion). ....	41
Figure 3.9	BOSS Simulation Model: Nonlinear Amplifier .....	42







Figure 4.34	IM products of the Complex Gain System with a Phase Shift in the Feedback Path. . . . .	104
Figure 4.35	IM Products and Spurs of the Cartesian System with Amplifier and Modulator Distortion.. . . .	105
Figure 4.36	IM Products and Spurs of the Cartesian System with Amplifier and Demodulator Distortion (Amplifier Output) . . . . .	106
Figure 4.37	IM Products and Spurs of the Cartesian System with Amplifier and Demodulator Distortion (Demodulator Output). . . . .	106
Figure 4.38	IM Products and Spurs of the Cartesian System with Modulator, Amplifier and Demodulator Distortion (Amplifier Output). . . . .	107



Table 4.1	Normalized Out-of-Band Power for the Class AB Amplifier with Input Power Levels of 100%, 90%, 80%, and 70% of Maximum . . . . .	68
Table 4.2	Normalized Out-of-Band Power for the Class B Amplifier with 70%, 80%, 90%, and 100% of Maximum Input Power . . . . .	71
Table 4.3	Normalized Out-of-Band Power for the Complex Gain System with Sampling Rates of 8, 16, and 32 Samples/Bit. . . . .	74
Table 4.4	Normalized Out-of-Band Power for Lookup Table Sizes of 16, 32, 64, and 128 Complex Entries. . . . .	75
Table 4.5	Normalized Out-of-Band Power for Input Power Levels of 100%, 90%, 80%, and 70% of Maximum . . . . .	77
Table 4.6	Normalized Out-of-Band Power for the Class AB, the Class B, and a Linear Amplifier. . . . .	79
Table 4.7	Comparison of the Normalized Out-of-Band Power for the Uncompensated Amplifiers and the Complex Gain Predistorter. . . . .	83
Table 4.8	Normalized Out-of-Band Power for the Cartesian System with Loop Gains of 2, 5, 10, and 15. . . . .	85
Table 4.9	Normalized Out-of-Band Power for the Cartesian System with Varying Input Power Levels . . . . .	88
Table 4.10	Normalized Out-of-Band Power for the Class AB Amplifier, the Class B amplifier, and a Linear Amplifier. . . . .	90
Table 4.11	Comparison of the Normalized Out-of-Band Power for the Uncompensated Amplifiers, a Linear Amplifier, and the Cartesian System. . . . .	92
Table 4.12	Comparison of the Normalized Out-of-Band Power Between a Linear Amplifier, the Class AB Amplifier, the Complex Gain Predistorter, and the Cartesian System. . . . .	94

**Table A1.2 The Normalized AM-AM and AM-PM  
Conversion Factors for the Class B  
Amplifier . . . . .123**

$\alpha$	roll-off factor for the transmit filter (square-root raised cosine)
$A$	constant amplifier gain in the Cartesian system
$\beta$	transfer function of the feedback network
$\Delta t$	simulation step size
$d_A(t)$	open loop distortion of the amplifier in the Cartesian system
$e_g$	error signal - difference between the actual amplifier output and the desired amplifier output in the complex gain system
$f$	frequency
$f_1$	frequency of tone 1 (two-tone input)
$f_2$	frequency of tone 2 (two-tone input)
$F$	gain characteristic of the complex gain predistorter
$G$	gain characteristic of amplifier based on the AM-AM and AM-PM conversion in the complex gain system
$I$	in-phase component of complex signal
$IM_3$	third order intermodulation product
$IM_5$	fifth order intermodulation product
$K$	constant amplifier gain in the complex gain system
$T$	symbol period
$Q$	quadrature-phase component of complex signal
$v_a$	amplifier output signal in the complex gain system (complex envelope)
$v_d$	predistorted signal in the complex gain system (complex envelope)
$v_m$	baseband signal in the complex gain system (complex envelope)
$V_{out}$	amplifier output signal in the Cartesian system

<b>AC</b>	<b>Alternating Current</b>
<b>AM-AM</b>	<b>Amplitude to Amplitude</b>
<b>AM-PM</b>	<b>Amplitude to Phase</b>
<b>BOSS</b>	<b>Block Oriented System Simulator (Comdisco Inc.)</b>
<b>DFT</b>	<b>Discrete Fourier Transform</b>
<b>DSP</b>	<b>Digital Signal Processor</b>
<b>EIA</b>	<b>Electronic Industries Association</b>
<b>FFT</b>	<b>Fast Fourier Transform</b>
<b>FM</b>	<b>Frequency Modulation</b>
<b>LINC</b>	<b>Linear Amplification Using Nonlinear Components</b>
<b>IM</b>	<b>Intermodulation Distortion</b>
<b>kb/s</b>	<b>kilobits per second</b>
<b><math>\pi/4</math> DQPSK</b>	<b><math>\pi/4</math> shifted Differential Phase Shift Keying</b>
<b>PA</b>	<b>Power Amplifier</b>
<b>PBO</b>	<b>Peak Back-Off</b>
<b>PSD</b>	<b>Power Spectral Density</b>
<b>QAM</b>	<b>Quadrature Amplitude Modulation</b>
<b>QPSK</b>	<b>Quadrature Phase Shift Keying</b>
<b>RF</b>	<b>Radio Frequency</b>
<b>TDMA</b>	<b>Time Division Multiple Access</b>
<b>TIA</b>	<b>Telecommunication Industry Association</b>
<b>VSELP</b>	<b>Vector Sum Excited Linear Prediction</b>

The popularity and growth of cellular radio has created capacity problems in large cities. The limited amount of available frequency spectrum has resulted in severe spectral crowding. Spectrally efficient linear modulation techniques, such as QAM and QPSK, are being considered in order to increase the system capacity [1, 2]. However, linear modulation techniques require linear power amplifiers. Using nonlinear power amplifiers with these modulation schemes causes the spectrum of the signal to widen, resulting in interference in adjacent channels. One suitable technique for reducing the nonlinear distortion involves the use of predistortion to linearize the power amplifier.

### **1.1 Digital Cellular Mobile Radio**

A second generation of cellular mobile communication systems is under development to overcome the capacity limitations of the analog cellular system. This new system is characterized by digital speech transmission and enhanced network capabilities. The system proposed for North America conforms to interim standard IS-54 [3]. This standard, published in May 1990, was prepared by the Electronic Industries Association/Telecommunication Industry Association (EIA/TIA) subcommittee TR45.3 on Digital Cellular Systems. Higher capacity is attained by using advanced transmission techniques, including efficient speech coding, error correcting channel codes, and bandwidth efficient modulation [1].

The IS-54 standard proposes that time division multiple access (TDMA) multiplexing be used to increase system capacity. The bit rate of the system is 48.6 kb/s with a frame duration of 40 ms, which is divided into six 6.67 ms time slots. For initial implementation, each user is allowed two of these time slots. These two time slots contain a 16 kb/s gross data rate, of which 13.2 kb/s represents digitally

control information [2]. To achieve the 13.2 kb/s of coded voice, the voice signal needs to be compressed. The speech coder uses a linear predictive coding technique called Vector Sum Excited Linear Prediction (VSELP). Future improvements in speech encoder technology are expected to allow speech to be compressed to 6.5 kb/s. Each user would then be allotted only one TDMA time slot, thereby doubling the capacity of the cellular system.

In the present analog cellular system FM is used, a modulation system that has a constant envelope. The proposed digital system will use a modulation technique called  $\pi/4$  shifted Differential Quadrature Phase Shift Keying ( $\pi/4$  DQPSK). One advantage of this modulation technique is its bandwidth efficiency. The transmission rate of 48.6 kb/s and a channel spacing of 30 kHz results in a spectral efficiency of 1.62 bits/s/Hz.

## **1.2 Digital Transmitter**

A simplified block diagram of the transmitter used for digital cellular radio is shown in Figure 1.1. This simplified model contains a speech encoder, a  $\pi/4$  DQPSK modulator and a power amplifier. A more detailed description of the modulator and the RF power amplifier is provided with the explanation of the computer simulation models (Chapter 3).

### **1.2.1 Speech Encoder**

As discussed in the previous section, the speech encoder digitizes and compresses the voice. Although voice conversation is continuous, the TDMA multiplexing scheme transmits the voice signal in bursts. This is achieved by digitizing the speech. The digitized speech is stored, transmitted in bursts, and then 'stretched' at the receiver to reproduce the original speech.

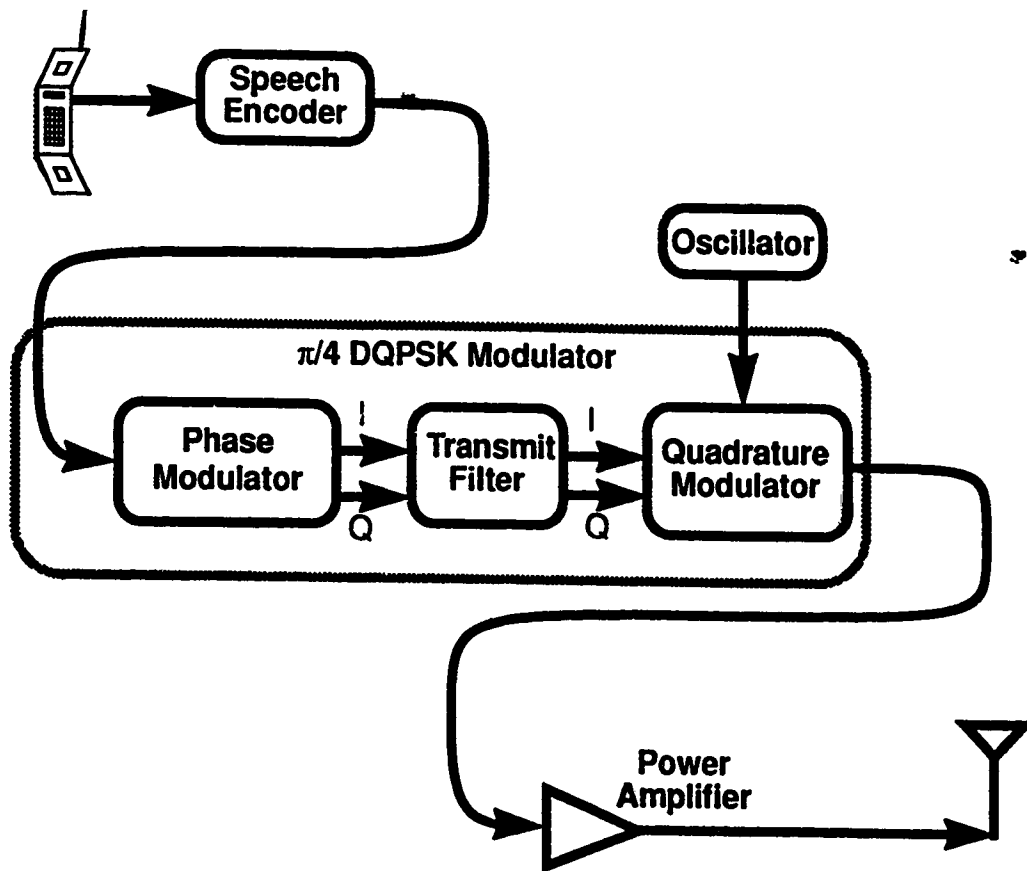


**Figure 1.1 Block Diagram of a Digital Transmitter**

### **1.2.2 Modulator**

The modulator produces a  $\pi/4$  DQPSK signal at the channel frequency from the baseband digital voice data. This is performed in three stages. First, the phase modulator performs the differential phase encoding of the digital voice data. Secondly, the transmit filter defines the spectral shape of the transmitted signal [4]. The IS-54 specification recommends that a transmit filter with a square-root raised-cosine amplitude response and a linear phase response be used. This allows bandlimited transmission with zero intersymbol interference. After filtering, the phase modulated signal is converted to the assigned channel frequency (in the 800 MHz band) by the quadrature modulator.

In the current analog cellular radio system, low index FM modulation is used. Therefore, because the signal has a constant envelope, efficient and nonlinear power amplifiers can be used.

The linear modulation method proposed for the digital cellular system is spectrally efficient but has significant RF envelope fluctuation. As a result, it is more susceptible to the nonlinearities of the power amplifier. This nonlinear distortion causes the spectrum of the signal to widen, causing adjacent channel interference. Thus, the digital transmitter requires a linear power amplifier.

Linear power amplifiers have a low dc-to-ac conversion efficiency. Nonlinear power amplifiers have higher theoretical maximum efficiencies. Class A power amplifiers have a theoretical maximum efficiency of 50%, while class B amplifiers have a theoretical maximum efficiency of 75% [5]. Class C power amplifiers have a still higher theoretical maximum efficiency, but are the least linear. Nonlinear power amplifiers can be characterized by amplitude-to-amplitude distortion (AM-AM) and amplitude-to-phase distortion (AM-PM). In order to reduce these distortion effects, and thereby limit the transmitted out-of-band power, some form of amplifier linearization must be used.

### **1.3 Adaptive Predistortion**

Predistortion is one approach that may be used to linearize a nonlinear amplifier. This technique operates on the principle of appropriately predistorting the signal at the amplifier input. The nonlinear amplifier then amplifies and distorts this complementary predistorted signal so that its output is an amplified minimally distorted version of the original signal. This work examines two different methods of predistortion, namely (a) Cartesian coordinate negative feedback, and (b)



compared. As well, the error sensitivity of the two techniques is examined.

The amplifier is not the only source of distortion in the transmitter. The non-ideal modulator and demodulator also introduce distortion in the output signal, such as dc offset, differential gain, and differential phase.

Computer simulation offers a time-efficient method of studying complex systems. The parameters and components of the system can be varied easily. Simulation-based analysis and design has proved to be a useful and effective tool for development and performance evaluations of communication systems. Complex envelope simulation models are used to analyze the two predistortion techniques.

#### **1.4 Thesis Outline**

RF power amplifier distortion and the effects of these nonlinearities are discussed in Chapter 2. The criteria for assessing amplifier nonlinearity are described and a survey of linearization techniques is presented. The two linearization techniques studied in this project are also described.

Chapter 3 is concerned with the simulation approach. The simulation software, the models used to analyze the digital cellular mobile radio transmitter, and the linearization techniques are described. The distortion generated by the modulator and the demodulator is analyzed. The measurement of the power spectral density, and the calculation of the out-of-band power are also described in this chapter.

simulations is presented and extensive simulation results are presented and discussed.

Chapter 5 summarizes the simulation approach used and the results obtained, discusses the implementation feasibility of the predistortion methods studied, and indicates areas of future desirable research.

## Amplifier Distortion and Linearization Techniques

This chapter provides background information on amplifier distortion and linearization techniques. The effects of the amplifier nonlinearities are examined and the different types of nonlinear distortion are explained. The intermodulation distortion products and out-of-band power are presented as criteria for assessing amplifier nonlinearity. Various amplifier linearization techniques that are available, or that have been proposed, are discussed.

### 2.1 Amplifier Distortion

The output of an ideal amplifier is an amplified replica of the input signal. However, in real power amplifiers, nonlinear distortions occur because of power supply and other gain mechanism limitations. The non-ideal characteristics of the amplifier cause the output amplitude and/or phase to vary nonlinearly with input signal level [6, 7]. Figure 2.1 shows a typical output power response for an amplifier.

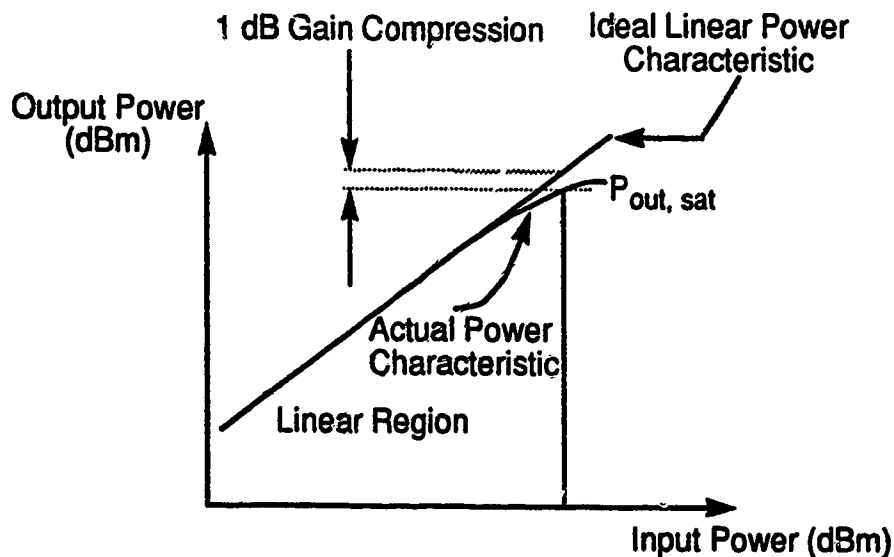
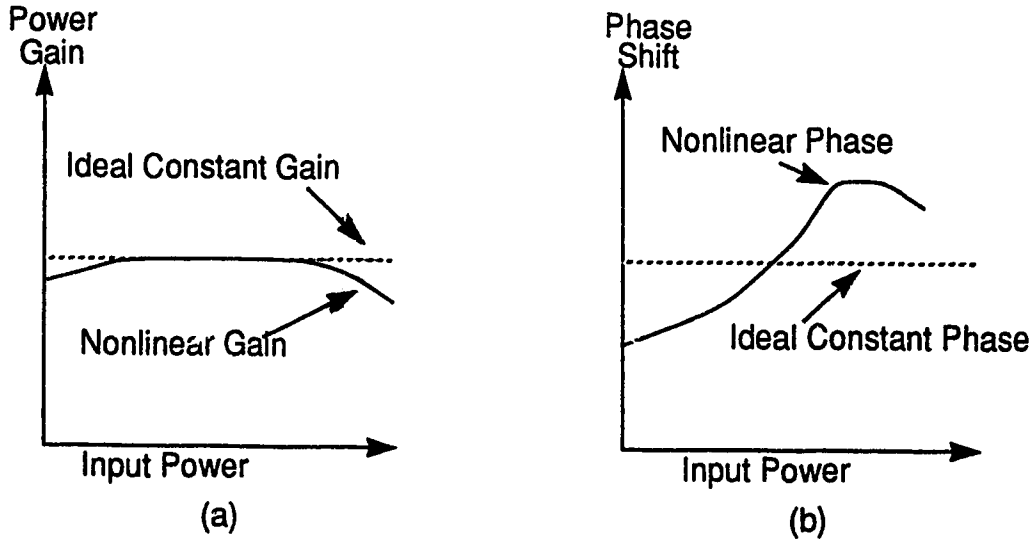


Figure 2.1 Output Power Characteristic

At low input power levels, the output power is normally a linear function of the input power. As the input power increases further, the output power begins to increase sublinearly until eventually a power level is reached at which the output power reaches a maximum, or may actually decrease. The dc-to-ac conversion efficiency of high frequency power amplifiers is highest at saturation. Hence, efficient operation of power amplifiers results in distortion of signals with amplitude modulation. Two primary distortion mechanisms are of interest: amplitude-to-amplitude distortion (AM-AM) and amplitude-to-phase distortion (AM-PM).

### 2.1.1 AM-AM Distortion

AM-AM distortion is a nonlinear amplitude or envelope distortion arising from a nonlinear power transfer characteristic. The power gain of an amplifier is the slope of the power transfer characteristic. The gain is dependent on the signal input power level (see Figures 2.1 and 2.2).



**Figure 2.2 Types of Amplifier Distortion (a) Nonlinear Amplitude (Envelope) Distortion (b) Nonlinear Phase Distortion**

When the amplifier is operated close to saturation, the output signal suffers from amplitude compression, resulting in harmonic and intermodulation distortion. Harmonic distortion is the generation of second, third, or higher harmonics of the input signal. Intermodulation distortion (IMD) results in spurious signals within the frequency band of the applied signal.

### **2.1.2 AM-PM Distortion**

AM-PM distortion is caused by an amplifier's nonlinear phase response. The phase of the output signal is a function of the instantaneous amplitude of the input signal (see Figure 2.2 b). This causes amplitude-to-phase conversion. These phase nonlinearities produce harmonic and intermodulation distortion [6].

## **2.2 Evaluation of Amplifier Nonlinearities**

### **2.2.1 Intermodulation Distortion**

A convenient measure for specifying the maximum allowable distortion of the amplifier is that of intermodulation distortion products. The output of an amplifier with a nonlinear transfer characteristic has spurious signals within the frequency band of the applied signal. An intermodulation distortion product is the ratio of the power of a spurious signal to the power of the desired output. Balanced two-tone tests are used to measure the intermodulation distortion. The test signal consists of two equal-level tones, at frequencies  $f_1$  and  $f_2$ . The frequency difference,  $\delta f = f_1 - f_2$ , is small compared to their individual frequencies. When these two frequencies pass through a nonlinear amplifier, spurious signals at additional frequencies are produced. These spurious signals contain the intermodulation products. For  $f_2 > f_1$ , the third-order distortion products appear at  $2f_2 - f_1$  (upper) and  $2f_1 - f_2$  (lower) while the fifth-order distortion products appear at  $3f_2 - 2f_1$  (upper) and

$3f_1-2f_2$  (lower). The third- and fifth-order products are the most important because they lie nearest to the original frequencies and usually dominate the distortion.

The third-order intermodulation distortion product,  $IM_3$ , may be defined as the ratio of the output power at a third-order product frequency,  $2f_2-f_1$  or  $2f_1-f_2$ , to the output power at one of the fundamental signals,  $f_1$  or  $f_2$ :

$$IM_3 \text{ (dB)} = 10 \log \left| \frac{P_3}{P_{1,2}} \right| \quad (2.1)$$

where:

$P_3$  = power of the third-order product at  $2f_2-f_1$  (upper) or  $2f_1-f_2$  (lower)

$P_{1,2}$  = power at  $f_1$  or  $f_2$ .

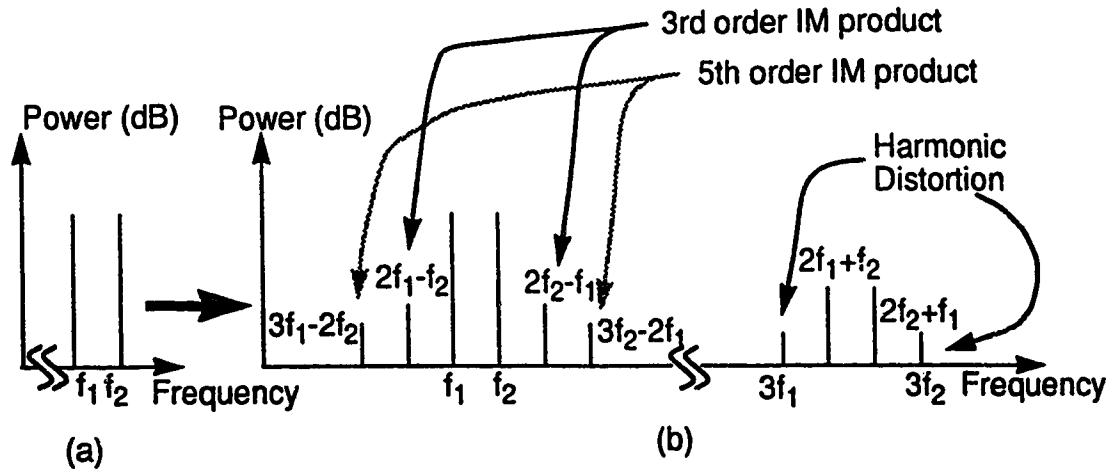
The fifth-order intermodulation distortion,  $IM_5$ , may be defined as:

$$IM_5 \text{ (dB)} = 10 \log \left| \frac{P_5}{P_{1,2}} \right| \quad (2.2)$$

where:

$P_5$  = power of the fifth-order product at  $3f_2-2f_1$  (upper) or  $3f_1-2f_2$  (lower).

The input and output spectra for a simple two-tone test are shown in Figure 2.3 [8].



$f_1$  and  $f_2$  are two tones. The amplifier nonlinearities give rise to sum and difference products.

**Figure 2.3 Harmonic and Intermodulation Spectra for a Nonlinear Power Amplifier (a) Input Spectra (b) Output Spectra**

## 2.2.2 Out-of-Band Power

Another measure of amplifier distortion is the out-of-band power of a transmitted signal. When a bandlimited signal is applied to an amplifier, any nonlinearity in the amplifier will lead to output power that lies outside the original signal bandwidth [5]. For  $\pi/4$  DQPSK modulation, the proposed system has a channel bandwidth of 30 kHz. In the adjacent channel (centered 30 kHz away), IS-54 [3] specifies that the maximum transmitted power is 26 dB below the mean output power in the main channel. In the next 30 kHz channel, centered 60 kHz away, the allowed power is -45 dB. And, 90 kHz and more away from the channel center, the maximum out-of-band power is -60 dB. This is illustrated in Figure 2.4.

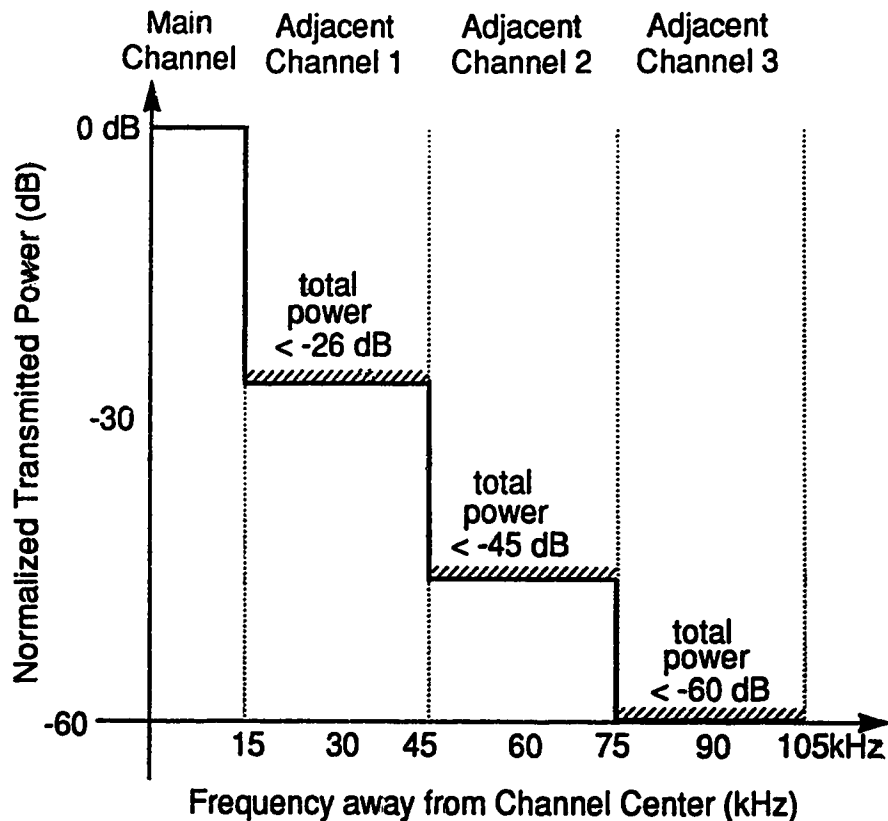


**Figure 2.4 Allowed Transmitted Power in Adjacent Channels**

### **2.3 Amplifier Linearization Techniques**

Although linear modulation techniques achieve high spectral efficiency, they are easily affected by the nonlinear distortion of power amplifiers. This distortion results in spectral spreading. Thus, linear power amplification techniques are required, otherwise the power amplifier eliminates any spectrum efficiency gained by using the linear modulation. To retain the spectral efficiency of the linear modulation method, an effective method must be used to reduce the effect of the nonlinear distortion produced by the amplifier. This section presents a literature survey of promising linearization methods proposed for digital mobile radio.

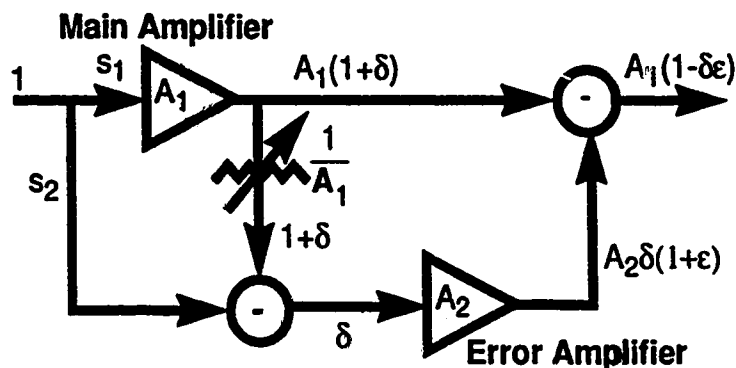
A simple linearizing method is to operate the amplifier at levels well below saturation, as is evident from Figure 2.1. This is referred to as backing-off [6, 9]. The effects of the amplifier nonlinearities decrease as the input signal level is



reduced. However, the amount of back-off results in a reduction in amplifier efficiency, since the dc operating conditions are still maintained at the original levels.

### 2.3.1 Feedforward Correction

This linearization technique involves the cancellation of unwanted distortion products. The input signal is split into two components, which are amplified and combined in such a way that the distortion products cancel [6, 10]. A diagram of a feedforward system is shown in Figure 2.5.



$A_1, A_2$  - main and error amplifier gain, respectively.

$\epsilon, \delta$  - first-order deviations from gain linearity of the main and error amplifier, respectively

**Figure 2.5 Feedforward Correction [6]**

$A_1$  refers to the high-level main amplifier and  $A_2$  refers to the low-level error amplifier. The gains of the two amplifiers are equal ( $A_1 = A_2$ ). The symbols  $\delta$  and  $\epsilon$  represent first order deviations from the gain linearity of the main amplifier and of the error amplifier, respectively. A portion of the output signal from the main amplifier is attenuated so that it has the same level as the signal  $s_2$ . The difference between the distorted and the undistorted signal is used to provide an error signal,  $\delta$ . The error signal is amplified and the output of the error amplifier is subtracted from the main amplifier to produce the output  $A_1(1-\delta\epsilon)$ . The output is seen to have

only a second order deviation from the gain  $A_1$ . Thus, the linearity of the output signal is improved considerably.

Stewart and Tusubira [10], reported on an experimental feedforward correction system for micro-cellular systems. Using a two-tone test in the 950 MHz region, they achieved a reduction in  $IM_3$  of 55 dB.

The advantages of the feedforward system are:

- ❑ System is open loop and thus is unconditionally stable
- ❑ Highly efficient nonlinear amplifiers can be used.

The disadvantages of this system are:

- ❑ Two amplifiers are required
- ❑ Cannot easily compensate for drift and temperature variations
- ❑ Requires more complex circuitry
- ❑ Primarily reduces only  $IM_3$  (first order nonlinearities).

### **2.3.2 LINC**

LINC, Linear Amplification Using Nonlinear Components [11 - 18], is a method of producing linear amplification by using two nonlinear amplifiers. As shown in Figure 2.6 [11], this linearization method separates the signal into two parts, amplifies each part separately, and then recombines the two signals such that the harmonics cancel.

This technique, also called out-phasing, was developed in the 1930's [17] to improve the efficiency and linearity of high power AM broadcast transmitters. It is similar to feedforward compensation in that both techniques use two amplifiers to cancel the unwanted distortion products. In the LINC technique, the overall transfer function of the amplifier system is linear, but the RF amplifiers are both high level, and can be nonlinear. The input signal to the system,  $S(t)$ , is an amplitude and/or

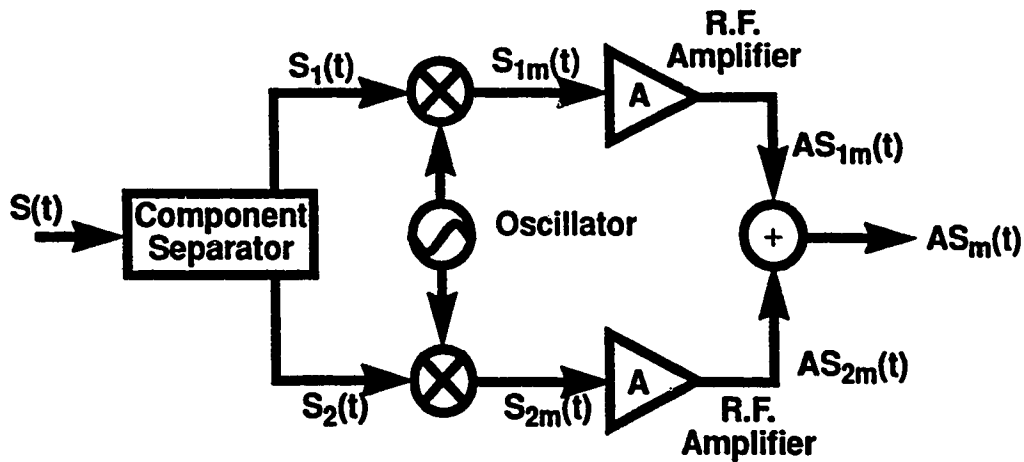


Figure 2.6 LINC Transmitter

phase modulated waveform. From  $S(t)$ , two complex signals,  $S_1(t)$  and  $S_2(t)$ , are generated. These signals vary in phase but have a constant amplitude. The two complex signals,  $S_1(t)$  and  $S_2(t)$ , are separately modulated and amplified through two well-matched nonlinear amplifiers, producing  $AS_{1m}(t)$  and  $AS_{2m}(t)$ . These signals are then passively summed to provide the modulated and amplified output signal,  $AS_m(t)$ .  $S_1(t)$  and  $S_2(t)$  are generated so that all undesired out-of-band components are in exact anti-phase at the output of the amplifiers, and hence, cancel when combined. The desired components are in phase and reinforce at the output of the summation circuit.

The LINC approach provides RF amplification by highly efficient, nonlinear amplifiers operating on constant envelope signals. However, the characteristics of the two amplifiers must be well-matched for the nonlinearities to cancel when the two amplified signals are summed [13, 14]. As well, any electrical length differences between the two amplification paths will cause phase errors.

Simulation results by Tomisto *et al.* [12] reported 60 dB suppression of adjacent channel interference. This was an OQPSK system using a Nyquist filter with a roll-off of 100%. A Nyquist filter provides a bandlimited output with zero

intersymbol interference [4]; an example of a Nyquist filter is the raised cosine filter. A roll-off of 100% corresponds to  $\alpha = 1$  for the raised cosine filter. The simulated system was designed for digital mobile radio applications. Another LINC system for digital mobile radio was constructed by Hetzel *et al.* [15]. This prototype system, operating at 170 MHz, used two class C amplifiers. Employing a two-tone test signal, the system achieved IM products 60 dB below the fundamental frequencies.

The advantages of the LINC system are:

- Simple to implement
- Highly efficient, nonlinear amplifiers can be used.

The disadvantages of this system are:

- Matching of the amplifiers is difficult
- Difficulty in the generation of the constant amplitude signals - although this can be done with a digital signal processor (DSP)
- System is sensitive to mismatches in phase between the two amplification paths.

### 2.3.3 Adaptive Predistortion

Adaptive predistortion [14, 19 - 22] operates on the basis of providing an appropriately distorted signal to the amplifier, so that the output of the amplifier is an amplified replica of the original input signal. This adaptive method of linearizing power amplifiers was first described by Salah and Salz in 1982 [19]. Several other adaptive techniques have since been developed, but the basic principles of operation are similar. Adaptive predistortion involves a transmitter-based recursive algorithm that predistorts the signal constellation to produce a virtually linear transmitted signal (see Figure 2.7). A calibration signal, which is generated by the

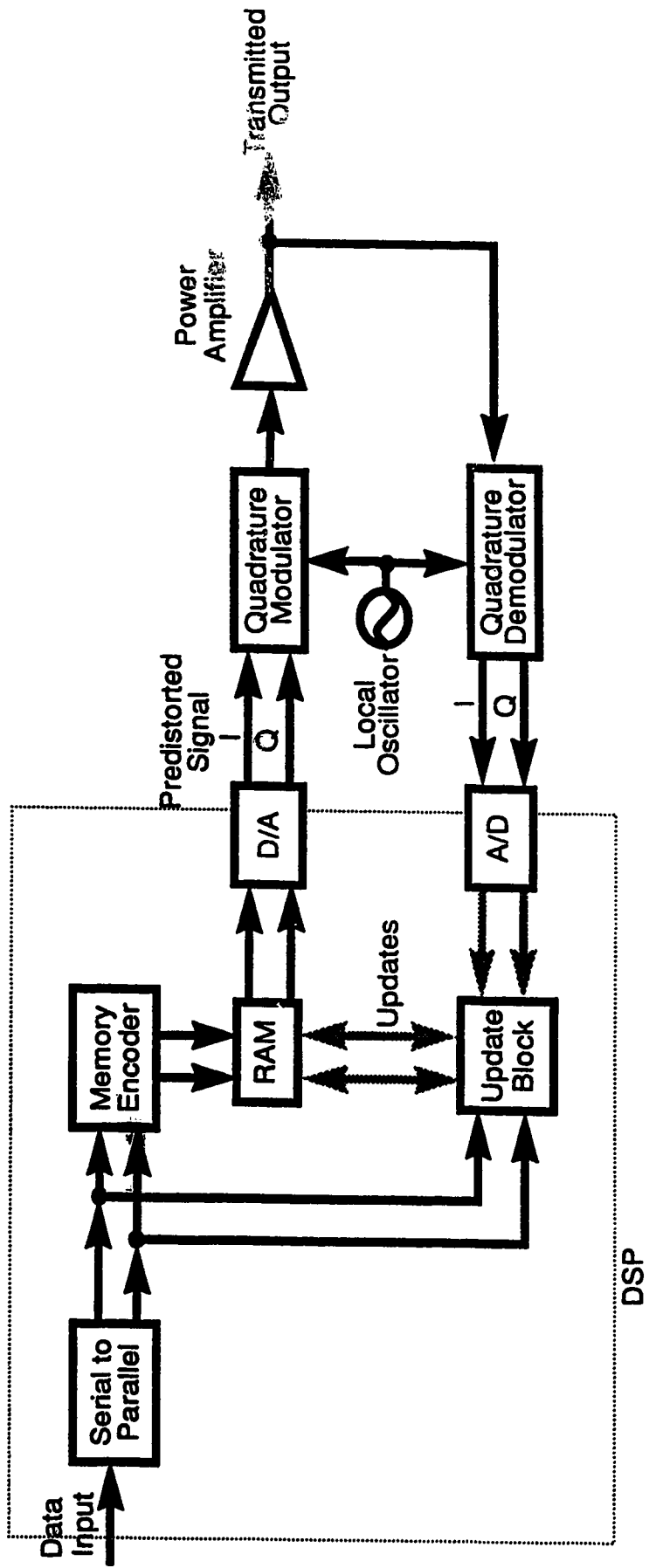


Figure 2.7 Adaptive Predistortion

baseband DSP (digital signal processor), is modulated and amplified by the nonlinear amplifier. The amplifier output is sampled by a directional coupler, demodulated, and fed back to the baseband processor. From this feedback information, the gain and phase distortion of the amplifier are fully characterized and stored in memory. The DSP then uses the measured distortion to predistort the modulating signal in a manner that is complementary to the power amplifier distortion. Thus, the overall transmitter characteristic is linearized.

The adaptive predistortion transmitter operates mainly in an open loop configuration. The loop is closed periodically to recalibrate the distortion table. To adapt for both frequency channel switches and thermal effects, the recalibration process must be quick and be performed periodically.

There are different methods of calculating the predistorted signal. Two of these, the mapping predistorter [20] and the complex gain predistorter [21, 22], are discussed in more detail in the following sections.

#### 2.3.3.1 Mapping Predistortion

This system maps the complex modulation plane onto itself by causing the complex signal trajectory to follow a new path. A block diagram of this system is shown in Figure 2.8. The complex modulating signal,  $S_i$ , is used as a pointer to a two-dimensional, memory-based, lookup table. A set of complex values,  $\phi_i$ , is stored in the lookup table. The vector sum of  $S_i$  and the appropriate  $\phi_i$  forms the predistorted signal. This signal is then modulated and amplified, producing  $T_i$ . The sampling loop demodulates  $T_i$  and generates the feedback signal  $P_i$ . If the amplifier is nonlinear,  $P_i$  is a distorted and delayed version of  $S_i$ . The update block corrects for the delay, and uses the error in  $P_i$  to calculate a new estimation for  $\phi_i$ .

The complex modulation plane is quantized in the in-phase (I) and quadrature (Q) dimensions. The input  $S_i$  is quantized with 8 to 10 bit accuracy in

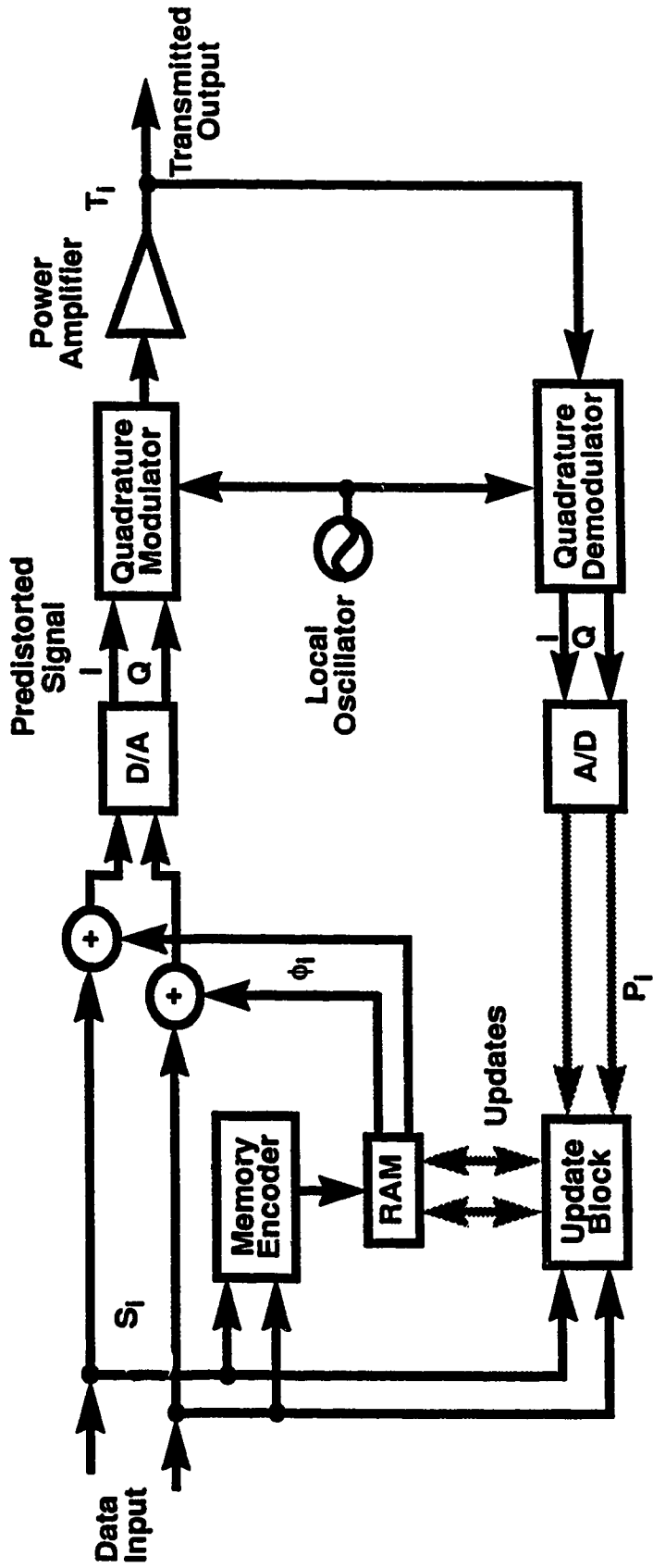


Figure 2.8 Mapping Predistortion

its real and imaginary parts separately, and these act as an index to the lookup table. The table size is determined by the number of bits required. For 10 bit quantization, the lookup table requires more than 1 MByte of memory [20]. A recursive technique is used to calculate the  $\phi_i$ 's for the lookup table. Although this technique involves simple calculations, the number of table entries and the slow convergence of the algorithm result in slow update times. If the channel frequency is changed, up to 10 seconds are required to calculate all of the new values of  $\phi_i$  for the lookup table [20, 21, 22]. Although this system does respond well to slow variations, such as temperature variations and component aging, it has slow update times.

Nagata [20] investigated a  $\pi/4$  DQPSK system for digital mobile radio which included a mapping predistorter. The system operated at 145 MHz and included a class AB amplifier. He achieved -60dB out-of-band power emission in simulation results and close to this in a prototype system. However, the system required update times of five to ten seconds.

The advantages of a mapping predistorter are:

- ❑ Linearizing process is open loop and therefore is stable
- ❑ Responds well to slow variations such as temperature and component aging.

The disadvantages of this system are:

- ❑ Very large memory requirement
- ❑ Very slow adaption and update mechanisms.

### 2.3.3.2 Complex Gain Predistortion

This adaptive predistortion approach [21, 22], shown in Figure 2.9, is similar to the mapping predistorter described above, but takes advantage of the amplitude



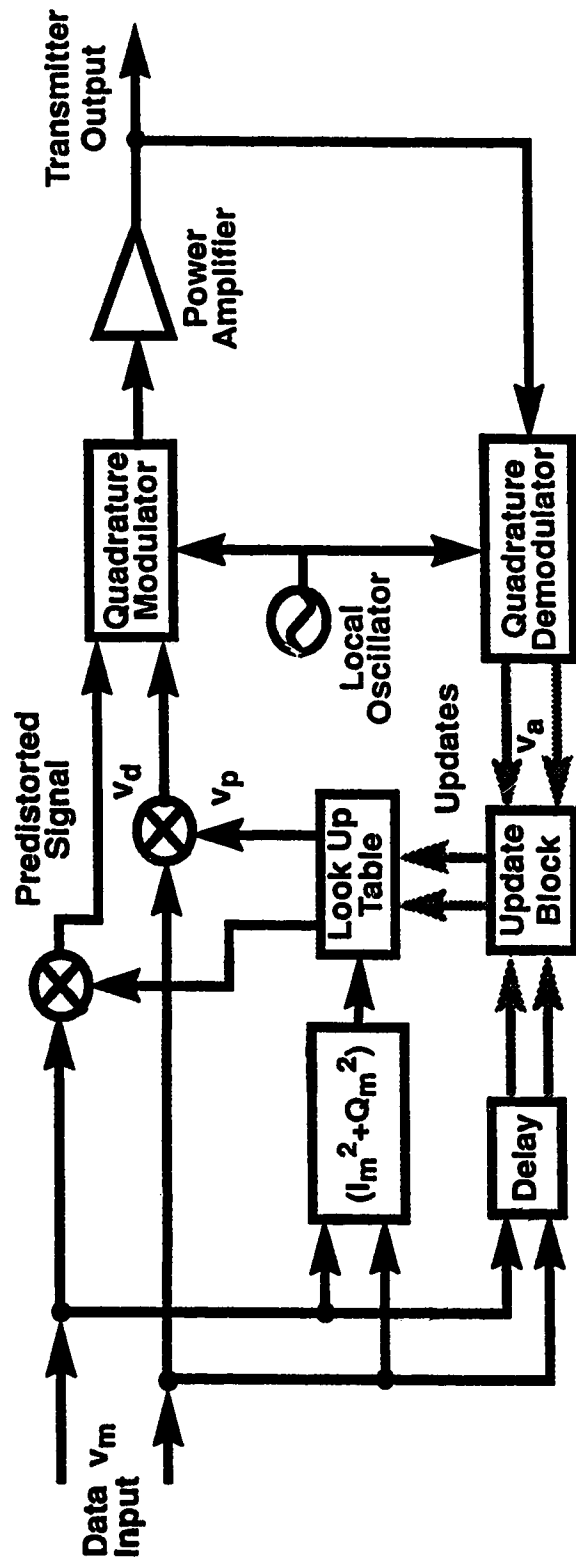


Figure 2.9 Complex Gain Predistorter

the speed of updating the memory.

The power amplifier is characterized by AM-AM and AM-PM distortion and both of these mechanisms are dependent on the input amplitude. Assuming that the power amplifier distortion does not depend on the phase of the input signal and that the distortion is memoryless, a complex signal of constant magnitude will have a constant degree of distortion. Thus, the complex gain predistorter requires only a one dimensional table to characterize the amplifier predistortion. This results in a smaller memory requirement and a faster convergence time than for the mapping predistorter.

The power of the baseband signal,  $|v_m|^2$ , is used to index a lookup table. The output of the lookup table is multiplied by the original signal,  $v_m$ , to give the predistorted signal,  $v_d$ . This signal is then modulated and amplified. If the demodulated signal,  $v_a$ , is not an amplified version of  $v_m$ , a new entry for the lookup table is generated.

This system assumes that the amplifier is memoryless and has a level-dependent complex gain. Thus, the complex envelope of the input,  $v_d$ , and output,  $v_a$ , are related by:

$$v_a = v_d G(|v_d|^2) \quad (2.3)$$

The complex amplifier gain,  $G(|v_d|^2)$ , includes the AM-AM and the AM-PM characteristics of the amplifier. The amplifier gain is dependent on the instantaneous power of the input signal and does not depend on its phase. The transfer function of the predistorter is based on this relationship. The input/output complex envelope relationship of the predistorter is given by:

$$v_d = v_m F(|v_m|^2) \quad (2.4)$$

power of its input signal.

The value of the predistorter's complex gain,  $F$ , is determined by setting the composite characteristics of both the predistorter and the amplifier equal to a constant amplitude gain,  $K$ .

From (2.3) and (2.4):

$$v_a = Kv_m = v_d G(|v_d|^2) = v_m F(|v_m|^2) G\left[|v_m|^2 |F(|v_m|^2)|^2\right] \quad (2.5)$$

Defining  $x_m = |v_m|^2$  gives:

$$K = v_m F(x_m) G(x_m |F(x_m)|^2) \quad (2.6)$$

For each value of  $v_m$ , the predistortion function  $F(|v_m|^2)$  needs to be determined. This value is the root of the equation:

$$e_g(F) = v_a(F) - Kv_m \quad (2.7)$$

The error signal,  $e_g(F)$ , is the difference between the actual amplifier output and the desired amplifier output.

A secant algorithm [24] is used to calculate the predistortion values. The equation used for the secant algorithm is:

$$F_i(k+1) = \frac{F_i(k-1) e_{gi}(F_i(k)) - F_i(k) e_{gi}(F_i(k-1))}{e_{gi}(F_i(k)) - e_{gi}(F_i(k-1))} \quad (2.8)$$

where "i" is the table entry and "k" is the iteration number

quadrature value.

The secant method is used because it has relatively fast convergence. Only about 10 iterations are needed to find a value for each  $F_i$ . A unique value of  $F$  is needed for each table value. Therefore, for a table size of 64, with 10 iterations per table value, 640 iterations are required.

Since the lookup table contains only corrections for magnitude, and not for both the I and Q values of the complex signal, the amount of memory required is much less than for the mapping predistorter. Good results have been obtained with a table size of 64 [21, 22]. This results in a memory requirement of 128 bytes (since  $F$  is a complex number). This is much less than the 1 Mbyte required for the mapping predistorter. The recursive technique used in the complex gain predistorter requires more complicated calculations than the mapping predistorter, but the fast convergence time and the small table size reduces the time needed to update the lookup table. Typical times for updates are of the order of 4 ms [21, 22].

Cavers [21, 22] reported on a complex gain system using a class AB amplifier backed-off by 0.22 dB. For two-tone simulation tests, he achieved IM products reduced below 60 dB.

The advantages of the complex gain predistorter are:

- Significant reduction in memory size compared to the mapping predistorter
- Rapid convergence time
- Responds well to slow variations such as temperature and component aging.

The disadvantages of this system are:

- Increased computational overhead.

Cartesian coordinate negative feedback [25 - 30] is similar to adaptive predistortion, but uses negative feedback to generate the predistorted signal and thus linearize the transmitter. A block diagram is shown in Figure 2.10.

The RF power amplifier output is sampled and this signal is then synchronously demodulated into its quadrature components,  $I_a$  and  $Q_a$ . These signals are used as the negative feedback information. They are subtracted from the quadrature input signals to generate a loop error signal. The loop error signal, after loop filtering, is the input to the quadrature modulator. If the loop gain is sufficiently high, the feedback loop will continuously correct for any nonlinearity in the transmitter. The feedback loop must also adjust for phase shifts generated by the amplifiers and the feedback path. The loop stability is determined by the phase shift and by the loop gain. The higher the loop gain, the more sensitive the stability is to phase adjustments [30]. As this is a closed loop system, it is conditionally stable and the loop time delay determines the maximum bandwidth of the system. The usable bandwidth is typically 10% of the operating frequency.

This system operates as a simple feedback loop, as shown in Figure 2.11. An estimation of the reduction in distortion from the power amplifier and modulator is easily calculated. The open loop distortion is given by  $d_A(t)$  and the voltage gain of amplifier is  $A$ . The complex envelope representation of the input is  $S(t)$ . The open loop output of the amplifier is given by:

$$V_{out} = AS(t) + d_A(t) \quad (2.9)$$

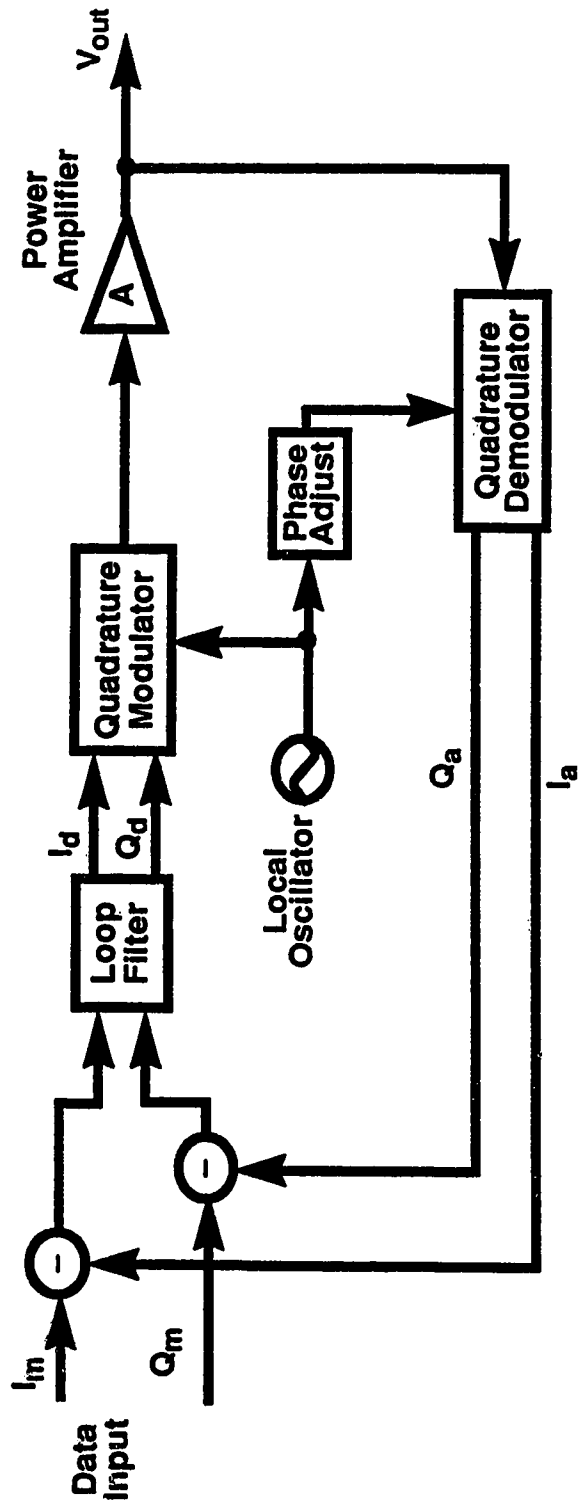


Figure 2.10 Cartesian Coordinate Negative Feedback System

output of the amplifier when the loop is closed is:

$$V_{out} = \frac{S(t)}{\beta} + \frac{d_A}{A\beta} - \frac{d_F(t)}{\beta} \quad (2.10)$$

where  $d_F(t)$  is the distortion in the feedback path.

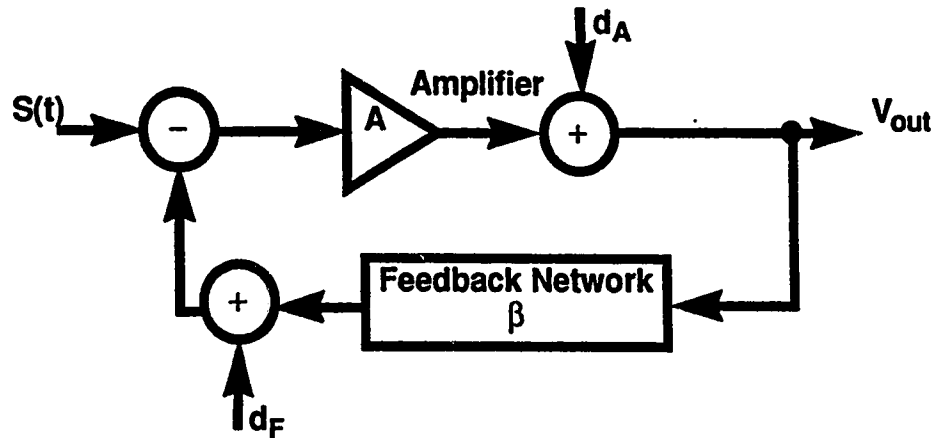


Figure 2.11 Basic Feedback Amplifier

Equation (2.10) demonstrates that distortion in the forward path ( $d_A$ ) is reduced by the loop gain ( $A\beta$ ), while distortion in the feedback path ( $d_F$ ) is actually increased for  $\beta < 1$ .

Akaiwa and Nagata [25] constructed an experimental system using  $\pi/4$  DQPSK modulation with Nyquist baseband filtering (50% roll-off). The system operated at 145 MHz and used a class AB amplifier. The relative out-of-band power was reduced by 28 dB to -60 dB.

Johansson and Mattsson [30] constructed an experimental system, in the 900 MHz range, using a class AB amplifier. In two-tone tests,  $IM_3$  was reduced by 29 dB to -62 dB.

The advantages of the Cartesian coordinate negative feedback are:

- Continuous correction (zero convergence time)
- Simple to implement.

- ❑ Potential instability of the feedback loop
- ❑ Restricted bandwidth.

## **2.4 Summary**

A linearization technique for digital cellular radio must, first of all, improve the composite linearity of the transmitter sufficiently to meet the out-of-band power requirements of the IS-54 specification (Section 2.2.2). An additional requirement is that the system must be able to respond to variations in the operating conditions. These include rapid changes such as frequency channel switches, slow changes resulting from changes in ambient and atmospheric conditions (temperature and humidity), and fluctuations and drifts due to component aging.

While all of the techniques discussed report improvements in the out-of-band power and intermodulation products sufficient for the application, not all meet the second requirement of adaptability. Of the described systems, feedforward compensation and LINC are the least suitable for mobile radio applications, as neither of these techniques is adaptive. The other methods, adaptive predistortion and Cartesian coordinate negative feedback, are adaptive. The two adaptive predistortion techniques discussed are the mapping predistorter and complex gain predistorter. The mapping predistorter updates slowly, and has a large memory requirement. The long convergence time and the prohibitive memory requirements reduce its suitability for the mobile radio environment. The complex gain predistorter has a faster update mechanism and uses less memory.

Adaptive predistortion and Cartesian coordinate negative feedback are similar systems. The Cartesian system is a closed loop, negative feedback system, while the predistortion scheme is mainly open loop; the loop is closed only briefly



during each calculation. Although closed loop operation restricts the bandwidth of the Cartesian feedback system, this is not a detriment to its applicability, as mobile radio is a narrowband system.

In summary, of the linearization techniques discussed, the most suitable methods for digital mobile radio are the complex gain predistortion system and the Cartesian coordinate negative feedback system. In the following chapters, these two systems are analyzed and compared.

## **2.5 Simulation Plan**

The project uses simulation to analyze the performance of two linearization techniques: Cartesian coordinate negative feedback and complex gain predistortion. The analysis uses  $IM_3$ ,  $IM_5$ , and the out-of-band power (defined by IS-54) to characterize the performance of the linearization methods. The overall simulation approach is outlined below:

The first phase of the project included preparing and verifying the computer models for a digital transmitter. The models include generation of  $\pi/4$  DQPSK modulated signals, pulse shaping filters, and amplifiers with AM-AM and AM-PM distortion. Models for the complex gain predistorter, the Cartesian coordinate negative feedback system, and a modulator and demodulator with representative distortion were also included.

The second phase involved simulations to analyze the effects of the nonlinear amplifier on the transmitter. Two different nonlinear amplifier characteristics were used. These simulations established a benchmark with which to compare the linearization techniques.

in the third phase, the linearization techniques were included in the transmitter model. The performance parameters of both the complex gain predistorter and the Cartesian feedback system were optimized. Also, the performance of the linearization techniques with the two different amplifiers was characterized.

The fourth phase included an error-sensitivity analysis of the two systems. The effects of the representative modulation and demodulation distortion on the transmitter and the ability of the predistortion techniques to compensate for this type of distortion were analyzed.

### 3. Computer Simulation Models

This chapter describes the models used to simulate a transmitter for digital cellular mobile radio. The simulation software, BOSS, is discussed and the simulation models used to analyze the digital cellular mobile radio transmitter are explained. The distortion generated by the modulator and demodulator is discussed, and the complex envelope representation of the distortion is developed. The measurement of the power spectral density and the calculation of the out-of-band power are also discussed.

#### 3.1 The BOSS Environment

The Block Oriented Systems Simulator (BOSS) software package by COMDISCO was used for the simulations. Version 2.7 of BOSS runs on a SUN SPARC 7 workstation and provides a highly interactive and graphic environment for simulation-based analysis and design of communication systems. The system is developed in a hierarchical manner by using block diagram representations of the various components of the system [31]. Each functional block is represented by a software subroutine block. A block can represent a simple function, such as a modulator, or a more complex function, such as an entire communication link. The system is constructed in topological form, similar to a block diagram representation of the hardware realization. In order to build a simulation system, each block diagram is constructed by bringing existing models from a library to the workstation's screen, and connecting them in the desired topology. New block diagrams are created from existing blocks and from library modules. If a functional block cannot be constructed from existing models, a new model is created by entering a FORTRAN subroutine. The models added to the libraries can be used by other users; some of the models used in this project were constructed for a previous project [32] and modified for these simulations. When the complete block

diagram has been constructed, the system may be simulated. Results from the simulations can be viewed using the post processor which can generate a variety of plots such as waveform plots, eye diagrams, and scatter (constellation) diagrams. Frequency domain plots are also available; these include power and phase plots.

### **3.2 System Model**

A block diagram for a  $\pi/4$  DQPSK transmitter is shown in Figure 3.1. The corresponding BOSS model representation for this transmitter is shown in Figure 3.2. Comparing the two block diagrams, one can see that the two block diagrams are similar. The main difference is that the BOSS simulations use an equivalent low-pass, complex envelope representation of the signals in order to reduce the sampling rate and conserve computing time. Simulation at the carrier frequency of 850 MHz requires a very small  $\Delta t$ , where the parameter  $\Delta t$  is used to specify the simulation step size. If the signal is sampled at the Nyquist rate (2·850 MHz), a  $\Delta t$  in the order of 0.6 ns is required. Simulations with such a small  $\Delta t$  would take a very long time to execute. Therefore, the simulations are carried out at baseband. The complex signals in BOSS contain both the in-phase and the quadrature signals,  $S(t) = I(t) + jQ(t)$ .  $S(t)$  refers to the complex envelope of the RF signal. A small square in a BOSS model indicates that there are input parameters which must be defined for the block. The parameters include variables such as the length of simulation, the bit rate, and the sampling rate. The parameters are either specified when the blocks are included in the system or when the system is simulated. The small blocks labeled "SINK" are simply used to terminate output signals. Most of these signals were used for testing and debugging the models. The routing of the lines between blocks is performed automatically by BOSS (and is not always aesthetically pleasing).

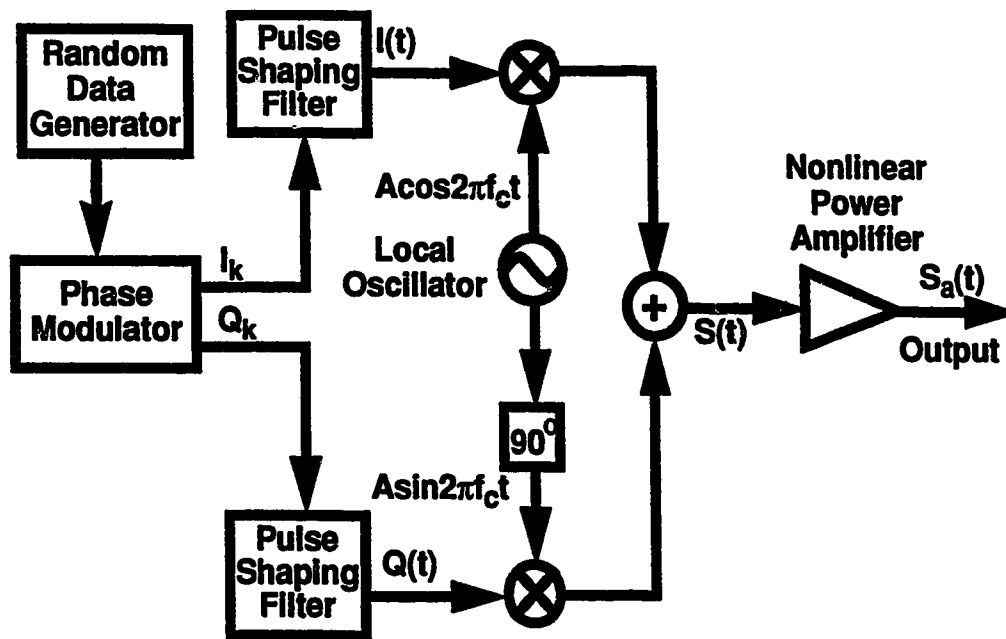


Figure 3.1 Block Diagram of a  $\pi/4$  DQPSK Transmitter

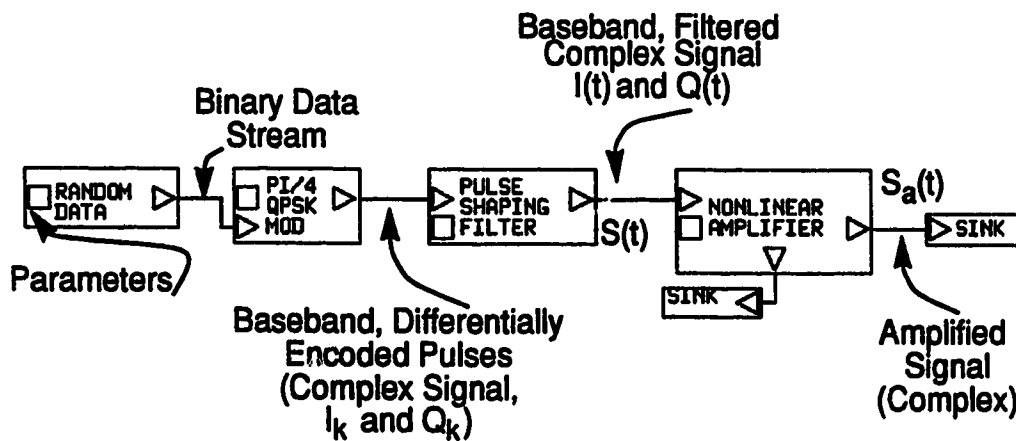


Figure 3.2 BOSS Simulation Model:  $\pi/4$  DQPSK Transmitter

The following sections discuss the modules in the  $\pi/4$  QPSK transmitter shown in Figures 3.1 and 3.2. The transmitter consists of the following blocks:

- Random data generator
- Phase modulator ( $\pi/4$  DQPSK modulator)
- Pulse shaping filters
- Nonlinear power amplifier.

### 3.2.1 Random Data Generator

The data generator is represented by a random data block that simulates a random digital data stream. The data rate is a parameter in this block. The IS-54 specifies a data rate of 48.6 kb/s. Using this data rate causes cumulative truncation errors to occur as the bit period is 20.5761316...  $\mu\text{s}$ . Thus, for these simulations, a data rate of 50 kb/s was used, corresponding to a bit period of 20.0  $\mu\text{s}$ , thereby avoiding this cumulative truncation error.

The simulation sampling rate must also be considered. The BOSS manual recommends a sampling rate of at least eight to sixteen times the bit rate. Thus, the simulation step size,  $\Delta t$ , must be small enough to avoid undue aliasing. That is, the aliased power falling into the simulation bandwidth must be small compared to the noise power in the same bandwidth. If the parameter  $\Delta t$  is a power of two, the internal binary representation of  $\Delta t$  will be the same as the entered value. As well, the bit rate should be chosen to be an integer of  $\Delta t$  intervals. Therefore, for these simulations, the minimum sampling rate was chosen to be sixteen times the bit rate giving:

$$\Delta t = \frac{1}{50 \text{ kHz} (16)} = 1.25 \mu\text{s}$$

## **3.2.2 Phase Modulator**

### **3.2.2.1 $\pi/4$ DQPSK Modulation**

The  $\pi/4$  DQPSK modulation scheme is being considered by the Electronic Industries Association (EIA) for the digital cellular system in North America [3, 2]. In this phase modulation method, the digital information is contained in the relative phase difference between two symbols, where a symbol consists of two data bits. The phase can take one of eight different values, resulting in a signal constellation with eight points (see Figure 3.3 (c)). The constellation is constructed by superimposing two QPSK signal constellations each having four possible states, offset by  $45^\circ$  ( $\pi/4$  radians. See Figure 3.3). Each constellation is used alternately to transmit each symbol. Hence, successive symbols have a relative phase difference of  $\pm 45^\circ$  or  $\pm 135^\circ$ .

There are three major factors which have led to the selection of  $\pi/4$  DQPSK for the North American system [25, 33, 34]. These are:

- Effects of amplifier nonlinearity
- Receiver implementation
- Performance in a fast-fading environment.

The first factor results in spectral spreading. In general, the spectral spread increases with increased envelope variation. As can be seen from Figure 3.3 (a, b), the QPSK system has a maximum envelope fluctuation of 100% due to possible  $180^\circ$  phase shifts. However,  $\pi/4$  DQPSK has a maximum phase change of  $135^\circ$ , hence the variation in the signal envelope and the spectral spread are not as large as for QPSK. The second factor is the receiver implementation. The  $\pi/4$  DQPSK modulation can be detected using a coherent detector, a differential detector, or a discriminator. Coherent detection is more complex than either differential or discriminator detection due to the necessity of recovering the carrier. In a fast

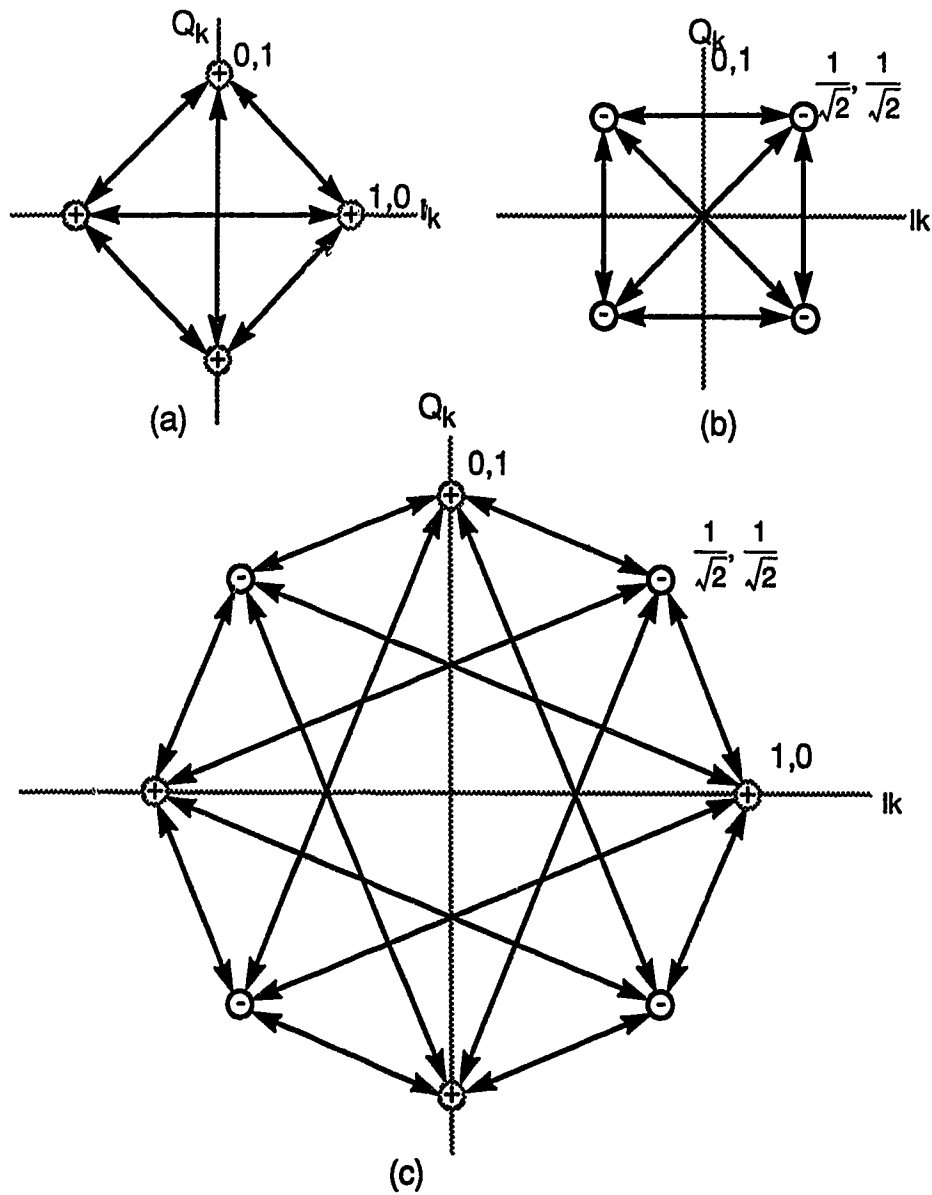


**Figure 3.3 Modulation Constellations: (a), (b) QPSK Constellation, (c)  $\pi/4$  DQPSK Constellation**

fading environment, coherent detection results in a higher irreducible BER than either differential detection or discriminator detection [25].

### 3.2.2.2 Simulation Model

The signal converter, shown schematically in Figure 3.4, generates the  $\pi/4$  DQPSK constellation. It converts the digital binary data into two separate



quadrature data streams and maps them onto the constellation. The resulting quadrature data streams are at 25 kHz.

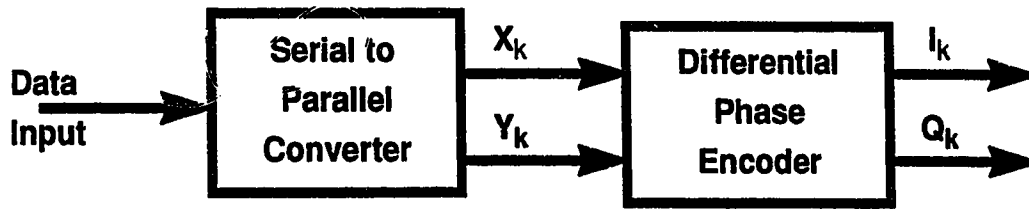


**Figure 3.4 Signal Converter**

This is done in two steps. First, the module performs a serial-to-parallel conversion on the incoming data stream. This produces 2 data streams,  $X_k$  and  $Y_k$ .  $X_k$  contains the odd-numbered bits and  $Y_k$  the even-numbered bits. Next,  $Y_k$  and  $X_k$  are mapped into  $I_k$  and  $Q_k$  according to the following expressions:

$$\begin{aligned} I_k &= I_{k-1} \cos\theta_k + Q_{k-1} \sin\theta_k \\ Q_k &= I_{k-1} \sin\theta_k - Q_{k-1} \cos\theta_k \end{aligned} \quad (3.1)$$

Where  $\theta_k$  is defined by Table 3.1.

**Table 3.1 Phase Mapping**

$X_k$	$Y_k$	$\theta_k$
1	1	$-\frac{3\pi}{4}$
0	1	$\frac{3\pi}{4}$
0	0	$\frac{\pi}{4}$
1	0	$-\frac{\pi}{4}$

The BOSS module calculates the phase changes based on the current values of  $X_k$  and  $Y_k$ . This phase change is added to the phase of the previous signal. This defines the phase of the current symbol and the amplitude of this signal is unity.

### 3.2.3 Pulse Shaping Filter

The purpose of the pulse shaping filter is to define the spectral shape of the transmitted signal [5]. The EIA IS-54 recommends a square-root raised cosine filter with a roll-off ( $\alpha$ ) of 0.35. The filter used in the cellular receiver has exactly the same response. The combination of the two filters forms a raised cosine (Nyquist) filter which has an impulse response going through zero at symbol period intervals. This ideally results in zero intersymbol interference. The roll-off factor  $\alpha$  determines the width of the transition band. The frequency response is given by [33]:

$$|H(f)| = \begin{cases} T & 0 < |f| < \frac{(1-\alpha)}{2T} \\ T \sqrt{\frac{1}{2} \left( 1 - \sin \left[ \frac{\pi T}{\alpha} \left( |f| - \frac{1}{2T} \right) \right] \right)} & \frac{1+\alpha}{2T} > |f| > \frac{(1-\alpha)}{2T} \\ 0 & |f| > \frac{1+\alpha}{2T} \end{cases} \quad (3.2)$$

where:

$T$  is the symbol period (twice as long as the bit period), and  
 $\alpha$  is the roll-off factor. For these simulations,  $\alpha = 0.35$ .

The frequency response is shown in Figure 3.5.

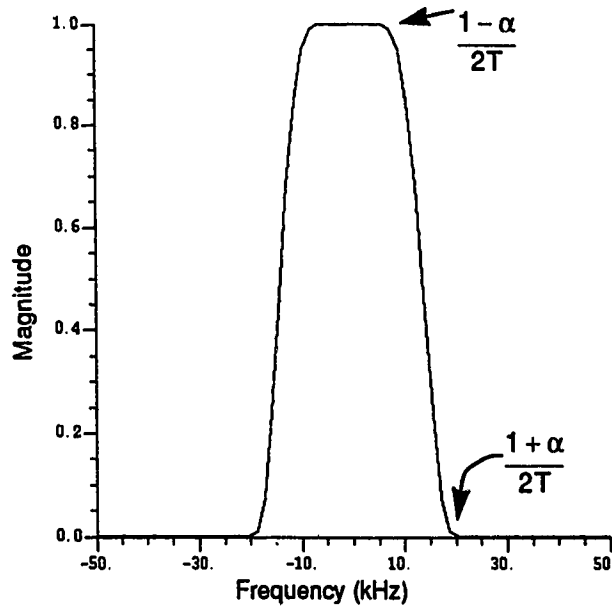


**Figure 3.5 Frequency Response of Square Root Raised Cosine Filter**

The filter is simulated by convolving the input waveform with the time domain impulse response of the filter. The time domain impulse response of the square-root raised cosine filter is defined by (3.3) [33] and is plotted in Figure 3.6. Pulse shaping is carried out independently in the I and Q channels.

$$h(t) = \begin{cases} 1 - \alpha + 4\frac{\alpha}{\pi} & t = 0 \\ \frac{\alpha}{\sqrt{2}} \left( \left(1 + \frac{2}{\pi}\right) \left(\sin \frac{\pi}{4\alpha}\right) + \left(1 - \frac{2}{\pi}\right) \cos \frac{\pi}{4\alpha} \right) & t = \pm \frac{T}{4\alpha} \\ \frac{\sin \left( \pi (1 - \alpha) \frac{t}{T} \right) + 4\alpha \frac{t}{T} \cos \left( \pi (1 - \alpha) \frac{t}{T} \right)}{\pi \frac{t}{T} \left( 1 - \left( 4\alpha \frac{t}{T} \right)^2 \right)} & t \neq 0, \pm \frac{T}{4\alpha} \end{cases} \quad (3.3)$$

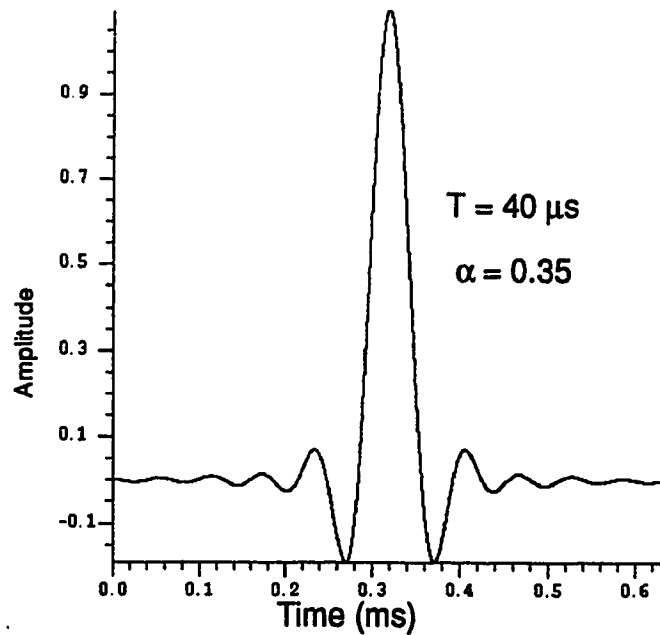


**Figure 3.6 Impulse Response of Square Root Raised Cosine Filter**

The constellation diagram of the signal after filtering is shown in Figure 3.7. The signal variation has increased over Figure 3.3 (c). The bandwidth and the amplitude variation are both dependent on the parameter  $\alpha$ . As  $\alpha$  decreases, the bandwidth of the signal decreases, but the amplitude variation increases [35].

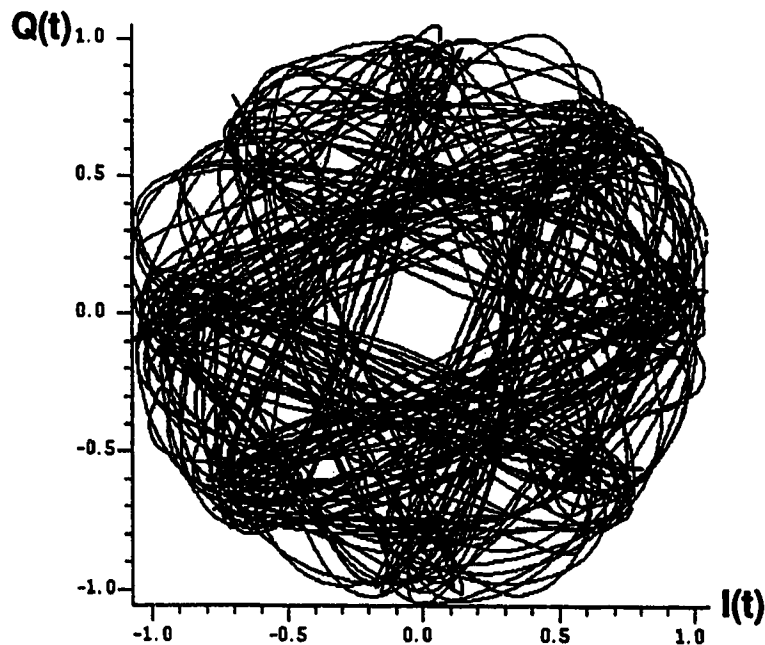


**Figure 3.7 Constellation of Square Root Raised Cosine Filter**

### 3.3 Nonlinear Power Amplifier

The nonlinear amplifier model in BOSS is implemented by two lookup tables that contain the AM-AM and AM-PM conversion factors. The normalized power of the input signal is used as a pointer to the AM-AM and the AM-PM tables. The data in the AM-AM table is normalized so that the maximum gain is unity (0 dB). The original signal is then multiplied by the AM-AM factor ( $a_1$ ) and the phase is shifted by the AM-PM factor ( $\phi$ ). An additional gain block (with gain  $a_2$ ) is included to increase the maximum gain to more than unity. This is shown in Figure 3.8.

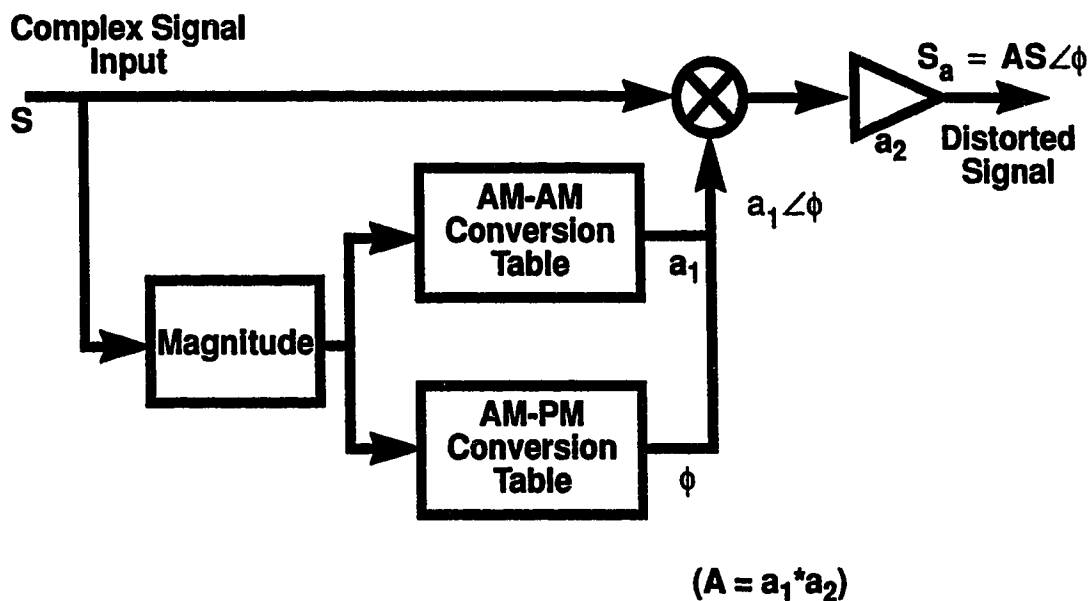


**Figure 3.8 Implementation of Nonlinear Amplifier in BOSS (AM-AM and AM-PM Conversion)**

The BOSS model for the nonlinear amplifier is in Figure 3.9.

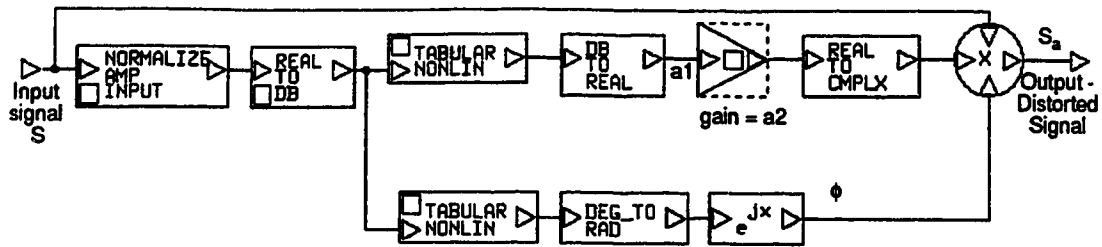


**Figure 3.9 BOSS Simulation Model: Nonlinear Amplifier**

The first amplifier modeled is an Avantek 6 Watt class AB amplifier specifically designed for the cellular frequency band. This amplifier was provided by NovaTel Communications Ltd. The data for the AM-AM and the AM-PM tables were obtained by measuring the output power and phase characteristics of the amplifier [36]. The output power and phase characteristics are shown in Figure 3.10 and the gain characteristic is shown in Figure 3.11.

The second amplifier modeled is an 8 Watt, single ended class B amplifier based on a BLV 93 transistor. Laboratory measurements of output power and phase were performed to obtain the AM-AM and AM-PM conversion parameters [37]. The AM-AM and AM-PM conversion tables for these two amplifier are listed in Appendix A. The output power/phase characteristics and the gain characteristic are shown in Figure 3.12 and Figure 3.13, respectively.

Comparing the characteristics of the two amplifiers, it is seen that the class B amplifier has greater gain expansion at low input levels and its gain compresses more quickly into saturation. Although the phase of the class B amplifier does not decrease at saturation, it has a greater variation ( $\sim 10^\circ$ ) than the class AB amplifier ( $\sim 4.5^\circ$ ).

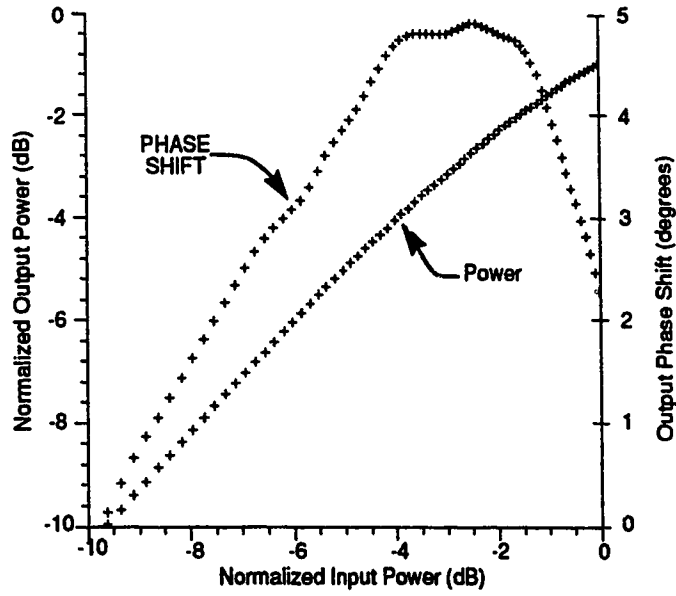


**Figure 3.10 Normalized Power and Phase Characteristics of Class AB Amplifier**

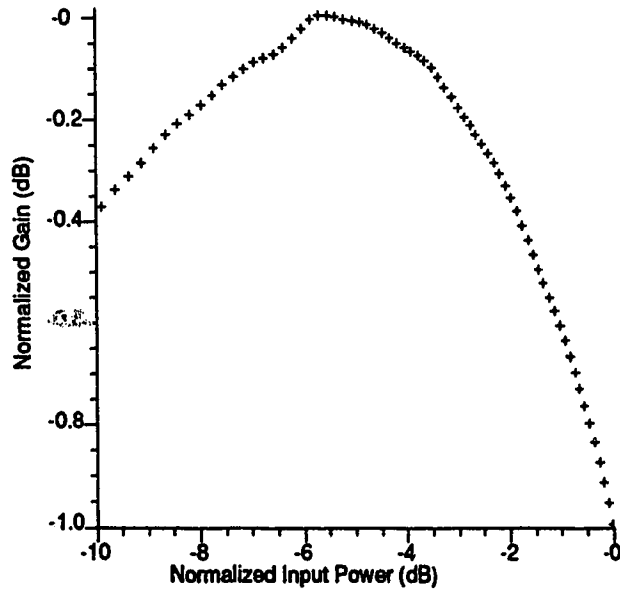


**Figure 3.11 Normalized Gain Characteristic of Class AB Amplifier**

NOTE: Gain is normalized so that the maximum gain is unity (0 dB).

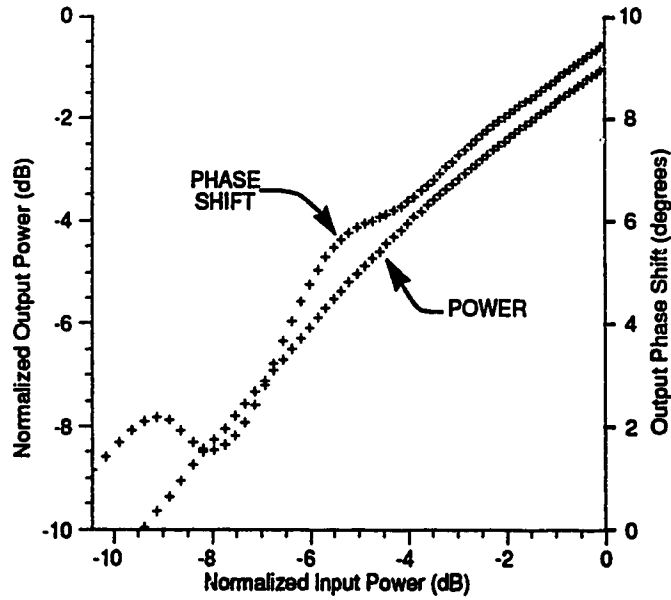


**Figure 3.12 Normalized Power and Phase Characteristics of Class B Amplifier**

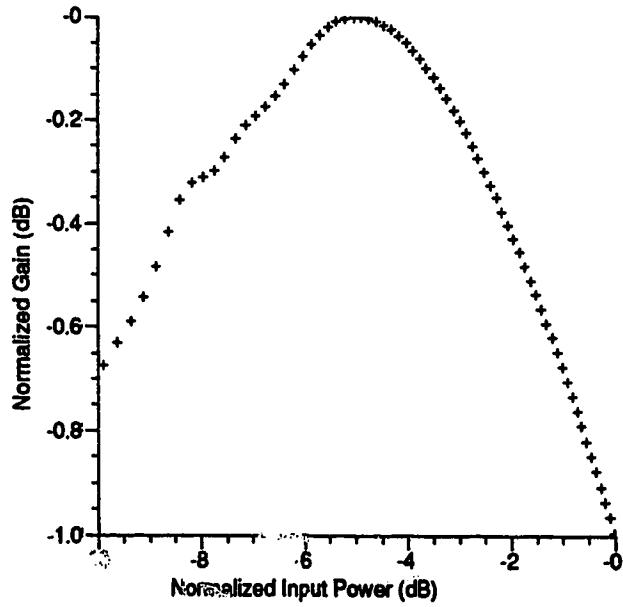


**Figure 3.13 Normalized Gain Characteristic of Class B Amplifier**

NOTE: Gain is normalized so that the maximum gain is unity (0 dB).



### 3.3.1 Complex Gain Predistorter

The complex gain predistorter distorts the input signal to the amplifier in a manner such that its output is an amplified replica of the original signal. The predistorter compares the output of the amplifier ( $v_a$ ) to the undistorted input signal ( $v_m$ ) and uses the difference ( $e_g$ ) to calculate the predistortion values ( $v_p$ ). The block diagram of the complex gain predistorter is shown in Figure 3.14.

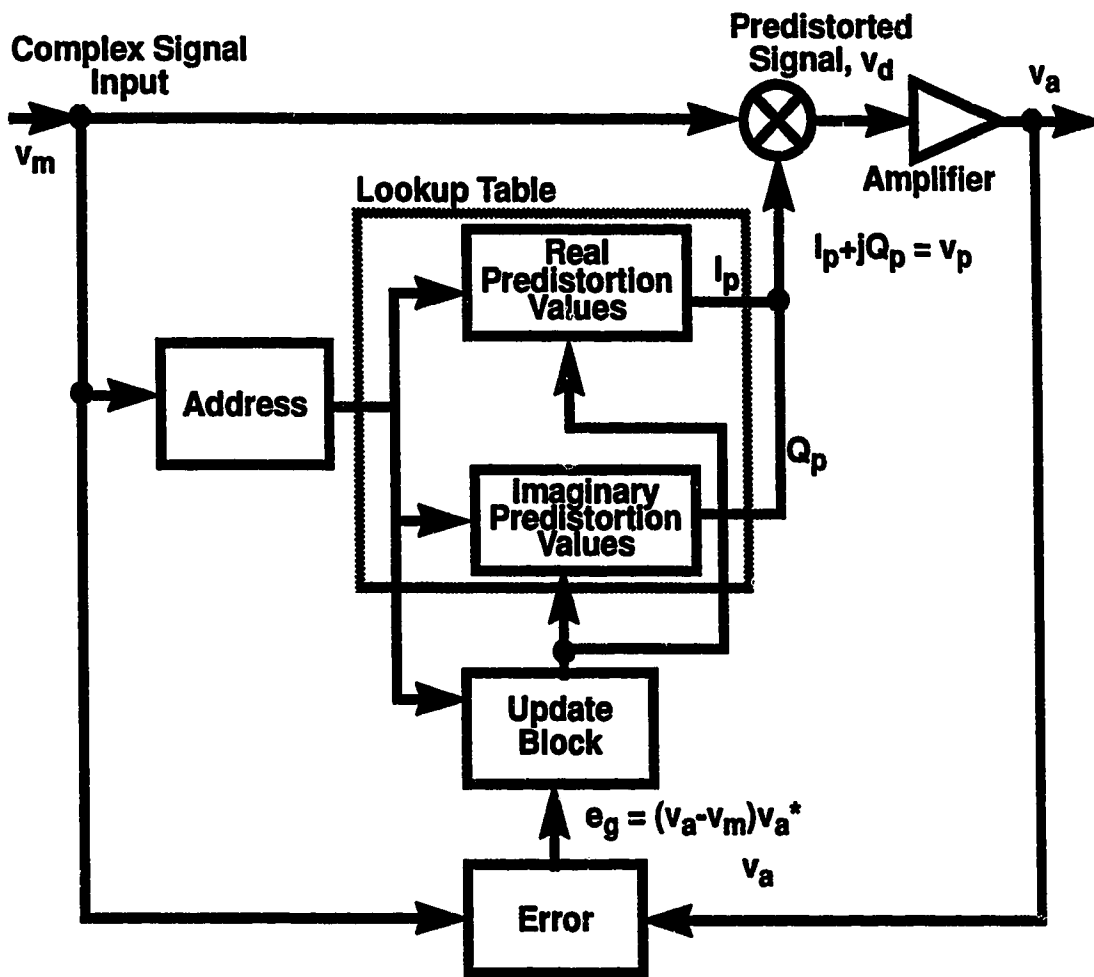


Figure 3 14 Block Diagram of Complex Gain Predistorter

Figure 3.15 shows the BOSS representation of the complex gain predistorter.

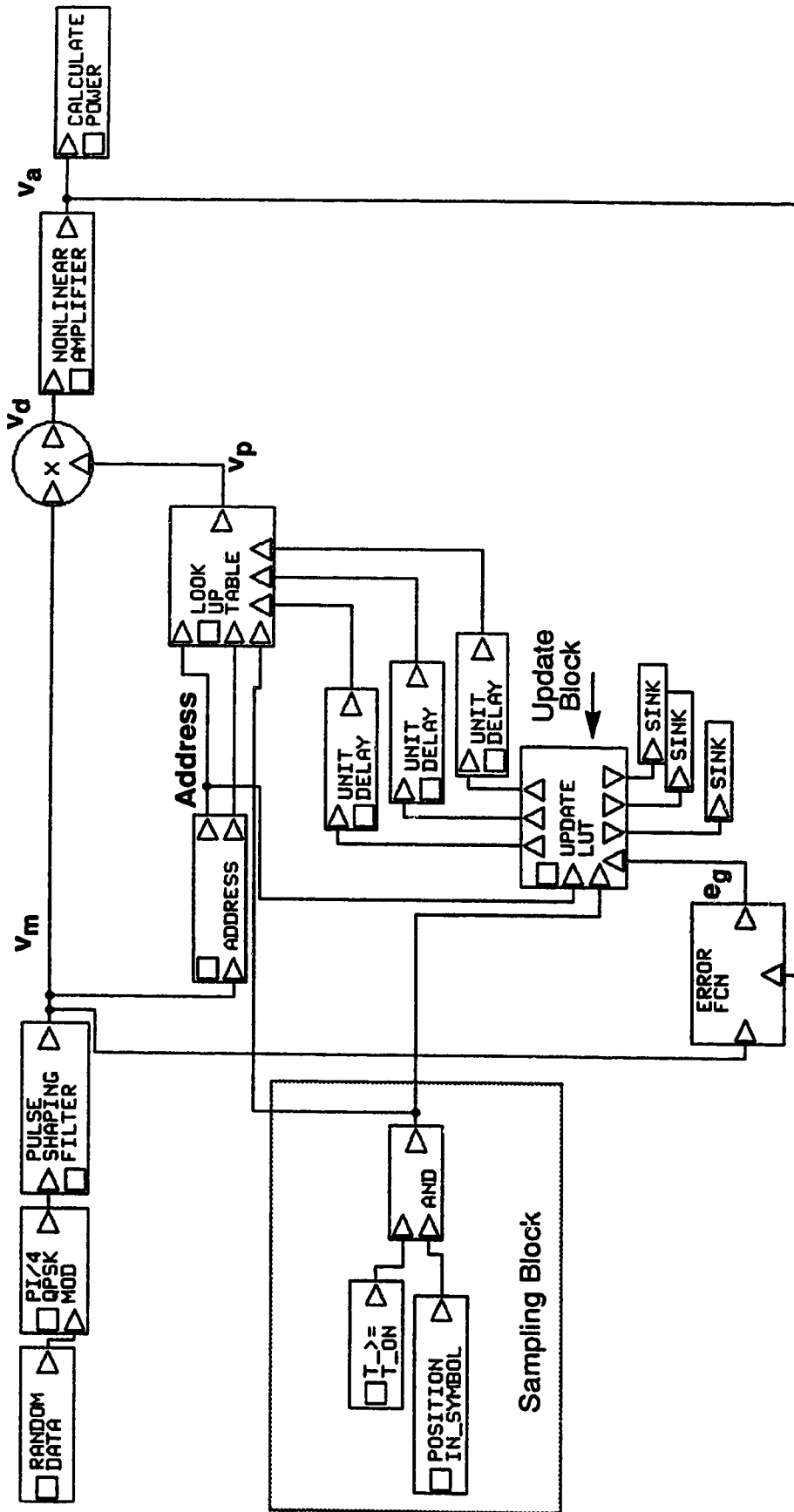


Figure 3.15 BOSS Simulation Model - Complex Gain Predistorter

The sampling block is used to generate a sampling signal at the update rate. The sampling or update rate is the number of times (per bit) that the predistortion table is accessed. The address block, look-up table, error block and the update block are discussed below.

### 3.3.2 Address Block and Lookup Table

The address block generates the index for the lookup tables. The index is an integer number between one and the table size. The address is calculated by the following relation:

$$\text{Address} = \text{INT} \left[ \left( \frac{|v_m|}{v_{m, \max}} \right)^2 (\text{tablesize} - 1) + 0.5 \right] + 1 \quad (3.4)$$

where:

the INT function takes the integer part of the real number  
and tablesize is the size of the lookup table.

The lookup table is a memory block that stores the predistortion values. The output of the lookup table is the predistortion value,  $v_p = I_p + jQ_p$ . These values are multiplied by the input signal to give the predistorted signal ( $v_d$ ). The predistortion values are calculated and updated by the update block.

### 3.3.3 Error and Update Blocks

The error block compares the undistorted signal and the amplified signal using the error relation:

$$e_g = (v_a - v_m) v_a^* \quad (3.5)$$

The error signal is normalized by multiplying it by the complex conjugate of the original signal ( $v_a^*$ ). If the error signal ( $e_g$ ) is too large, the update block

calculates new complex predistortion values,  $v_p$ , which are stored in the lookup tables. Figure 3.16 shows a block diagram of the update block. A listing of the FORTRAN subroutine that performs the update calculation is in Appendix B.

The update block also includes memory tables. The number of iterations is stored in the N-table. The  $v_p$ - and  $v_{p(n-1)}$ -tables store the current predistortion value and the previous predistortion value, respectively. The  $e_{g(n-1)}$ -table stores the error associated with the  $v_{p(n-1)}$  value.

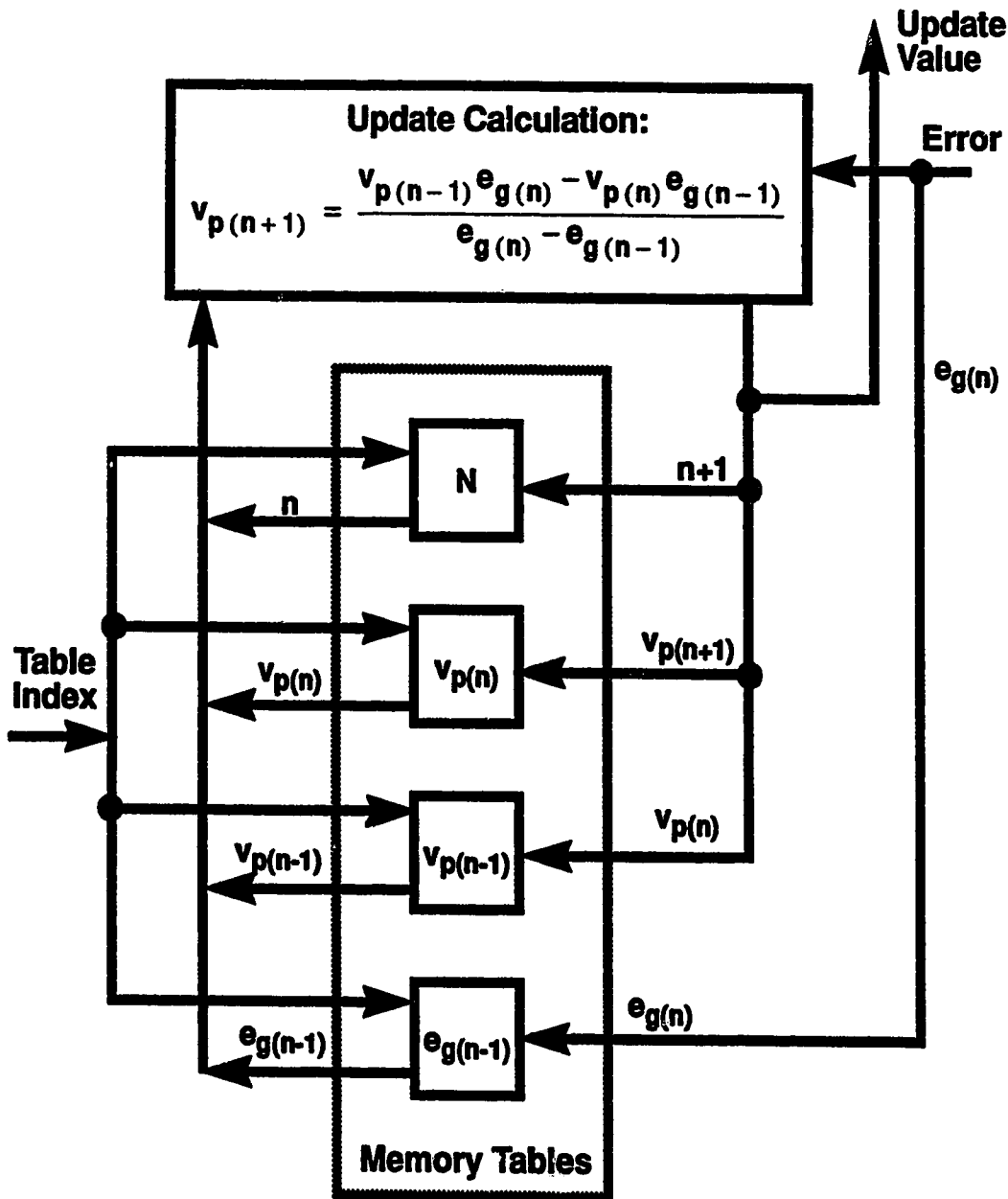


Figure 3.16 Update Block

### 3.4 Cartesian Coordinate Negative Feedback

This system uses negative feedback to predistort the amplifier input signal. A block diagram of this system is shown in Figure 3.17. The output of the nonlinear power amplifier is used as a feedback signal  $v_a$ . The feedback signal is amplified by the feedback amplifier, which has a gain of  $\beta$  ( $\beta < 1$ ) giving  $v_f$ . This signal is then subtracted from the input signal to generate a loop error signal ( $v_e$ ). The loop error signal is filtered, giving  $v_d$ , which is the input of the nonlinear power amplifier. If the loop gain is sufficiently high, the feedback loop will correct for the nonlinearity of the amplifier.

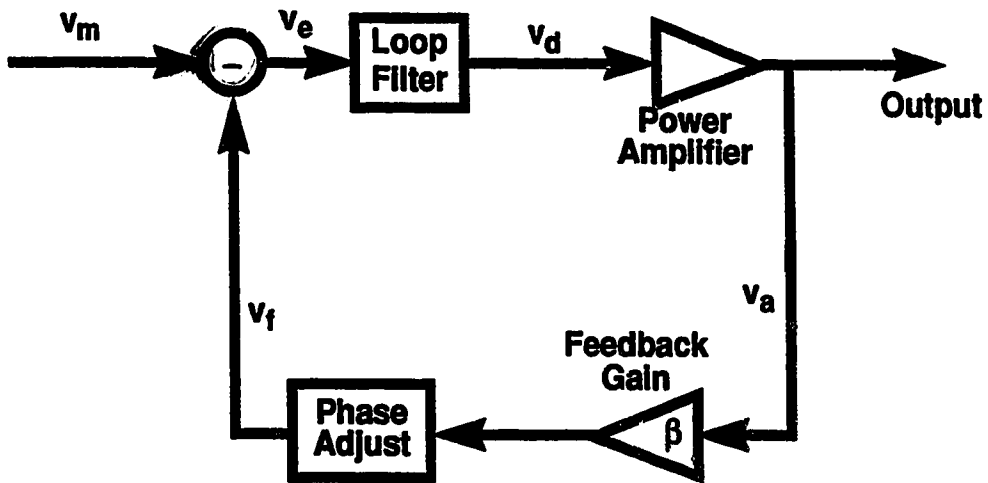


Figure 3.17 Block Diagram of Cartesian Coordinate Negative Feedback System

The BOSS system diagram is shown in Figure 3.18.

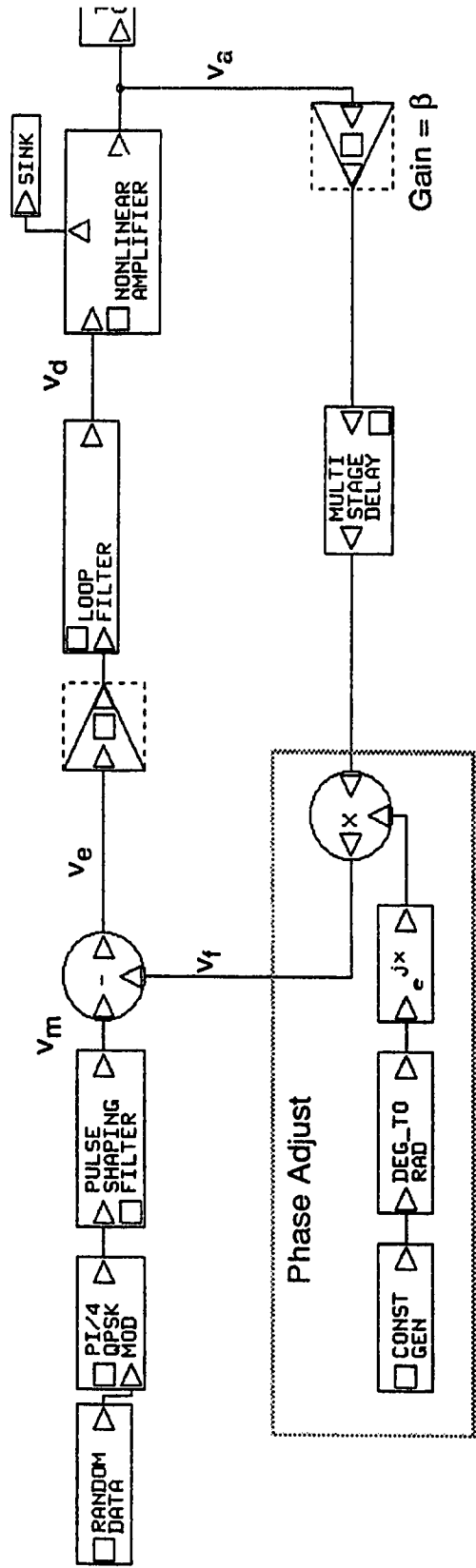


Figure 3.18 BOSS Simulation Model - Cartesian Coordinate Negative Feedback System

narrowband response in order to increase the stability of the system. A single pole Butterworth filter is used. This is approximated in BOSS as a lowpass infinite impulse response (IIR) filter. The 3 dB cutoff frequency is at 75 kHz.

The phase adjustment is critical to the system. The transmitter configuration is highly dependent on the correct setting of the phase adjuster. The RF amplifiers create significant phase shifts, which have to be corrected [16]. Incorrect phase adjustments lead to oscillations within the loop. Reduction in the open-loop gain leads to a less critical phase adjustment. The phase adjustment is achieved by delaying the local oscillator signal to the detector. In the simulation model, this was achieved by adjusting the phase of the complex envelope signal. The required phase adjustment must be recalibrated for each frequency channel and output power level.

### **3.5 Modulator and Demodulator Errors**

Although the simulation models involve complex envelope representation, both the complex gain predistorter and the Cartesian coordinate negative feedback system require modulators to shift the frequency to 850 MHz. A block diagram of the quadrature modulator shown in Figure 3.19.

The demodulators are necessary because the output of the amplifier is demodulated and used for feedback. A block diagram of the quadrature demodulator shown in Figure 3.20.

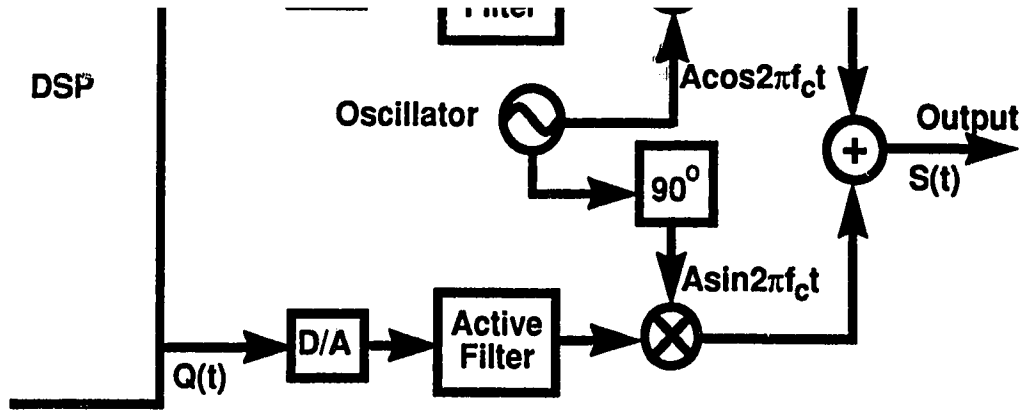


Figure 3.19 Quadrature Modulator

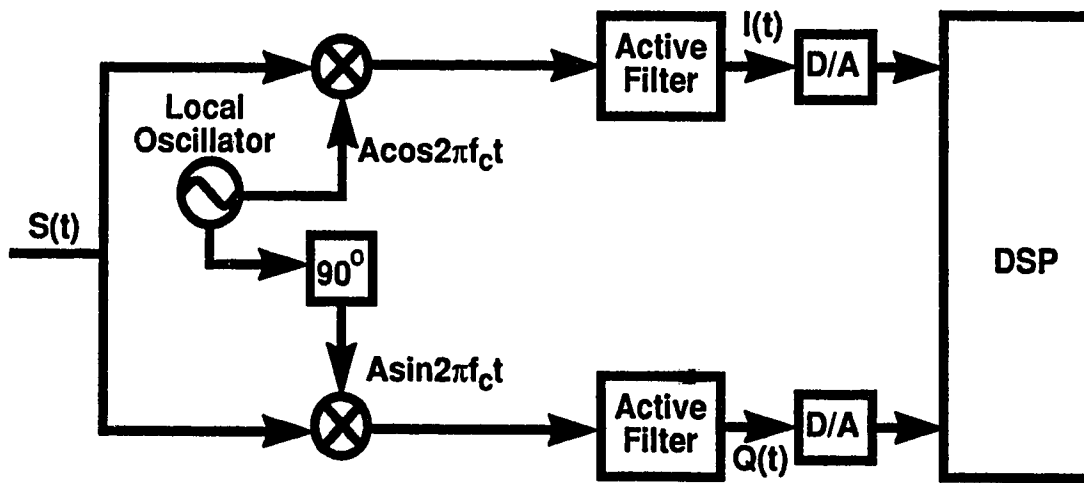


Figure 3.20 Quadrature Demodulator

Quadrature modulators use analog mixers, combiners, ninety degree phase splitters, and active filters. These produce various types of distortion including carrier leakage, differential gain, and differential phase shift [38, 39, 40]. A block diagram of a modulator and a demodulator with this distortion is shown in Figure 3.21. The modulator distortion is explained below:

- Carrier leakage in the mixers cause self mixing of the local oscillator references, resulting in dc offset. The DAC and active filter also add dc offset. This is modeled as a dc offset of  $b_1$  and  $b_2$ .



components caused by the DAC and active filter and the mixers. The gain imbalance is modeled by gain amplifiers with gain  $a_1$  and  $a_2$ .

- The phase splitter at the local oscillator does not produce an exact  $90^\circ$  phase shift. This is modeled as separate phase shifts of  $\phi_1$  and  $\phi_2$ .

The demodulator provides similar distortion. The phase shifter at the local oscillator does not produce an exact  $90^\circ$  phase shift. The DAC and active filters add dc offset and gain differences between the I and Q signals. The mixers are not perfectly balanced, resulting in gain differences. The leakage in the mixers causes self mixing of the local oscillator references causing dc offset. The coupling of the power amplifier output into the feedback path also adds a phase shift ( $\theta$ ). The demodulator dc offset is modeled as  $b_3$  and  $b_4$ . The gain imbalance is denoted as  $a_3$  and  $a_4$  and the phase imbalance is  $\phi_3$  and  $\phi_4$ .

### 3.5.1 Complex Envelope Modulator and Demodulator Distortion

As discussed earlier, simulation at the carrier frequency of 850 MHz take a very long time to execute. Therefore, the simulations are carried out at baseband, with an equivalent distortion added to the system. In this sub-section, the equivalent baseband distortion for the modulator and demodulator are derived.

From Figure 3.21, the input signals to the modulator are  $I(t)$  and  $Q(t)$  so, after including the dc offset and gain imbalance, the input signals to the multiplier are:  $a_1I(t) + b_1$  and  $a_2Q(t) + b_2$ .

The signals at the output of the modulator are:

$$S(t) = [a_1I(t) + b_1] \cos(2\pi f_c t + \phi_1) + [a_2Q(t) + b_2] \sin(2\pi f_c t + \phi_2) \quad (3.6)$$

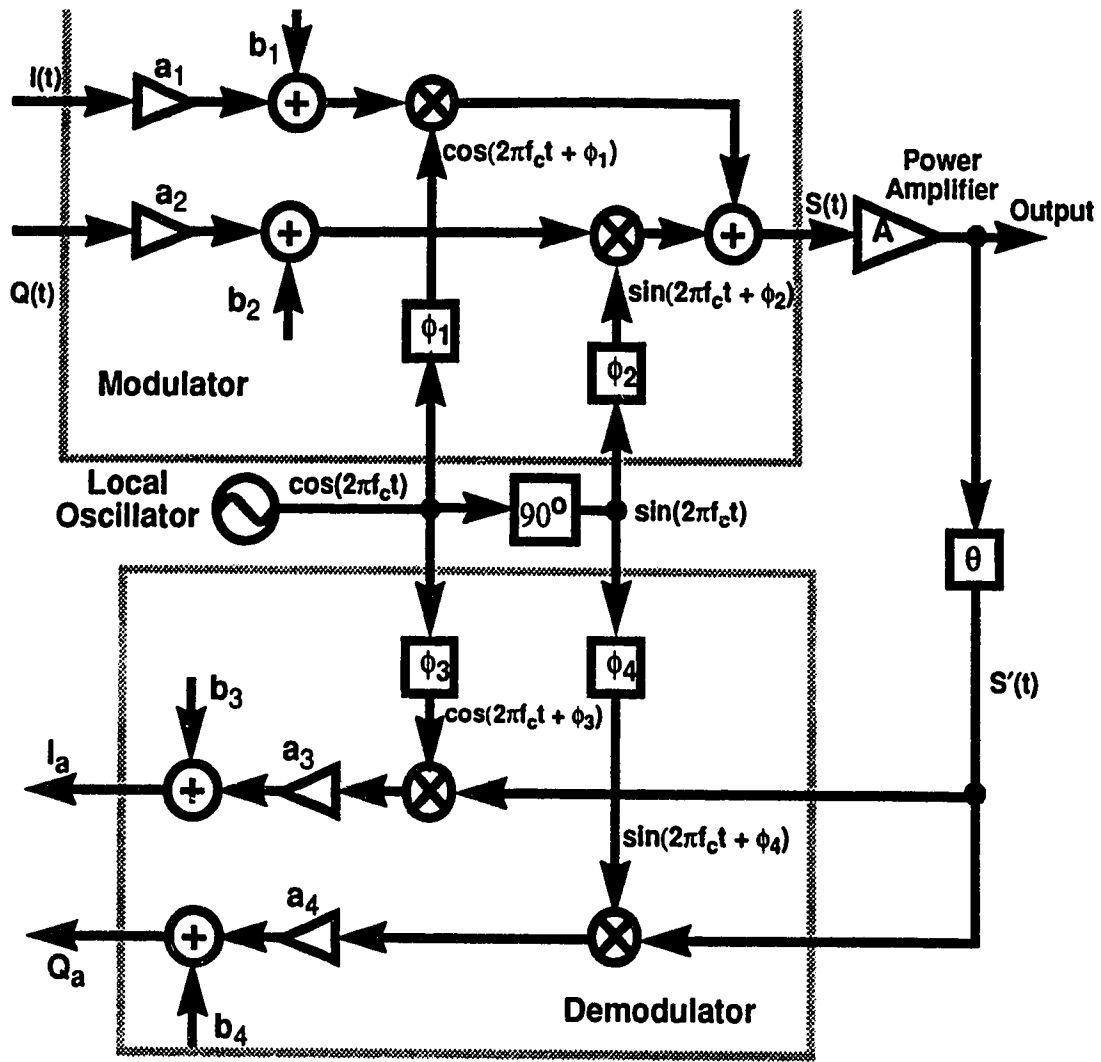


Figure 3.21 Modulator/Demodulator with Errors.

Equation (3.6) can be rewritten as:

$$S(t) = (a_1 I(t) + b_1) [\cos(2\pi f_c t) \cos(\phi_1) - \sin(2\pi f_c t) \sin(\phi_1)] + (a_2 Q(t) + b_2) [\sin(2\pi f_c t) \cos(\phi_2) + \cos(2\pi f_c t) \sin(\phi_2)] \quad (3.7)$$

$$S(t) = \{ [a_1 I(t) + b_1] \cos(\phi_1) + [a_2 Q(t) + b_2] \sin(\phi_2) \} \cos(2\pi f_c t) + \{ [a_1 I(t) + b_1] \sin(-\phi_1) + [a_2 Q(t) + b_2] \cos(\phi_2) \} \sin(2\pi f_c t) \quad (3.8)$$

This reduces to:

$$S(t) = I'(t) \cos(2\pi f_c t) + Q'(t) \sin(2\pi f_c t) \quad (3.9)$$

where:

$$\begin{aligned} I'(t) &= [a_1 I(t) + b_1] \cos(\phi_1) + [a_2 Q(t) + b_2] \sin(\phi_2) \\ Q'(t) &= [a_1 I(t) + b_1] \sin(-\phi_1) + [a_2 Q(t) + b_2] \cos(\phi_2) \end{aligned} \quad (3.10)$$

Assuming that the power amplifier does not distort  $S(t)$ , the signal at the input to the demodulator is then:

$$S'(t) = I''(t) \cos(2\pi f_c t + \theta) + Q''(t) \sin(2\pi f_c t + \theta) \quad (3.11)$$

where:

$$I''(t) = AI'(t)$$

$$Q''(t) = AQ'(t)$$

The demodulator multiplies (3.11) by  $\cos(2\pi f_c t + \phi_3)$  and  $\sin(2\pi f_c t + \phi_4)$ . The expressions for the two signals are given below:

In-phase (I) signal

$$\begin{aligned} &\frac{I''(t)}{2} \{ \cos(4\pi f_c t + \theta + \phi_3) + \cos(\theta - \phi_3) \} + \\ &\frac{Q''(t)}{2} \{ \sin(4\pi f_c t + \theta + \phi_3) + \sin(\theta - \phi_3) \} \end{aligned} \quad (3.12)$$

$$\begin{aligned} & \frac{I''(t)}{2} \{ \sin(4\pi f_c t + \theta + \phi_4) - \sin(\theta + \phi_4) \} + \\ & \frac{Q''(t)}{2} \{ \cos(\theta - \phi_4) - \cos(4\pi f_c t + \theta + \phi_4) \} \end{aligned} \quad (3.13)$$

These signals are passed through a lowpass filter to eliminate the high frequency ( $4\pi f_c t$ ) components. Including the dc offset and the gain imbalance, the output of the demodulator is given by (3.14) and (3.15).

$$I_a = a_3 \left( \frac{I''(t)}{2} \cos(\theta + \phi_3) + \frac{Q''(t)}{2} \sin(\theta - \phi_3) \right) + b_3 \quad (3.14)$$

$$Q_a = a_4 \left( \frac{I''(t)}{2} (-\sin(\theta + \phi_4)) + \frac{Q''(t)}{2} \cos(\theta + \phi_4) \right) + b_4 \quad (3.15)$$

As these signals are not dependent on  $f_c$ , but only on the original data signal and the added distortion, the modulation and demodulation distortion can be represented by a baseband model. This is shown in Figure 3.22. Figure 3.23 shows the corresponding BOSS representation of the modulation and demodulation distortion. The distortion generated by these BOSS models compares favorably to results obtained in [36].

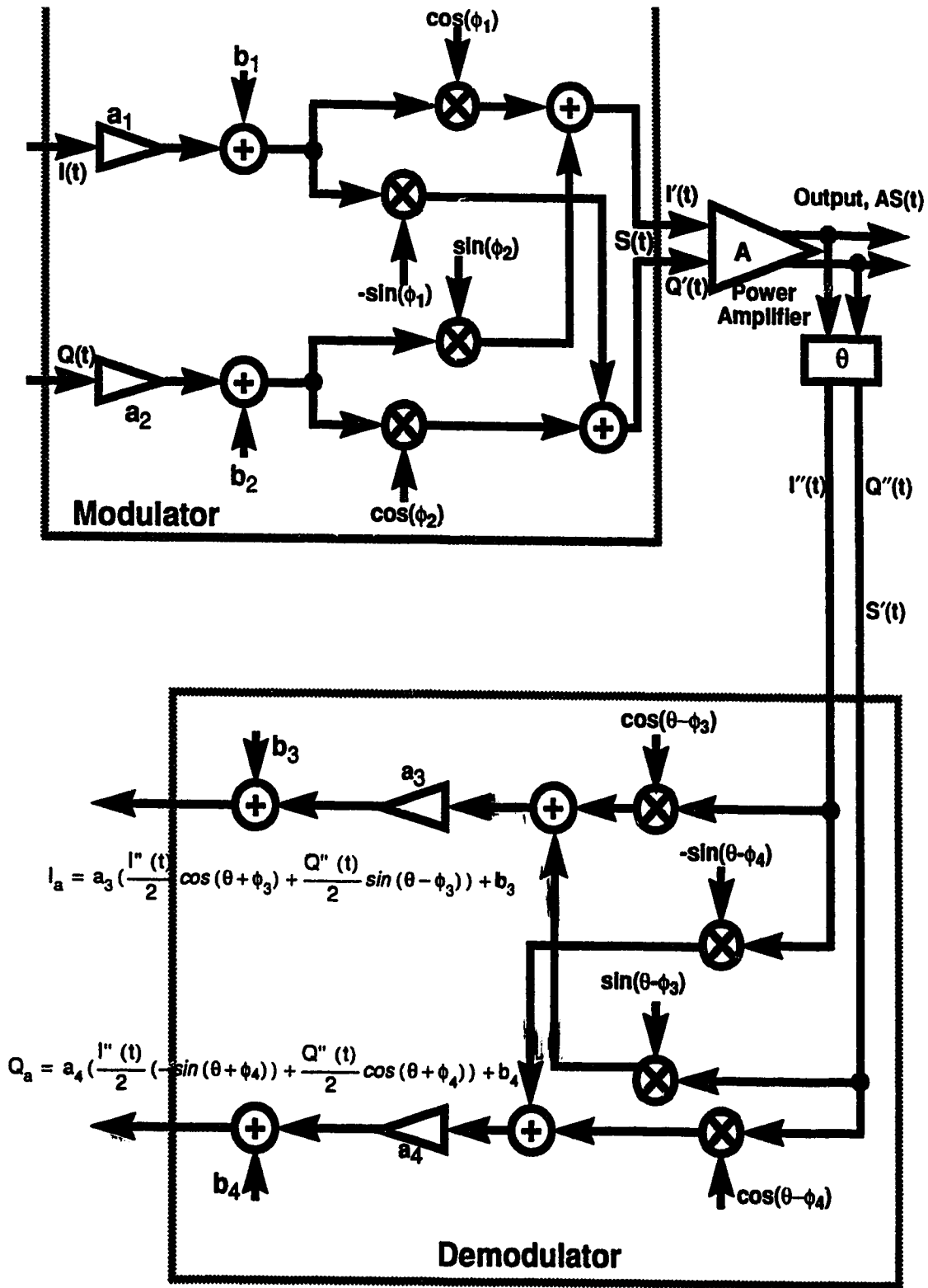


**Figure 3.22 Baseband Representation of Modulator/Demodulator with Errors**

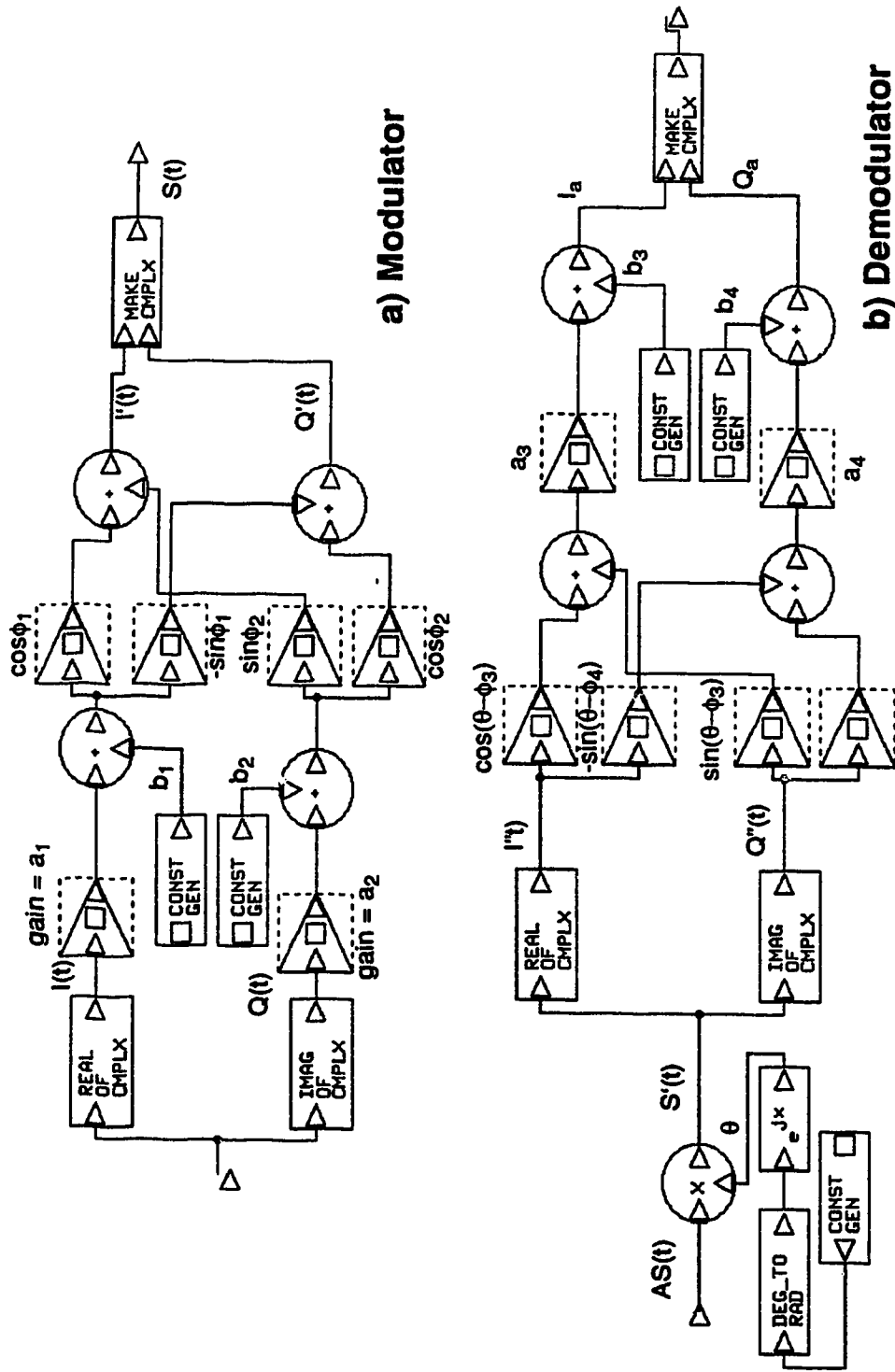


Figure 3.23 BOSS Simulation Model:  
 a) Modulator b) Demodulator

Simulation models to obtain the out-of-band power were also developed. An estimate of the power spectral density (PSD) can be made from the amplitude-squared of the discrete Fourier transform of some finite, sampled set of the data [41]. This estimate is called a periodogram. Although the periodogram method of estimating the PSD has poor variance [41 - 44], the use of the efficient fast Fourier transform (FFT) algorithm to find the discrete Fourier transform (DFT) provides a straight forward and convenient method of estimating the power spectral density. The PSD of a signal  $c(t)$  is estimated by sampling the signal at  $M$  points to produce the values  $c_0 \dots c_{M-1}$ ; these points span a range of time  $T$ , where  $T = (M-1)\Delta$ , and  $\Delta$  is the sampling interval.

The total power of the signal  $c(t)$ , is given by its mean squared amplitude:

$$\frac{1}{T} \int_0^T |c(t)|^2 dt \approx \frac{1}{M} \sum_{j=0}^{M-1} |c_j|^2 \quad (3.16)$$

The FFT algorithm is used to calculate the DFT of  $c(t)$ , where the DFT is given by:

$$C_k = \sum_{j=0}^{M-1} c_j e^{\frac{2\pi ijk}{M}} \quad k = 0, \dots, (M-1) \quad (3.17)$$

The periodogram estimate of the power spectrum at  $M/2+1$  discrete frequencies is:

$$\begin{aligned}
 P(0) &= P(f_0) = \frac{1}{M^2} |C_0|^2 \\
 P(f_k) &= \frac{1}{M^2} [|C_k|^2 + |C_{M-k}|^2] \quad k = 1, 2, \dots, \left(\frac{M}{2} - 1\right) \\
 P(f_c) &= P(f_{M/2}) = \frac{1}{M^2} |C_{M/2}|^2
 \end{aligned} \tag{3.18}$$

where  $f_k$  is defined only for zero and positive frequencies:

$$f_k \equiv \frac{k}{M\Delta} = 2f_c \frac{k}{M} \quad k = 0, \dots, \frac{M}{2} \tag{3.19}$$

and  $f_c$  is the Nyquist frequency.

There are two problems with the use of a periodogram to estimate the PSD. As mentioned above, the periodogram has a high variance. In fact, the variance of each  $P(f_k)$  is  $P^2(f_k)$  for all  $T$  and for all  $f_k$  [41, 42]. Although the periodogram is a good estimate over the whole frequency range, for each individual frequency the estimate is not very accurate. Unfortunately, the variance does not decrease if more data points are used (larger  $M$ ). If a longer run of data is sampled, with the same sampling rate, the Nyquist frequency ( $f_c$ ) is unchanged, but there is a finer frequency resolution (more  $f_k$ 's) within the Nyquist frequency interval. If the same length of data is sampled with a finer sampling interval (smaller  $\Delta$ ), then the frequency resolution is unchanged, but the Nyquist range extends up to a higher frequency. In neither case do the additional samples reduce the variance of any one particular frequency's estimated PSD.

To reduce the variance, several runs are averaged together [41, 42, 43]. This may be done in two different ways. In the first method, the sampled data is partitioned into  $K$  segments. The FFT is calculated for each segment and this is



used to produce a periodogram estimate. Then, the K periodogram estimates are averaged together at each frequency. This reduces the variance of the estimate by a factor of K [41, 42] (the standard deviation is reduced by a factor of  $\sqrt{K}$ ). Alternatively, the K data segments are overlapped by one half of their length. For this case, since the segments are not statistically independent, the variance is now reduced by a factor of 9K/11 [43]. This method requires fewer points to reduce the variance. For example, if there are N\*K samples, the first method reduces the variance by a factor of K whereas the second method reduces the variance by a factor of  $\frac{(2K-1)9}{11}$ .

The second problem with using the DFT to estimate the PSD is leakage [41, 42]. The signal  $s(t)$  is time-limited to a finite interval  $0 < t < T$ ; in effect, the infinite-time data was multiplied by a data window of unity magnitude and width of T. This results in the convolution of the actual DFT with the data window. This windowing results in significant leakage from one discrete frequency to another in the periodogram estimate. This leakage can be reduced by using a function to window the data. There are many different window types that can be used. They all involve compromises between the width of the main lobe and the attenuation of lower sidelobes. The choice of a data window type depends on the application. Since this application requires measurement of the out-of-band power, which is small compared to the in-band power, a window with low sidelobes is appropriate. The window used in this application is called the Blackman window (see Figure 3.24).

The Blackman window function is defined by [42, 44]:

$$w(t) = 0.42 + 0.5 \cos \frac{2\pi t}{T} + 0.08 \cos \frac{4\pi t}{T} \quad \text{for} \quad |t| \leq \frac{T}{2} \quad (3.20)$$

The Fourier transform of the Blackman window is [42, 44]:

$$W(f) = \frac{\sin \pi f T}{\pi f T} \left[ 0.42 + \frac{0.5 (fT)^2}{1 - (fT)^2} - \frac{0.08 (fT)^2}{4 - (fT)^2} \right] \quad (3.21)$$

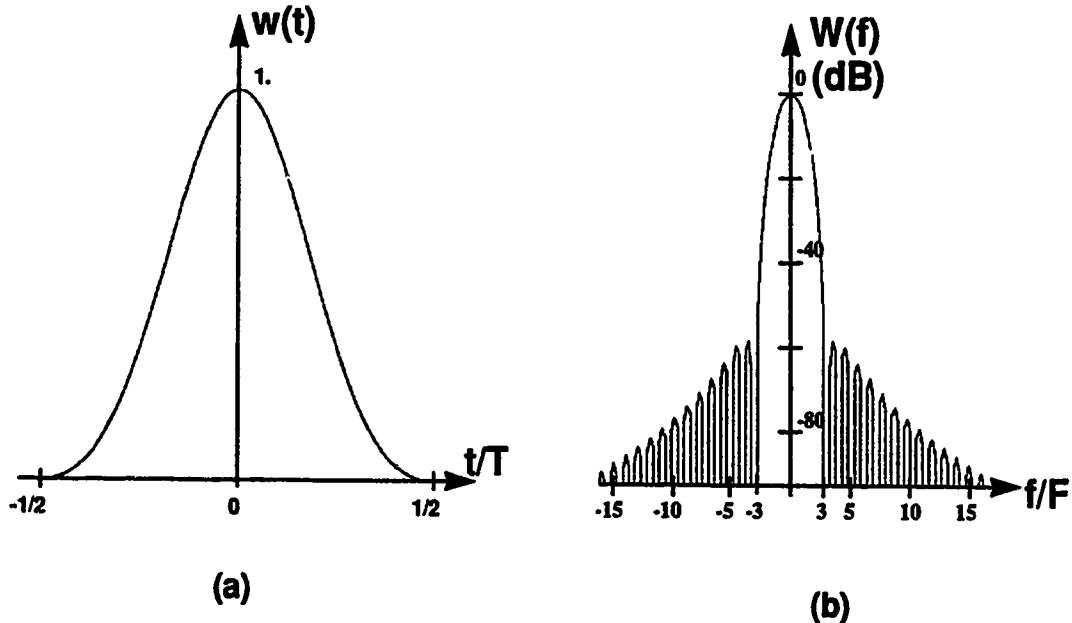


**Figure 3.24 Blackman Window: a) Time Domain Response  
b) Amplitude Response**

A block diagram of the power measurement model is shown in Figure 3.25.

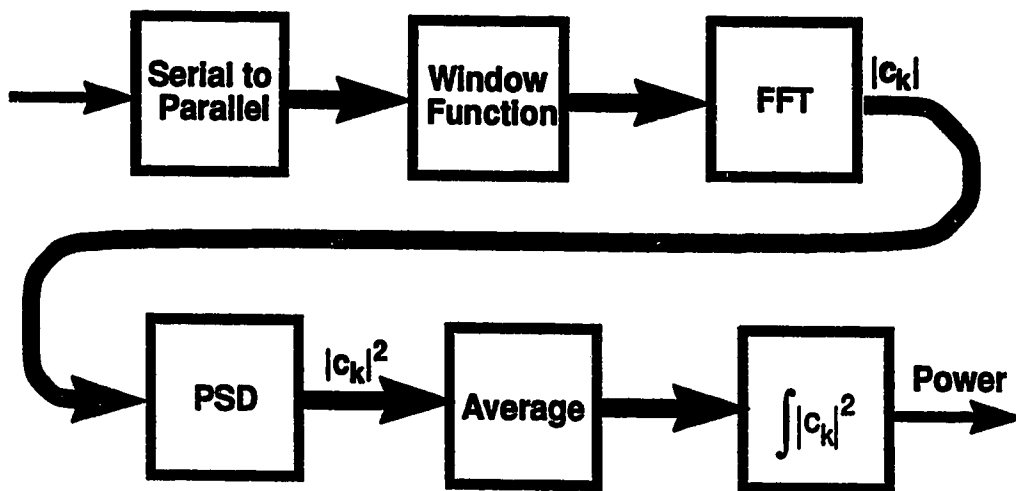


**Figure 3.25 Block Diagram of Power Measurement**

The PSD is estimated by first collecting  $M$  points of sampled data, where  $M$  is a power of two. The serial-to-parallel block in Figure 3.25 performs this function: it collects the  $M$  samples and passes a parallel data stream containing the  $M$  samples to the next block. The windowing function is applied to the collected samples and the FFT is used to find the DFT of the data. The PSD is estimated as the squared amplitude of the DFT. This model averages together several PSDs in order to reduce the variance. The data segments in the PSDs are overlapped by one-half their length in order to reduce the computing time. Thus, the standard deviation of the PSD is given by:

$$\sigma = \frac{100 \%}{\sqrt{\frac{9(K)}{11}}} \quad (3.22)$$

This estimate of the PSD provides the power spectral density across the whole frequency band, for  $0 < f < f_c$  (Nyquist critical frequency). In order to find the power in each channel,  $P(f_{\text{chan}})$ , the averaged, estimated PSD is integrated over the frequency range of each channel:

$$P(f_{\text{chan}}) = \frac{\frac{1}{2} \cdot \int_{f_1}^{f_2} P(f) df}{\int_0^{f_c} P(f) df} = \frac{\frac{1}{2} \sum_{f_k=f_1}^{f_2} P(f_k)}{\sum_{f_k=0}^{f_c} P(f_k)}, \quad (3.23)$$

where the channel is defined to be the frequency range  $f_1 < f < f_2$ . The factor of  $1/2$  in the numerator is due to the PSD being one-sided; it is only defined for  $0 < f < f_c$ . The allowed power in each channel is limited by IS-54 and this is discussed in Section 2.2 and shown in Figure 2.4.

subroutines that perform these functions are in Appendix C.

For the simulations, the BOSS model was configured to use  $2^{13}$  (8192) samples in each PSD calculation. With a sampling rate of  $1.25 \mu\text{s}$ , and a symbol rate of 25 kHz, this corresponds to 256 symbols. As well, the BOSS model was configured to average together 100 PSD calculations. The data sets used for each PSD calculation overlap by 50%, which corresponds to 13,056 symbols. From (3.22), the standard deviation is then:

$$\frac{100 \%}{\sqrt{\frac{9(100)}{11}}} = 11 \% \quad (3.24)$$

### 3.7 Summary

In this chapter, the basic simulation models for the  $\pi/4$  DQPSK transmitter, the power amplifier, the complex gain predistorter, and the Cartesian coordinate negative feedback linearizer were developed and discussed. The complex envelope equivalent model for the quadrature modulator and demodulator were developed. The techniques used to calculate the out-of-band power were presented. The next chapter describes the simulations carried out, and discusses the results.

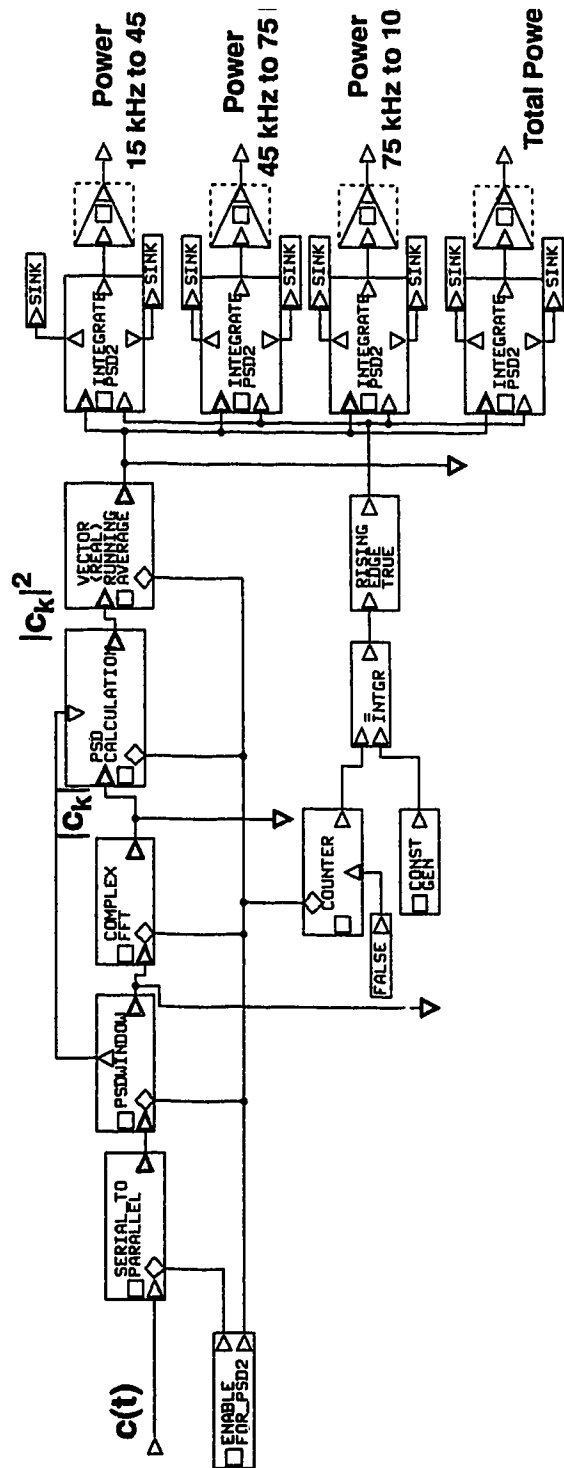


Figure 3.26 Boss Simulation Model: Out-of-Band Power Measurement

This chapter presents the results obtained from simulations of the models described in Chapter 3. The simulations are used to measure the performance of the gain predistortion method and of the Cartesian feedback system. First, an outline of the simulations is given and then the results obtained from these simulations are presented and discussed.

#### **4.1 Simulation Outline**

The first set of simulations was done in order to analyze the effects of the nonlinear amplifier on the transmitter. These results are presented in Section 4.2. The next set of simulations was carried out with the complex gain predistortion system. These simulations examined the effect of varying some of the parameters of this system. These parameters include the sampling rate, the table size, and the input power to the amplifier. As well, two different amplifiers were tested in the system. These results are presented in Section 4.3. The simulation results for the Cartesian feedback system are given in Section 4.4. These results include the effect of varying the loop gain and the input power to the amplifier. Two different amplifiers were also used in this system. Section 4.5 provides a comparison of the two predistortion methods. The inclusion of representative modulation and demodulation distortion, and the effect of this distortion on the effectiveness of the two predistortion methods are considered in Section 4.6. Section 4.7 presents a summary of the results.

#### **4.2 RF Power Amplifier Characteristics**

The power amplifiers are characterized by AM-AM and AM-PM conversion. This causes the spectrum of the input signal to widen. Two different amplifiers are

distortion on the transmitted signal.

#### 4.2.1 Class AB Amplifier

The first amplifier considered is a Class AB amplifier. The AM-AM and AM-PM characteristics of this amplifier are discussed in Chapter 3.3. Figure 4.1 shows the output PSD of the amplifier with a  $\pi/4$  DQPSK input signal at different power levels (backing-off), as well the spectrum for the input signal (or, the output spectrum for a linear amplifier). Backing-off is used for two different purposes:

- a) it is the simplest method of linearization
- b) the cellular RF amplifier is required to operate at various power levels for interference control in surrounding cells.

For these simulations, the back-off levels used are: 70% (-1.55 dB), 80% (-0.97 dB), 90% (-0.45 dB) and 100% (no back-off) of the maximum (peak) input power level. The maximum input power level is specified such that the maximum peak input level of the  $\pi/4$  DQPSK signal corresponds to the 1 dB compression point of the amplifier gain characteristic (saturation). The out-of-band power is given in Table 4.1, and using a two-tone input, Figure 4.2 shows the variation of the  $IM_3$  and  $IM_5$  products with the amplifier power level.

Table 4.1 indicates that there does not appear to be a significant difference in the out-of-band power in adjacent channel 1 between the various cases. However, Figure 4.1 reveals a significant difference in the spectra. The power in the 15 - 20 kHz range is seen to dominate the characteristic and the power in the 20 - 45 kHz range is small compared to this. Hence, it is necessary to consider both the measured out-of-band power and the PSD characteristics.

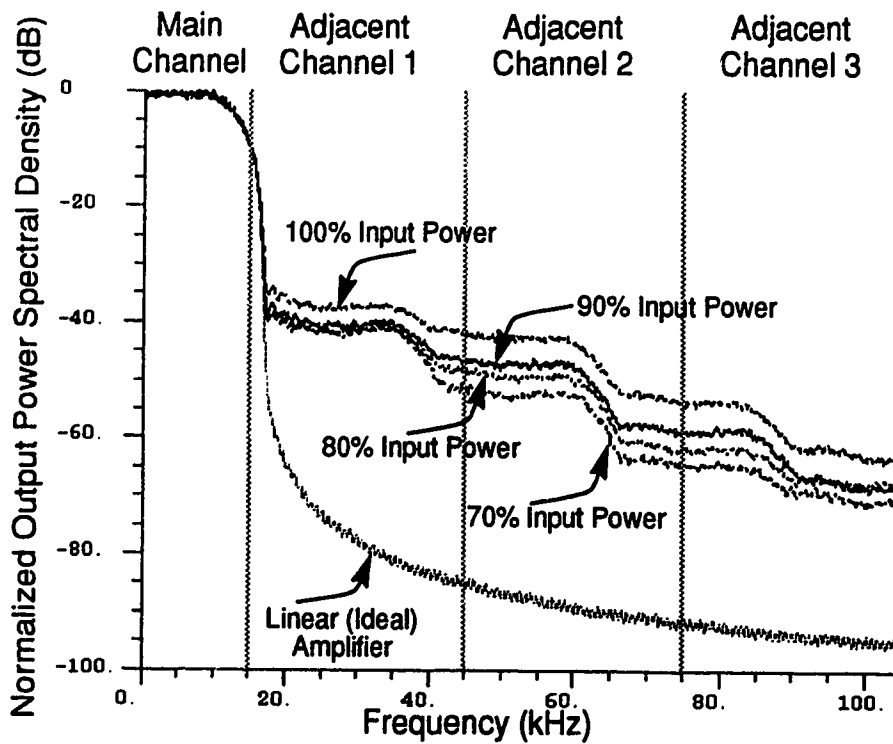


**Figure 4.1 Class AB Amplifier Spectra with Input Power Levels of 100%, 90%, 80%, and 70% of Maximum**

**Table 4.1 Normalized Out-of-Band Power for the Class AB Amplifier with Input Power Levels of 100%, 90%, 80%, and 70% of Maximum**

Input Power (% of maximum)	Adjacent Channel Power (dB)		
	#1	#2	#3
Linear (Ideal) Amplifier	-26.85	-85.6	-90.86
100	-26.23	-43.18	-55.44
90	-26.37	-47.86	-60.45
80	-26.71	-49.91	-62.79
70	-26.78	-52.99	-65.66
IS-54 Recommended	-26	-45	-60



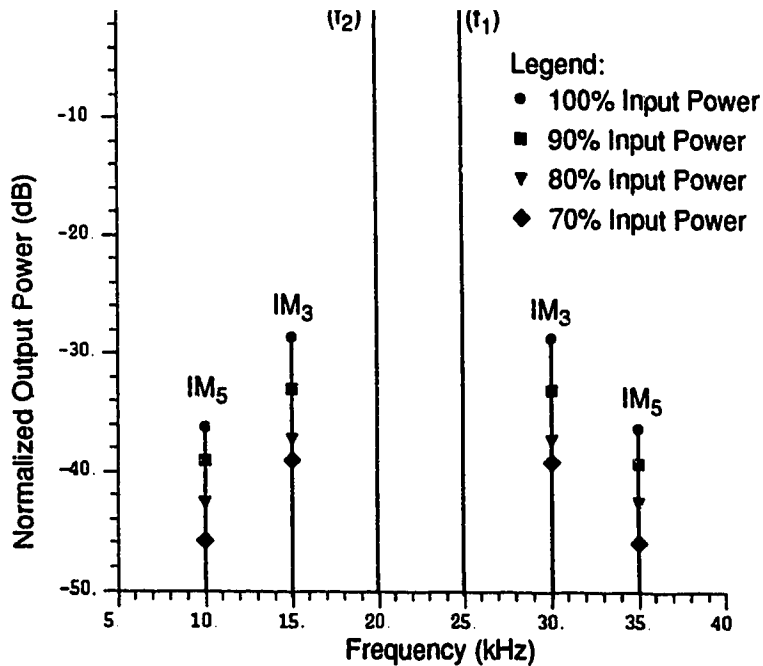


**Figure 4.2 IM Products of the Class AB Amplifier with Input Power Levels of 100%, 90%, 80%, and 70% of Maximum**

Although, from Table 4.1, only the second case (full input power) does not meet IS-54, Figure 4.1 shows a significant difference between the amplified (nonlinearly amplified) spectra and the original (linearly amplified) spectrum. There is up to 40 dB degradation in the out-of band power between the amplified spectra and the original spectrum in adjacent channels 1 and 2, and about 20 dB difference in channel 3. As the power level decreases, Figure 4.2 shows that IM<sub>3</sub> varies from -28.6 dB to -39.2 dB and IM<sub>5</sub> varies from -36.3 dB to -45.9 dB. Thus, backing-off does decrease the IM distortion.

The IM products show the effects of the amplifier on the spectra close to the frequency of the transmitted signal, while the PSD plots show the effects further away from the center frequency. Thus, both the IM products and the out-of-band power provide useful information on the linearity of the power amplifier.

The second amplifier used in the simulations is a Class B amplifier. The AM-AM and AM-PM characteristics of this amplifier are discussed in Chapter 3.3. Figure 4.3 shows the PSD of the amplifier output, operating at different back-off levels, along with the spectrum of the  $\pi/4$  DQPSK input signal (or, the output of an ideal, linear amplifier). These simulations also used back-off levels of 70% (-1.55 dB), 80% (-0.97 dB), 90% (-0.45 dB) and 100% of the maximum input power level. The out-of-band power is presented in Table 4.2, and the IM products for the amplifier are in Figure 4.4.

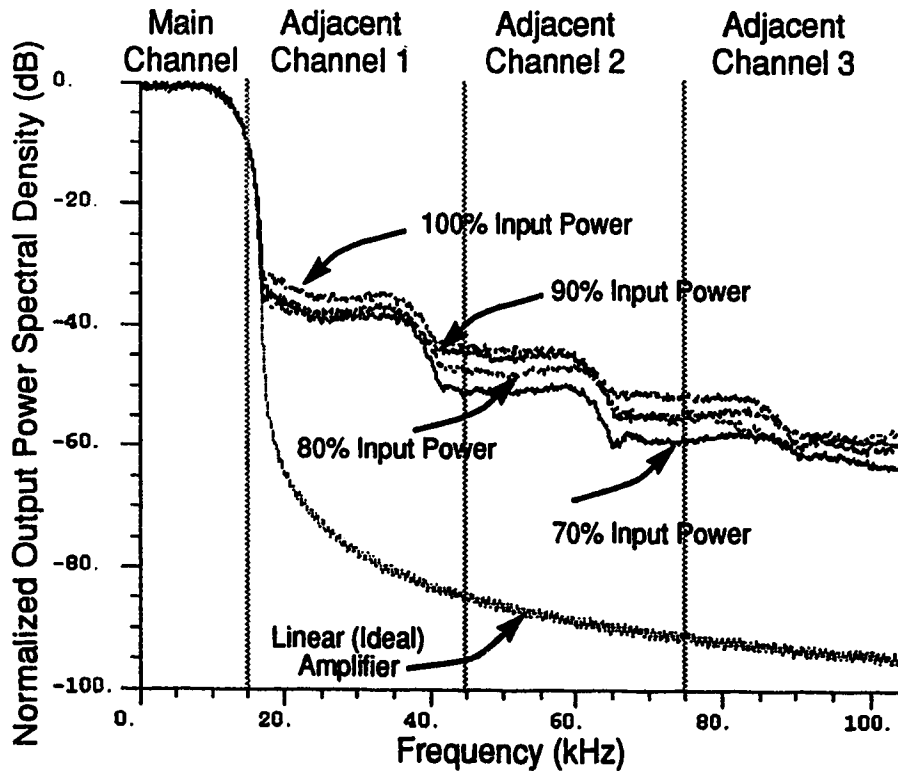


**Figure 4.3 The Class B Amplifier Spectra with 70%, 80%, 90%, and 100% of Maximum Input Power**

**Table 4.2 Normalized Out-of-Band Power for the Class B Amplifier with 70%, 80%, 90%, and 100% of Maximum Input Power**

Input Power (% of maximum) \ Adjacent Channel Power (dB)	#1	#2	#3
Linear (Ideal) Amplifier	-26.85	-85.6	-90.86
100	-26.0	-44.53	-53.43
90	-26.66	-45.61	-54.90
80	-26.56	-47.76	-55.83
70	-26.74	-51.34	-58.75
IS-54 Recommended	-26	-45	-60

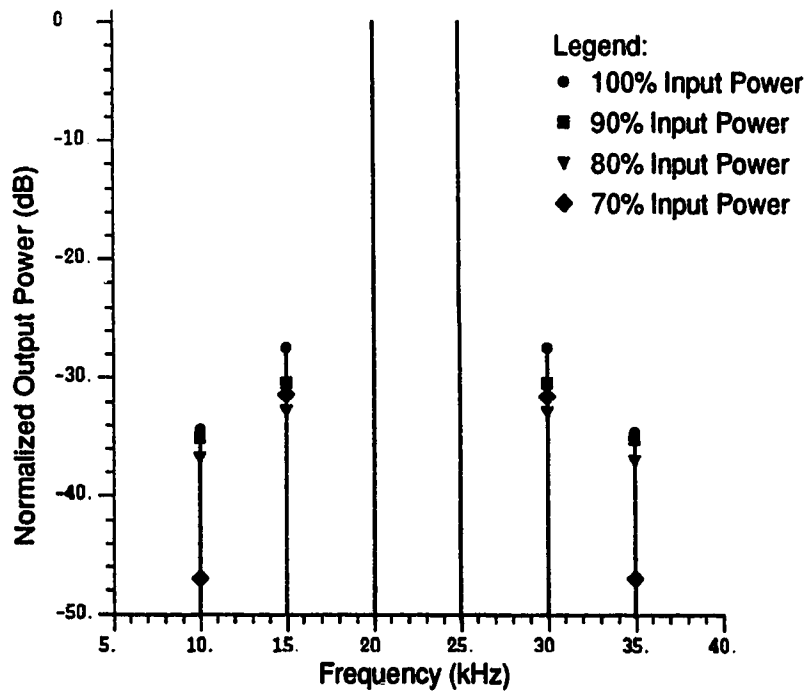


**Figure 4.4 IM Products of the Class B Amplifier with 70%, 80%, 90%, and 100% of Maximum Input Power**

dB above the ideal amplifier. In channel 2, there is between 34 dB to 40 dB difference between the amplified and ideal signal, while in channel 3 there is between 32 dB to 37 dB difference. These spectra do not meet the IS-54 recommended values for out-of-band power.  $IM_3$  varies from -27.5 dB to -32.9 dB and  $IM_5$  varies from -34.5 dB to -47.0 dB.

#### **4.2.3 Amplifier Distortion Comparison**

The results obtained from the simulations of both amplifiers demonstrates the effect of the amplifier's nonlinearity on the spectrum of the output signal. Both amplifiers increase the out-of-band power significantly. The out-of-band power for the class AB amplifier is slightly higher than for the class B amplifier. The amplifiers also introduce intermodulation distortion. The IM products for the class B amplifier are slightly higher than those of the class AB amplifier. These results also demonstrate that backing-off the amplifier is not an adequate method of linearizing. The out-of-band power improves only slightly as the input power is decreased, although the IM products are reduced significantly at the 70% input power level.

#### **4.3 Complex Gain Predistortion**

The previous section described the widening of the spectrum of the input signal caused by nonlinear amplification. The first method considered to reduce this spectral widening is the complex gain predistorter. This technique is described in Chapter 2 and its implementation is discussed in Chapter 3. The first simulations investigate the effect of varying the sampling rate and the lookup table size on the performance of the system. These simulations used the class AB amplifier. Simulations were also run with the Class B amplifier. Finally, analytical expressions for the performance of the system are given.

The minimum sampling or update rate needed for an acceptable aliasing level is the first parameter examined. This is the number of times (per bit) that the predistortion table is accessed. The bit rate is 50 kb/s so that a predistortion sampling rate of 16 samples/bit (or 32 samples/symbol) corresponds to a system sampling rate of 800 kHz. Figure 4.5 shows the PSD for sampling rates of 8 samples/bit, 16 samples/bit, and 32 samples/bit. The out-of-band power is shown in Table 4.3 and the IM products are displayed in Figure 4.6. These simulations used the class AB amplifier and a table size of 64 complex entries.

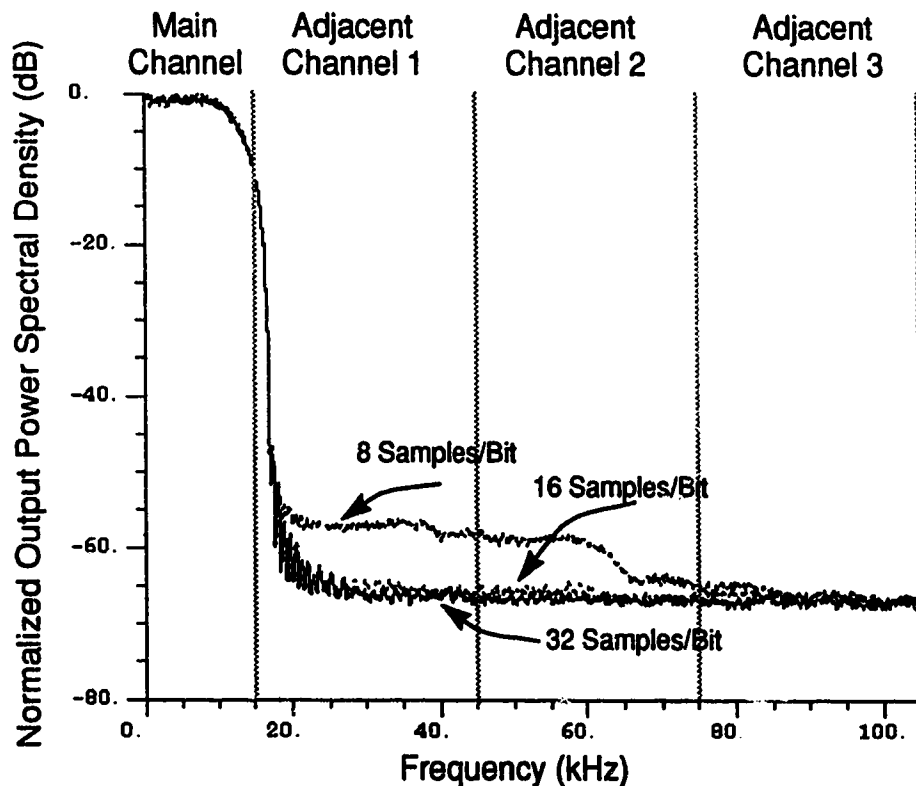


**Figure 4.5 Spectra of the Complex Gain System for Sampling Rates of 8, 16, and 32 Samples/Bit**

### System with Sampling Rates of 8, 16, and 32 Samples/Bit

Sampling Rate (Samples/Bit) \ Adjacent Channel Power (dB)	#1	#2	#3
8	-26.80	-58.82	-64.55
16	-26.86	-65.00	-65.37
32	-26.81	-65.20	-65.49

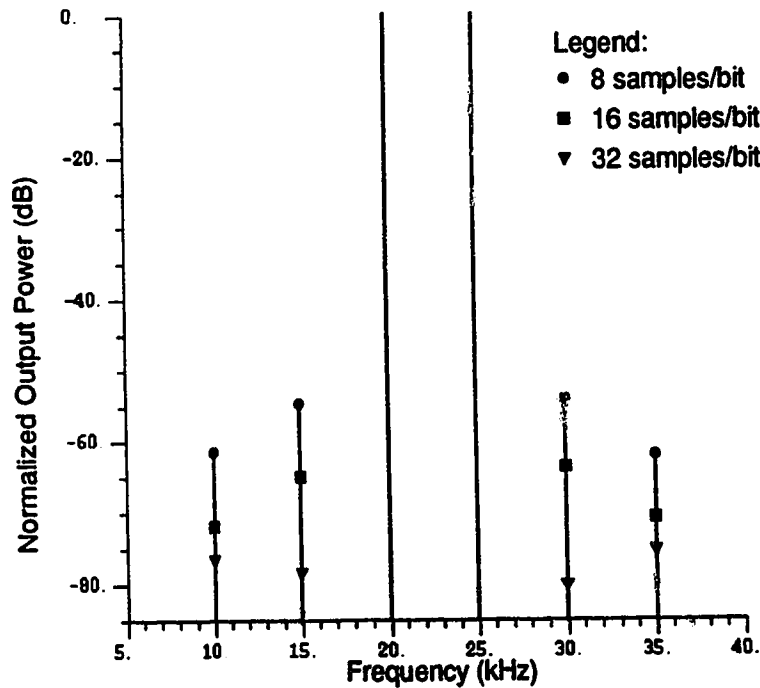


**Figure 4.6 IM products of the Complex Gain System for Sampling Rates of 8, 16, and 32 Samples/Bit**

Figure 4.5 and Table 4.3 show that there is close to a 10 dB improvement in channels 1 and 2 between 8 samples/bit and 16 samples/bit with minimal improvement between 16 samples/bit and 32 samples/bit. Figure 4.6 reveals that there is approximately a 9 dB difference in  $IM_5$  and a 10 dB difference in  $IM_3$  between 8 and 16 samples/bit. However, between 16 and 32 samples/bit there is

2.5 dB difference in  $IM_5$  and almost a 15 dB difference in  $IM_3$ . This large difference in  $IM_3$  demonstrates that the higher sampling rate has a large effect only close to the original signal frequency, and has a smaller effect further away from the center frequency. This can also be seen in Figure 4.5, since in adjacent channel 3, all of the sampling rates exhibit approximately the same out-of-band power and Table 4.3 shows less than 1 dB difference for all cases. Since there is minimal improvement in the out-of-band power between 16 and 32 samples/bit, 16 samples/bit is sufficient to ensure minimal aliasing, and was therefore used.

#### 4.3.2 Table Size

The next parameter studied for the complex gain predistorter is the size of the predistortion lookup table. This table stores the complex predistortion values. Table 4.4 shows the estimated out-of-band power for the table sizes of 16, 32, 64, and 128 complex entries and Figure 4.7 displays the PSD. Figure 4.8 shows the intermodulation products for the different predistortion lookup table sizes.

**Table 4.4 Normalized Out-of-Band Power for Lookup Table Sizes of 16, 32, 64, and 128 Complex Entries**

Lookup Table Size \ Adjacent Channel Power (dB)	#1	#2	#3
16	-26.71	-53.56	-55.16
32	-26.99	-58.49	-59.85
64	-26.86	-65.00	-65.37
128	-27.00	-69.95	-70.48

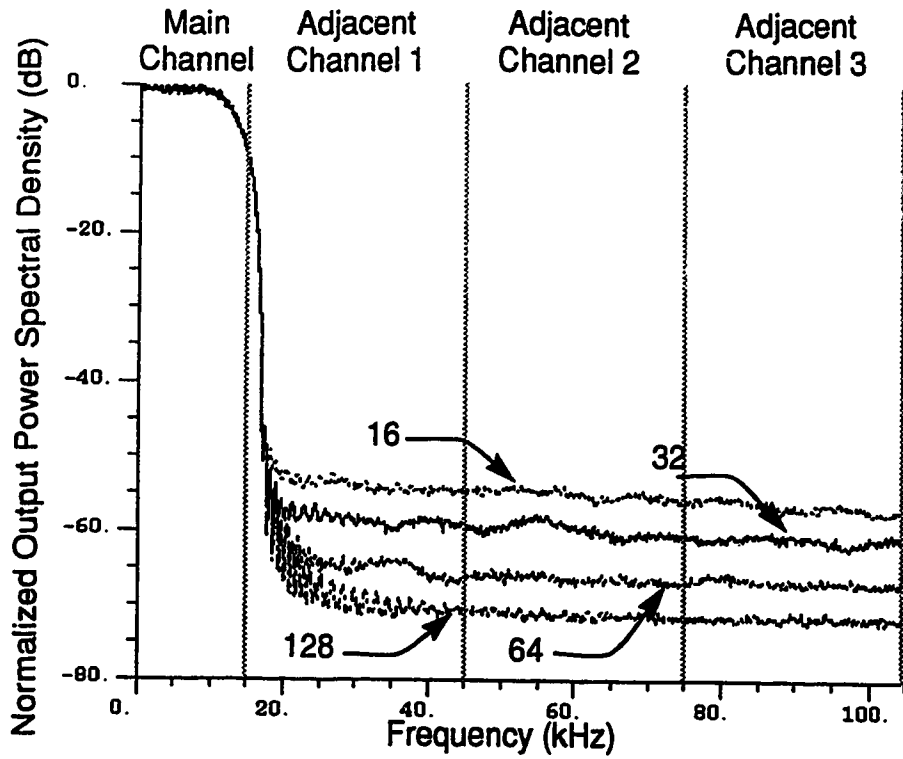


**Figure 4.7 Spectra of the Complex Gain System for Lookup Table Sizes of 16, 32, 64, and 128 Complex Entries**

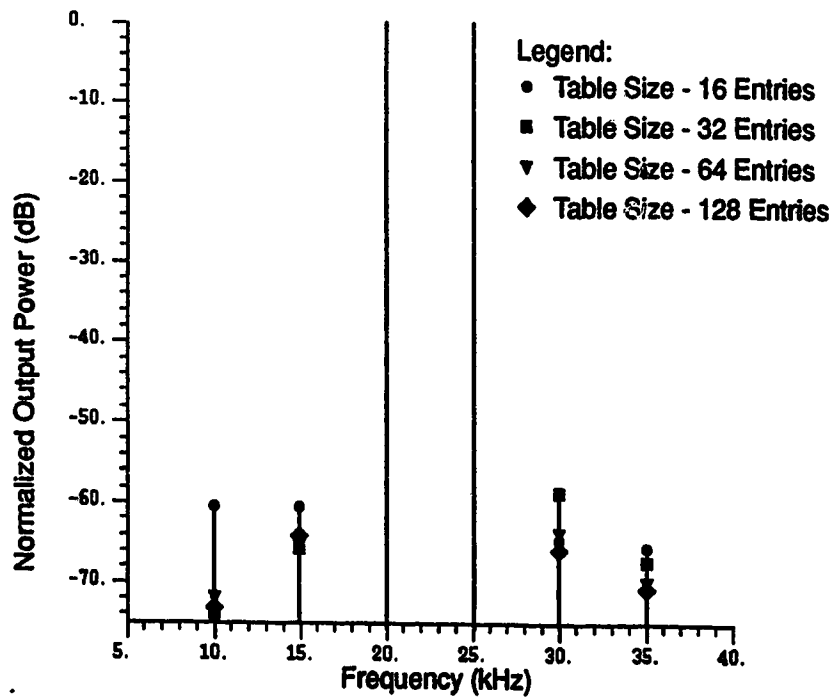


**Figure 4.8 IM Products of the Complex Gain Predistorter for Lookup Table Sizes of 16, 32, 64, and 128 Complex Entries**



Both Table 4.4 and Figure 4.7 demonstrate that for all channels, doubling the predistortion table size leads to a 5 dB to 6 dB improvement in the out-of-band power. This is consistent with other work in this area [22].

Figure 4.8 shows the effect that the table size has close to the center transmitting frequency.  $IM_3$  varies from -60 dB to -67 dB and  $IM_5$  varies from -60 dB to -74 dB. The IM products show less variation for the various table sizes than does the out-of-band power, and there is not a consistent difference as the table size increases. Thus, the table size does not have a large effect close to the center frequency. Since the out-of-band power with a table size of 64 complex entries is adequate to meet IS-54, this table size was used.

### 4.3.3 Power Level

The next set of simulations used in analyzing the performance of the complex gain predistorter involved varying the input power level of the amplifier. Table 4.5 shows the estimated out-of-band power at the output of a class AB amplifier with input power levels of 100%, 90%, 80%, and 70% of maximum. Figure 4.9 shows the PSDs, and the intermodulation products are shown in Figure 4.10.

**Table 4.5 Normalized Out-of-Band Power for Input Power Levels of 100%, 90%, 80%, and 70% of Maximum**

Input Power (% of maximum) \ Adjacent Channel Power (dB)	#1	#2	#3
100	-26.86	-64.99	-65.37
90	-26.81	-71.83	-72.26
80	-26.96	-73.56	-74.12
70	-26.73	-75.11	-75.92

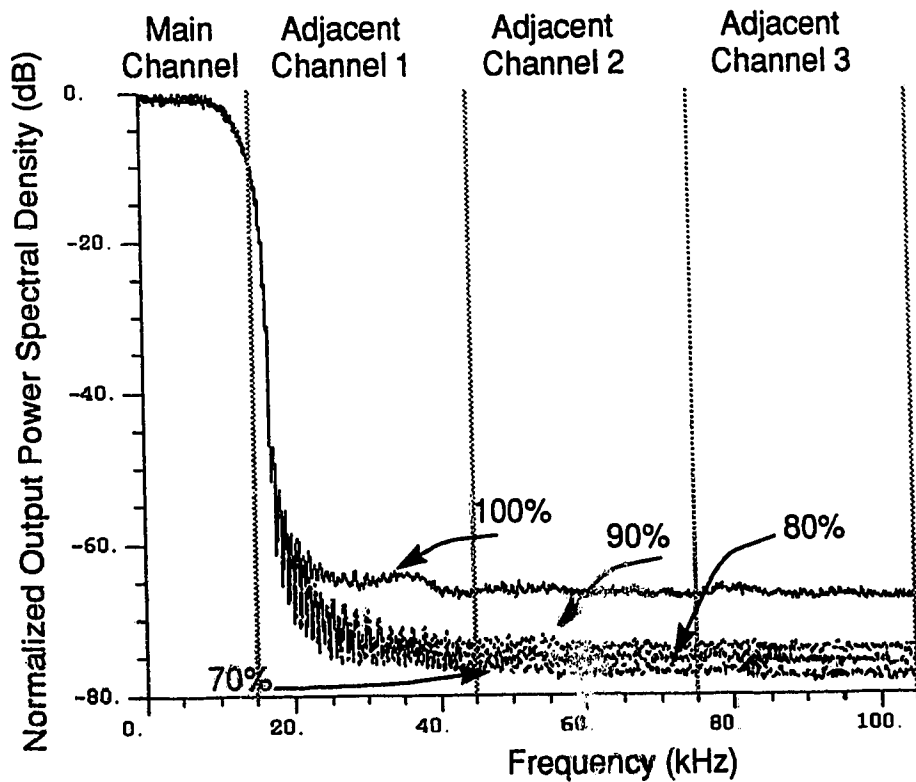


**Figure 4.9 Spectra of the Complex Gain System for Power Levels of 100%, 90%, 80%, and 70% of Maximum**

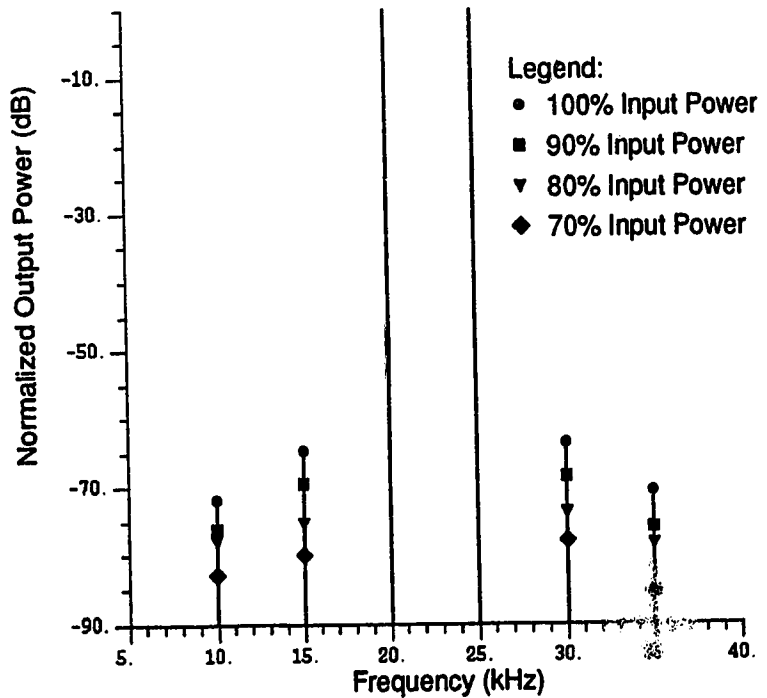


**Figure 4.10 IM Products of the Complex Gain Predistorter for Input Power Levels of 100%, 90%, 80%, and 70% of Maximum**

Figure 4.9 and Table 4.5 demonstrate that as the input power level decreases, the normalized out-of-band power is also decreased because the amount of distortion is decreased. Thus, the out-of-band power is dependent on the input power level. The out-of-band power, for all input power levels, is reduced by approximately 30 dB in channel 1, 20 dB in channel 2, and 10 dB in channel 3.

Figure 4.10 shows that as the input power decreases, the IM products also decrease. Each decrease in input power results in approximately a 5 dB decrease in  $IM_3$ , which ranges from approximately -64 dB to -80 dB.  $IM_5$  also decreases as the input power level decreases.  $IM_5$  ranges from -71 dB to -85 dB.

#### 4.3.4 Amplifiers

Finally, the effect of the different amplifiers on the performance of the system is examined. The simulations were repeated using the class B amplifier instead of the class AB amplifier used previously. The estimated out-of-band power is given in Table 4.6, the PSDs are shown in Figure 4.11, and the IM products are shown in Figure 4.12.

**Table 4.6 Normalized Out-of-Band Power for the Class AB, the Class B, and a Linear Amplifier**

Adjacent Channel Power (dB) Amplifier	#1	#2	#3
Class AB	-26.86	-65.00	-65.37
Class B	-26.07	-65.78	-66.84
Linear (Ideal)	-26.78	-85.60	-90.86
IS-54 Recommended	-26	-45	-60

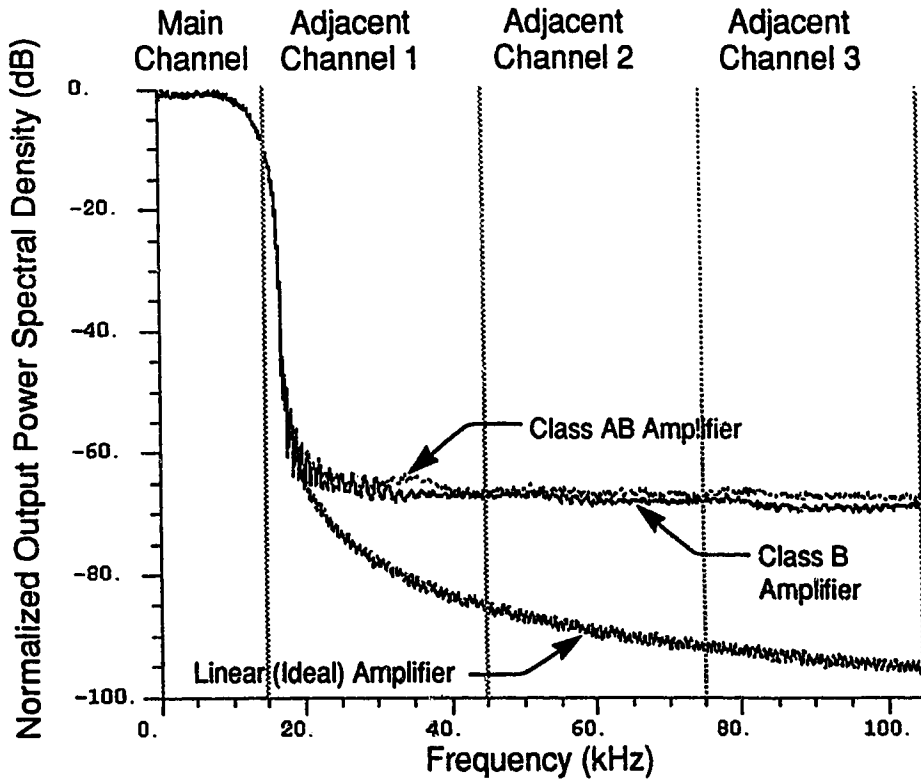


**Figure 4.11 Spectra of Complex Gain System for the Class AB Amplifier, the Class B Amplifier, and a Linear Amplifier**

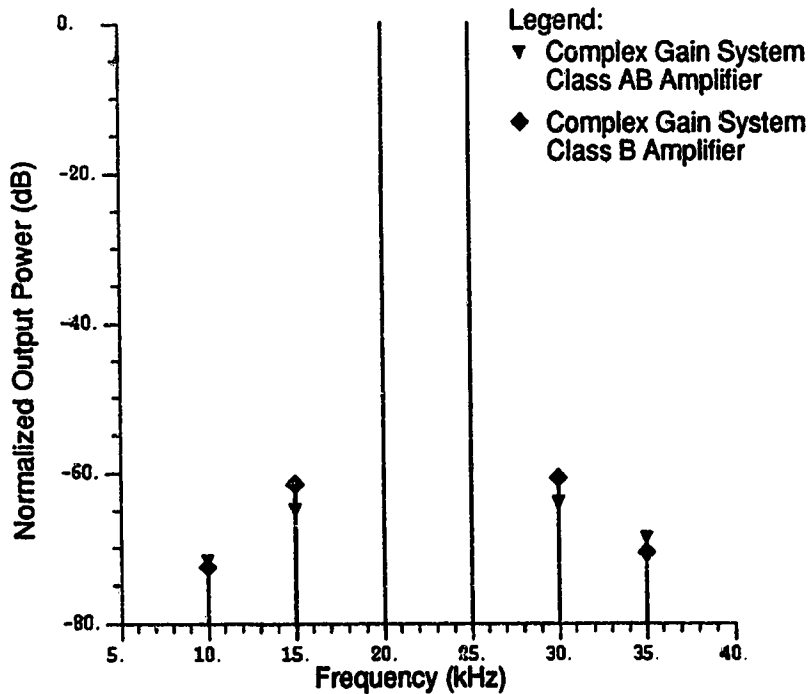


**Figure 4.12 IM Products for a Complex Gain Predistorter with the Class AB Amplifier and the Class B Amplifier**

These results indicate that the sampling rate and the table size do not have to be adjusted for the system to compensate for the change in amplifier. In channel 2, the out-of-band power is reduced by about 20 dB for both amplifiers. In channel 3, the out-of-band power is reduced by approximately 10 dB for the class AB amplifier and 13 dB for the class B amplifier.

Figure 4.12 shows that  $IM_3$  is reduced by approximately 35.5 dB for the class AB amplifier and by approximately 33.5 dB for the class B amplifier.  $IM_5$  is reduced by close to 34.5 dB for the class AB amplifier and by about 34 dB for the class B amplifier.

#### 4.3.5 Performance Analysis

One factor limiting the performance of the complex gain system is the quantization error in the look-up table entries. In addition to this, there is also adaption jitter in the convergence procedure. The table index is calculated to indicate the midpoint of each step. The step size,  $D_g$ , is given by:

$$D_g = x_m / N \quad (4.1)$$

where  $x_m$  is the table index (input power) and

$N$  is the number of table entries.

The value of  $x_m$  for each iteration varies over the range  $-D_g/2$  to  $D_g/2$ . Thus, during convergence, the value of  $x_{mi}(k)$  is different for each successive iteration for the same table value. This means that the calculated value for  $F(x_{mi})$  is not necessarily the same for each successive iteration and the final value is not necessarily at the center of the table entry. This causes variance in the output of the amplifier for each table entry level which increases the output error and limits the performance of the complex gain system. However, increasing the lookup table size minimizes this error, since this decreases the step size.

Another factor in the performance of the complex gain system is the characteristics of the amplifier. Since the complex gain system tries to find the 'inverse' distortion to the amplifier, it is reasonable to expect that the performance of the complex gain system is limited by the amplifier characteristics. As well, this system operates by predistorting the amplifier input signal, that is, if the amplifier reduces a signal by a factor of 'x', the complex gain system predistorts the input by '1/x'. Thus, if the amplifier is operated well into saturation, predistorting the input by '1/x' will only push the amplifier further into saturation, thus increasing the distortion. The complex gain system will not converge.

#### **4.3.6 Complex Gain System Summary**

A summary of the performance of the complex gain system is shown in Table 4.7 and Figures 4.13, 4.14. The complex gain predistortion system reduces the out-of-band power in adjacent channel 1 by approximately 30 dB, in channel 2 by about 20 dB, and in channel 3 by close to 10 dB. This clearly ensures that the transmitted out-of-band power will fall within the IS-54 recommendation. The system reduces  $IM_3$  and  $IM_5$  by approximately 35 dB. A sampling rate of 16 samples/bit (800 kHz) is sufficient to compensate for the amplifier nonlinearities. Increasing the look-up table size by a factor of two results in a 6 dB reduction in the out-of-band power.

The system uses a secant algorithm to calculate the predistortion values. These values are stored in a lookup table which contains 64 complex values. The algorithm requires at most, 10 iterations to converge and this occurs within 5 ms. This compares favorably to results obtained in [22].

**Table 4.7 Comparison of the Normalized Out-of-Band Power for the Uncompensated Amplifiers and the Complex Gain Predistorter**

Amplifier \ Adjacent Channel Power (dB)	#1	#2	#3
Uncompensated Class AB	-26.23	-43.18	-55.44
Uncompensated Class B	-26.0	-44.53	-53.43
Complex Gain, Class AB	-26.86	-65.00	-65.37
Complex Gain, Class B	-26.07	-65.78	-66.84
Linear (Ideal)	-26.85	-85.6	-90.86
IS-54 Recommended	-26	-45	-60

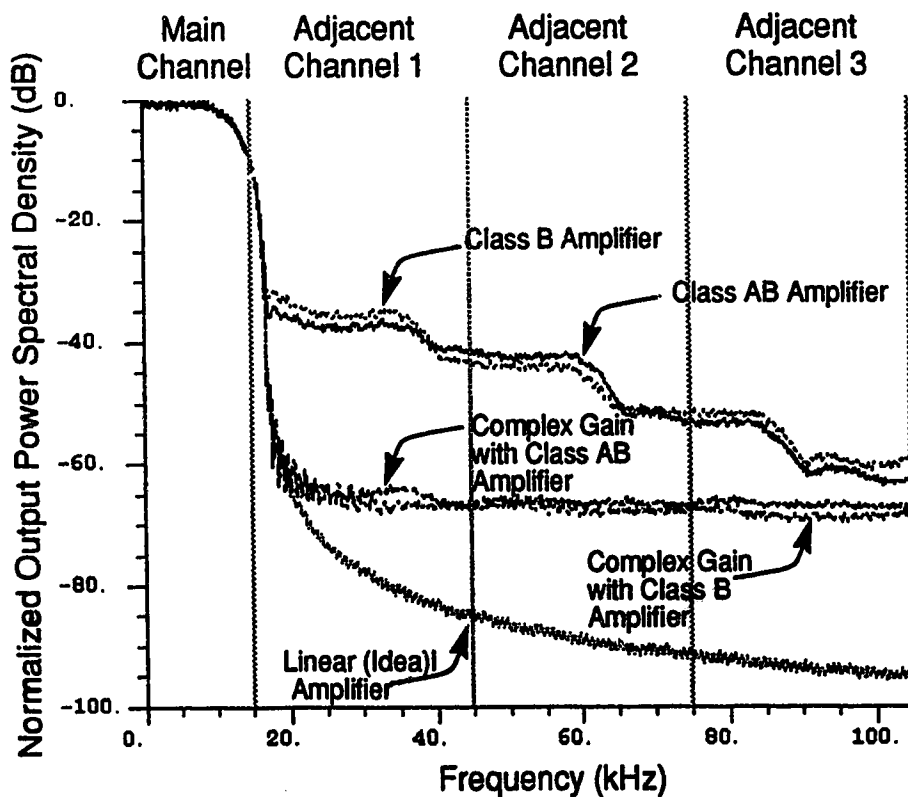


**Figure 4.13 Comparison of the Spectra of the Uncompensated Amplifiers and the Complex Gain Predistorter**

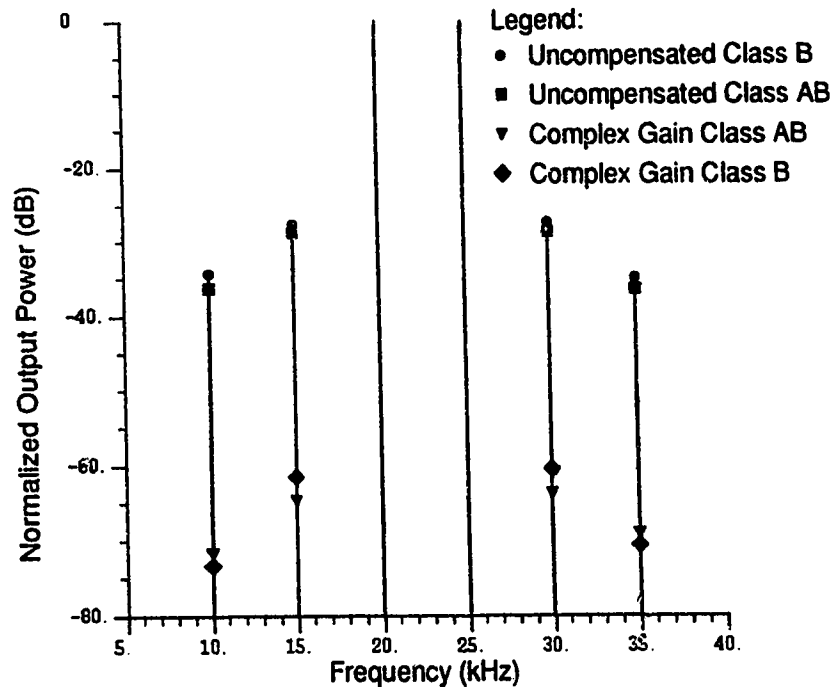


**Figure 4.14 Comparison of the IM Products of the Uncompensated Amplifiers and the Complex Gain Predistorter**

#### **4.4 Cartesian Coordinate Negative Feedback**

The second method considered to linearize the power amplifier is the Cartesian coordinate negative feedback system. This system, as described in Chapters 2 and 3, uses negative feedback to linearize the power amplifier. The system is much simpler than the complex gain system, and thus has fewer parameters. Basically, the only parameter of this system is the loop gain. Simulations varying the input power and simulations with a different amplifier were also run.

In the Cartesian system, a phase adjuster is required to ensure the stability of the system. If the phase adjustment is outside a certain range, the system oscillates and is unstable. The phase adjustment can be done automatically as described in [14, 30]. In this simulation system, the phase adjustment is complicated by the delay required by the simulation program in the feedback path.



In order to minimize this delay, the sampling rate of the simulated system must be sufficiently high. In an actual system, this would not be a problem because the feedback is done with an analog circuit. Thus, several simulations were done to ensure that the sampling rate was sufficient and to determine the required range of the phase adjustment.

#### 4.4.1 Loop Gain

From Chapter 2, the closed loop gain of a basic closed loop feedback amplifier is given by:

$$\frac{V_{out}}{V_{in}} = \frac{A}{(1 + \beta A)} \quad (4.2)$$

and the loop gain is defined as  $\beta A$  ( $\beta A \gg 1$ ).

The loop gain has an effect on the stability of the system. If it is too high, the system may oscillate and become unstable. From (2.10), the amplifier distortion is reduced by the loop gain. Thus, this parameter also controls the amount of linearization. If the loop gain is too low, the system will not correct for amplifier nonlinearities.

Table 4.8 gives the estimated out-of-band power for loop gains of 2, 5, 10, and 15. Figure 4.15 shows the PSDs and Figure 4.16 shows the IM products for these loop gains.

**Table 4.8 Normalized Out-of-Band Power for the Cartesian System with Loop Gains of 2, 5, 10, and 15**

Adjacent Channel Power (dB) \ Loop Gain	#1	#2	#3
2	-26.50	-49.88	-62.75
5	-26.79	-57.54	-69.98
10	-26.87	-65.12	-77.57
15	-26.32	-68.31	-81.16

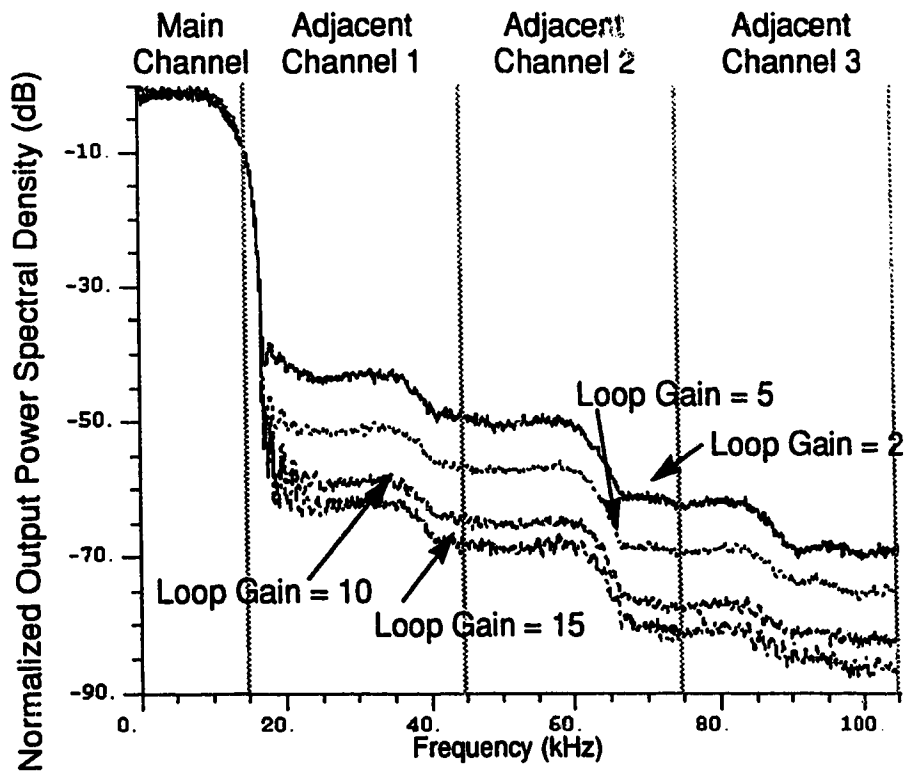


**Figure 4.15 Spectra for the Cartesian Feedback System with Loop Gains of 2, 5, 10, and 15**

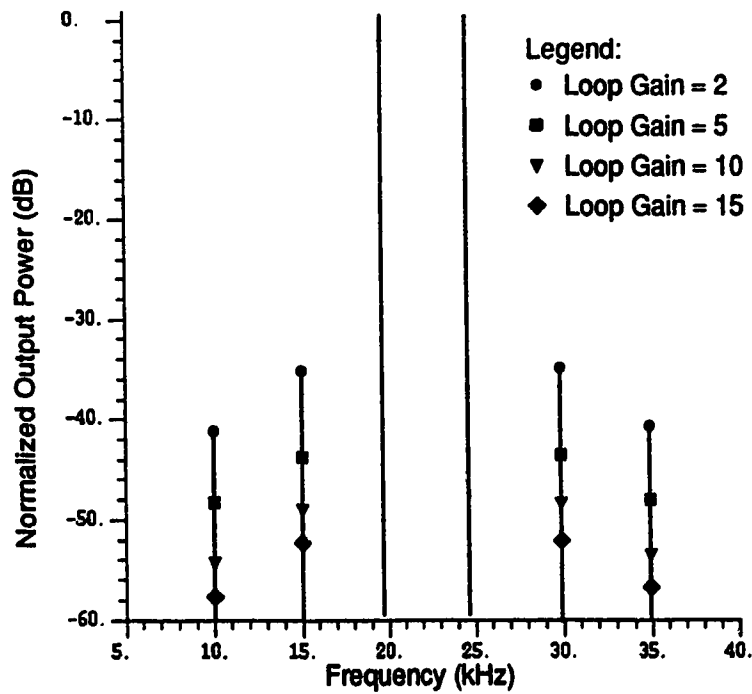


**Figure 4.16 IM Products of the Cartesian Feedback System With Loop Gains of 2, 5, 10, and 15**

If the loop gain is increased beyond 15, the system becomes unstable. As well, the range of phase adjustments for each loop gain was different. These simulations used the class AB amplifier model.

Figure 4.15 and Table 4.8 show that as the loop gain increases, the out-of-band power decreases. There is only a 3 dB difference in the out-of-band power for loop gains of 10 and 15 while the difference between loop gains of 2 and 5 is more than 7 dB and the difference between loop gains of 5 and 10 is approximately 7.5 dB. This small decrease in the out-of-band power between the loop gains of 10 and 15 shows that the loop gain is near its maximum. If the loop gain is increased much beyond 15, the system becomes unstable.

The results for the out-of-band power and the IM products are quite consistent. Figure 4.16 shows that as the loop gain increases, the IM products decrease. The IM products for a loop gain of 5 are 7 dB lower than the IM products for a loop gain of 2. The IM products for a loop gain of 10 are an additional 5 dB to 6 dB down, and for a loop gain of 15, there is an additional 3 dB difference. This compares closely to the estimated out-of-band power shown in Figure 4.15 and Table 4.8. A loop gain of 10 was used for the subsequent simulations.

#### **4.4.2 Input Power Level**

These simulations show the effects of varying the input power level of the amplifier. The input power levels are 100%, 90%, 80%, and 70% of full input power. The estimated out-of-band power is given in Table 4.9. The PSDs are displayed in Figure 4.17 and Figure 4.18 shows the IM products.

**Table 4.9 Normalized Out-of-Band Power for the Cartesian System with Varying Input Power Levels**

Adjacent Channel Power (dB) \ Input Power (% of Maximum)	#1	#2	#3
100	-26.87	-65.12	-77.57
90	-26.89	-67.40	-78.49
80	-27.16	-70.40	-80.12
70	-26.45	-73.05	-81.26

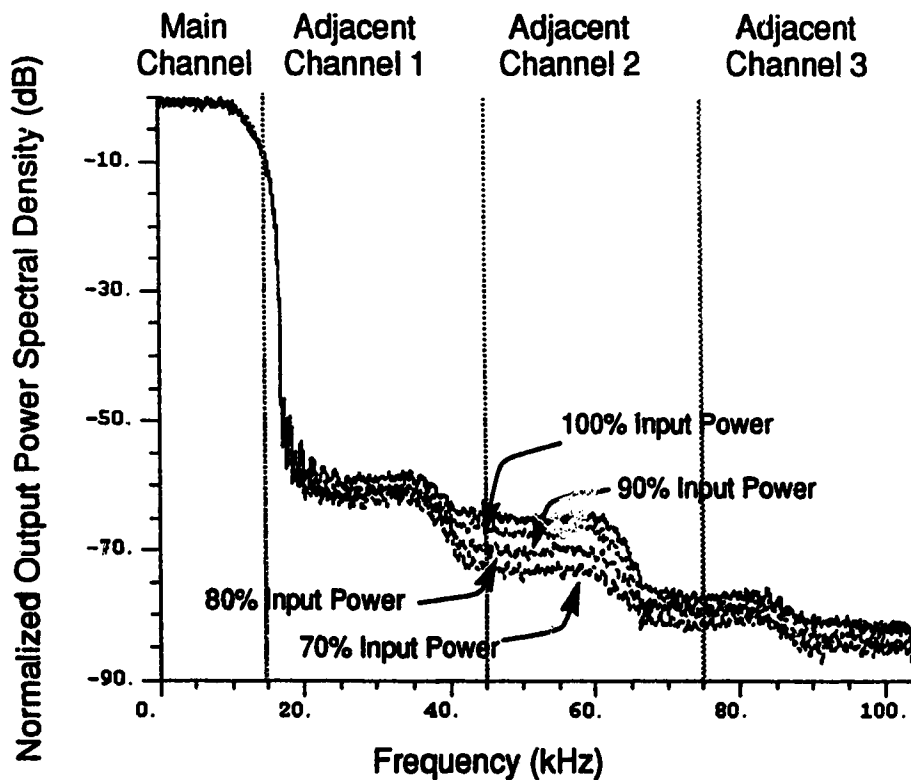


**Figure 4.17 Spectra of the Cartesian System for Input Power Levels of 100%, 90%, 80%, and 70% of Maximum**

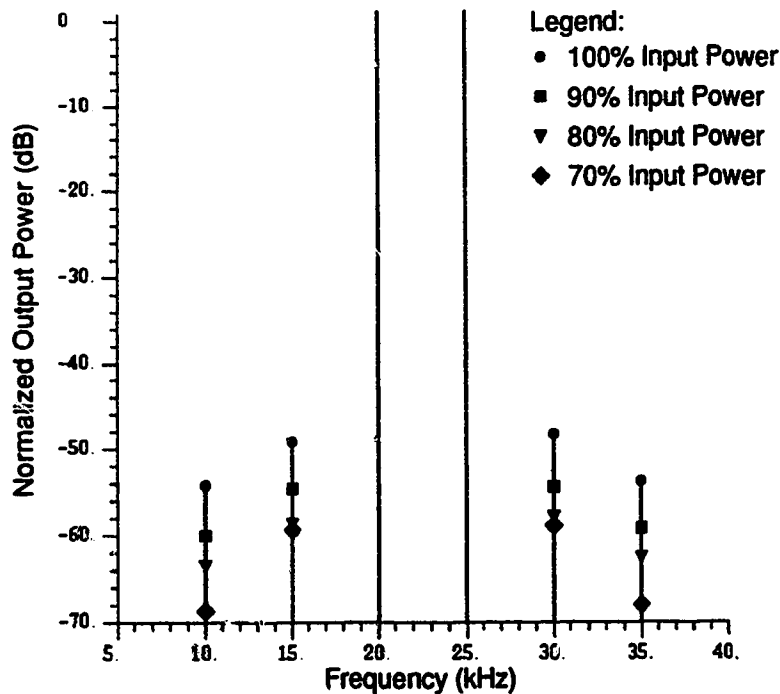


**Figure 4.18 IM Products of the Cartesian System for Input Power Levels of 100%, 90%, 80%, and 70% of Maximum**

Figure 4.17 and Table 4.9 show that as the input power decreases, the out-of-band power also decreases. This is expected, since the negative feedback system reduces the distortion by the loop gain. The out-of-band power, for all input power levels, is reduced by 19 dB to 22 dB in each channel.

Figure 4.18 shows that the IM products also decrease as the power level decreases. For all input power levels, the IM products are reduced by 20 dB to 21 dB. This is consistent with the results shown in Figure 4.17 and Table 4.9.

#### **4.4.3 Amplifier**

For this simulation, the class AB amplifier was replaced by the class B amplifier. The maximum loop gain and phase adjustment had to be changed for the class B amplifier. The loop gain used is now 20. The estimated out-of-band power

is displayed in Table 4.10. The PSDs of the two amplifiers are shown in Figure 4.19 and the IM products are shown in Figure 4.20.

**Table 4.10 Normalized Out-of-Band Power for the Class AB Amplifier, the Class B amplifier, and a Linear Amplifier**

Amplifier \ Adjacent Channel Power (dB)	#1	#2	#3
Class AB	-26.87	-65.12	-77.57
Class B	-26.69	-70.14	-78.52
Linear (Ideal)	-26.85	-85.6	-90.86
IS-54 Recommended	-26	-45	-60

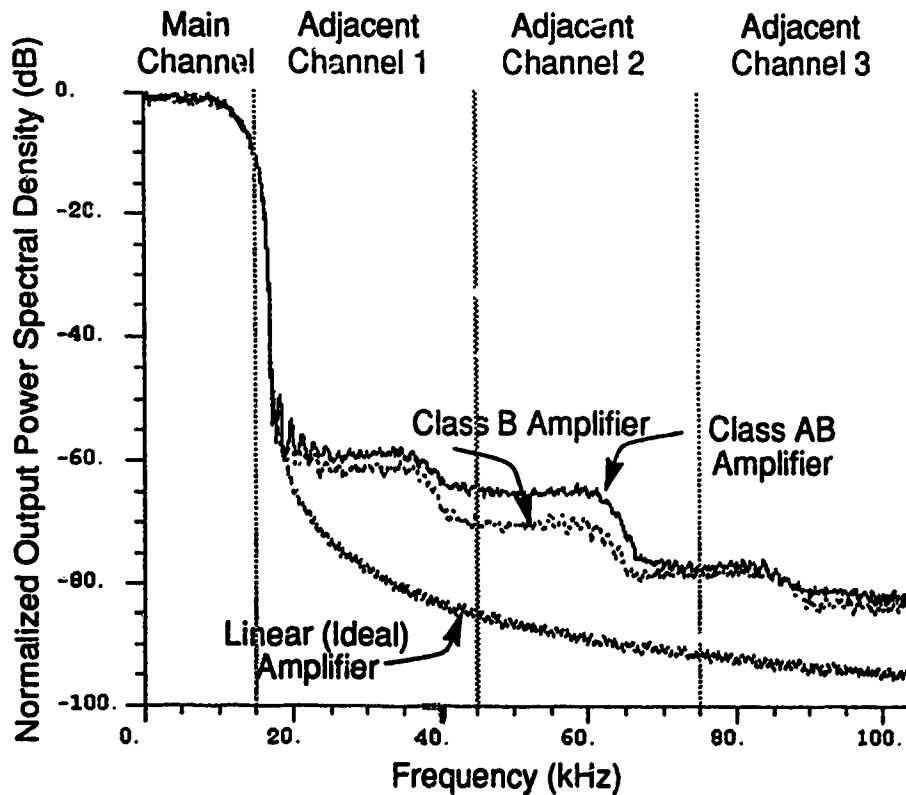


**Figure 4.19 Spectra of the Cartesian System for the Class AB Amplifier, the Class B Amplifier, and a Linear Amplifier**

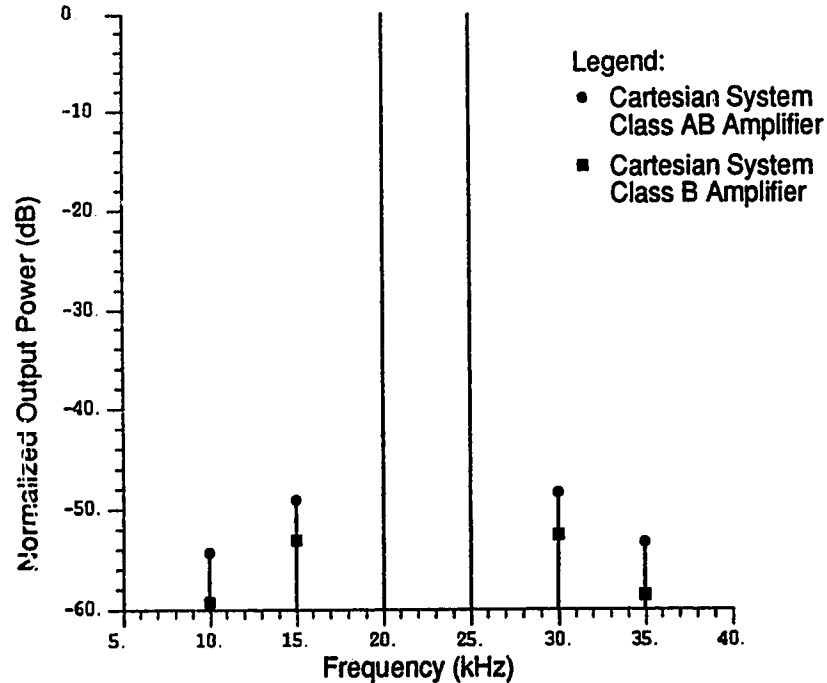


**Figure 4.20 IM Products for a Cartesian System with the Class AB Amplifier and the Class B Amplifier**

These simulations show that the system parameters need to be adjusted for each amplifier. The out-of-band power is reduced by approximately 22 dB for the Class AB amplifier and by 25 dB for the Class B amplifier. The difference in this improvement is due to the difference in the system loop gain between the two amplifiers.

The IM products for the class AB amplifier are reduced by approximately 20 dB while the IM products for the class B amplifier are reduced by close to 25 dB. Again, this difference between the two amplifiers is due to the difference in the loop gains between the two systems.

#### **4.4.4 Performance Evaluation**

From (2.10), the amplifier distortion is reduced by the loop gain. The simulations using the class AB amplifier had a loop gain of 10. The estimated out-

of-band power in channels 2 and 3 for the uncompensated system is -43.18 dB and -55.44 dB, respectively. The out-of-band power in channels 2 and 3 for the compensated system is -65.12 dB and -77.57 dB, respectively. Thus the reduction in out-of-band power is approximately 22 dB in each channel. The theoretical loop gain of 10 should result in an improvement of:

$$20\log(10) = 20 \text{ dB.} \quad (4.3)$$

This is close to the simulated improvement.

For the class B amplifier, the improvement in the out-of-band power in channels 2 and 3 is approximately 25 dB. A loop gain of 15 corresponds to a calculated improvement of:

$$20\log 15 = 23.5 \text{ dB.} \quad (4.4)$$

Again, this is reasonably close to the simulated improvement.

#### 4.4.5 Cartesian Coordinate Negative Feedback Summary

The performance of the Cartesian coordinate negative feedback linearization system is summarized in Table 4.11 and Figure 4.21 for the  $\pi/4$  DQPSK input signal. The IM products for a two-tone input are summarized in Figure 4.22.

**Table 4.11 Comparison of the Normalized Out-of-Band Power for the Uncompensated Amplifiers, a Linear Amplifier, and the Cartesian System**

Amplifier \ Adjacent Channel Power (dB)	#1	#2	#3
Uncompensated Class AB	-26.23	-43.18	-55.44
Uncompensated Class B	-26.0	-44.53	-53.43
Cartesian Class AB	-26.87	-65.12	-77.57
Cartesian Class B	-26.69	-70.14	-78.52
Linear (Ideal)	-26.85	-85.6	-90.86
IS-54 Recommended	-26	-45	-60



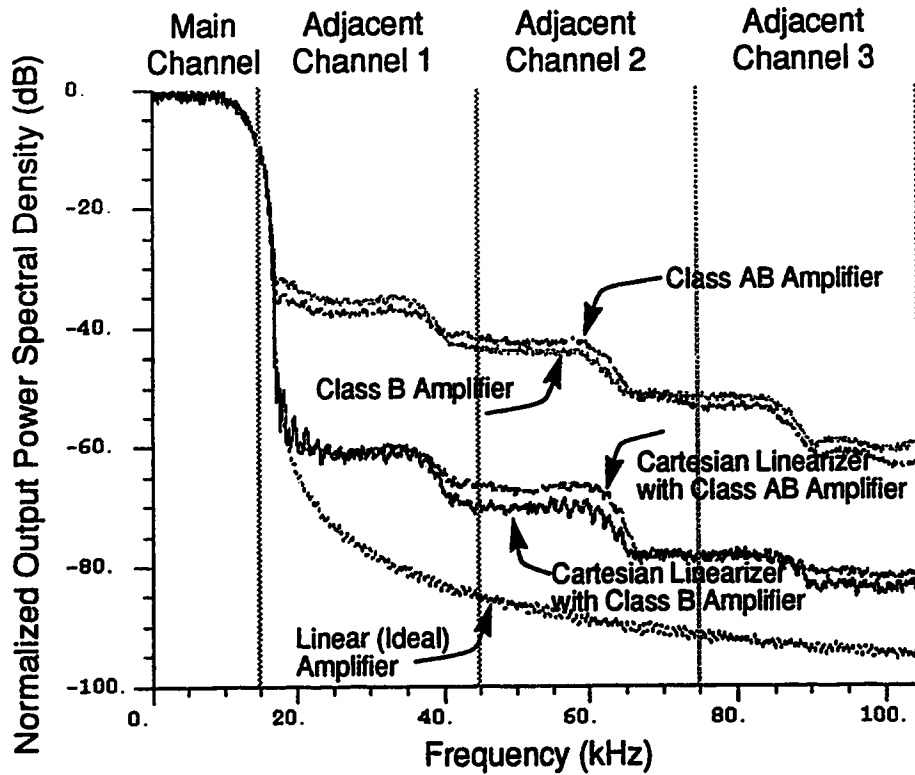


**Figure 4.21 Comparison of the Spectra of the Uncompensated Amplifiers, the Cartesian System, and a Linear Amplifier**

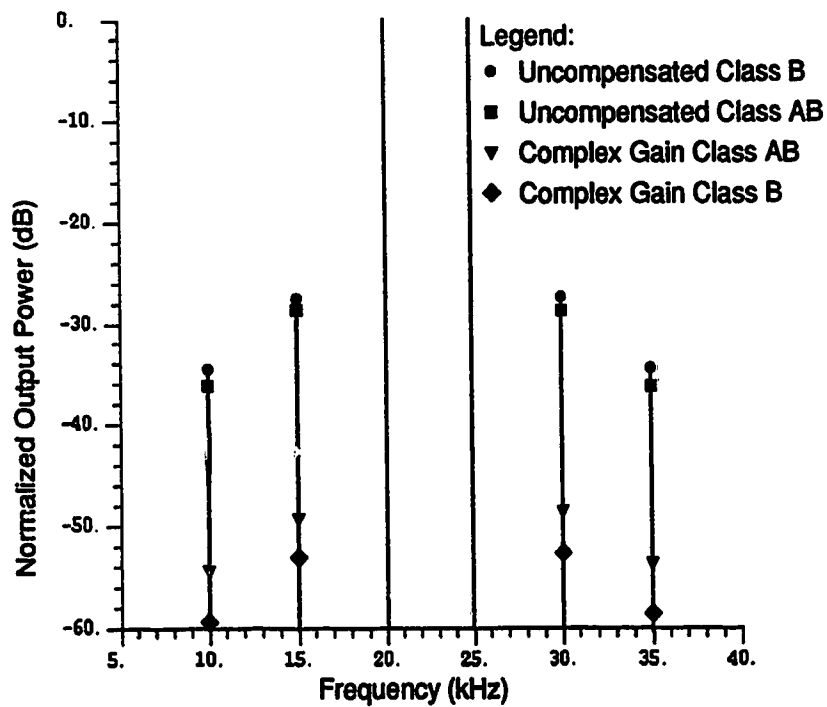


**Figure 4.22 IM Products for a Comparison of the Uncompensated Amplifiers and the Cartesian System**

The Cartesian system reduces the out-of-band power in all channels by about 22 dB for the class AB amplifier system and by 25 dB for the class B amplifier. The IM products are reduced by about 22 dB for the class AB amplifier and by 25 dB for the class B amplifier.

The reduction in out-of-band power is directly related to the loop gain of the system. However, if the loop gain is too high, the system becomes unstable and oscillates. As well, the loop gain and the phase adjustment need to be modified for each amplifier.

#### 4.5 Comparison of the Complex Gain and the Cartesian Systems

Table 4.12 and Figure 4.23 offer a comparison of the out-of-band power for the Cartesian system and the complex gain system with the class AB amplifier, and a  $\pi/4$  DQPSK input signal. The IM products for a two-tone input signal are displayed in Figure 4.24. The Cartesian system used a loop gain of 10. The complex gain system had a sampling rate of 16 samples/bit and a lookup table size of 64 complex entries.

**Table 4.12 Comparison of the Normalized Out-of-Band Power Between a Linear Amplifier, the Class AB Amplifier, the Complex Gain Predistorter, and the Cartesian System**

Adjacent Channel Power (dB) / RF Amplification	#1	#2	#3
Linear (Ideal)	-26.85	-85.6	-90.86
Uncompensated Amplifier	-26.23	-43.21	-55.46
Complex Gain System	-26.86	-65.00	-65.37
Cartesian System	-26.87	-65.12	-77.57
IS-54 Recommended	-26	-45	-60

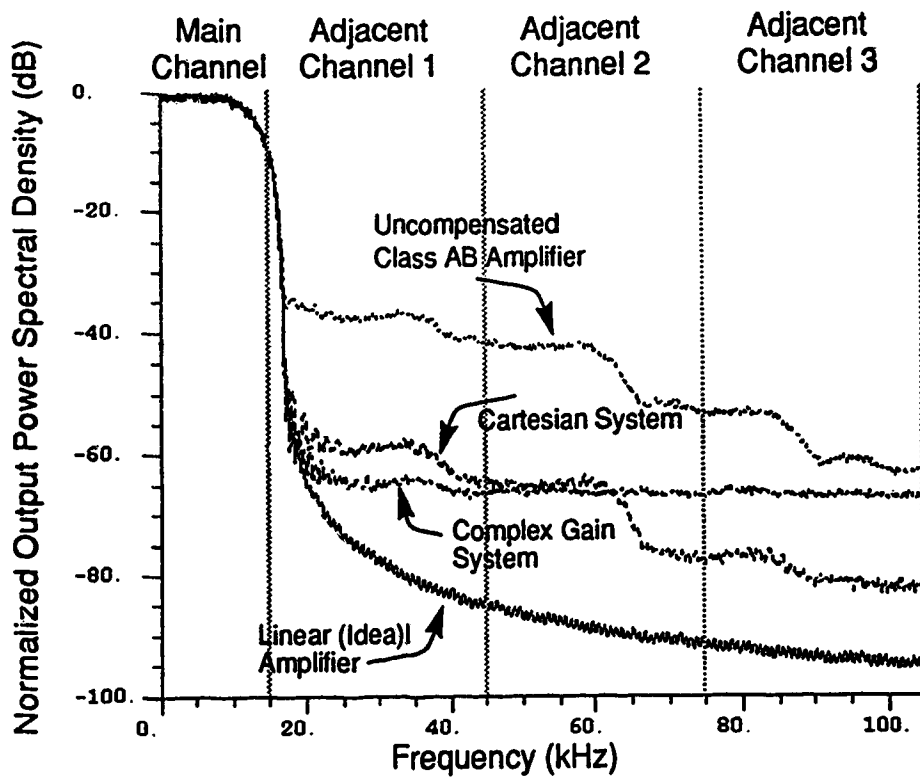


**Figure 4.23 Comparison of Spectra of the Class AB Amplifier, the Cartesian System, the Complex Gain System, and a Linear Amplifier**

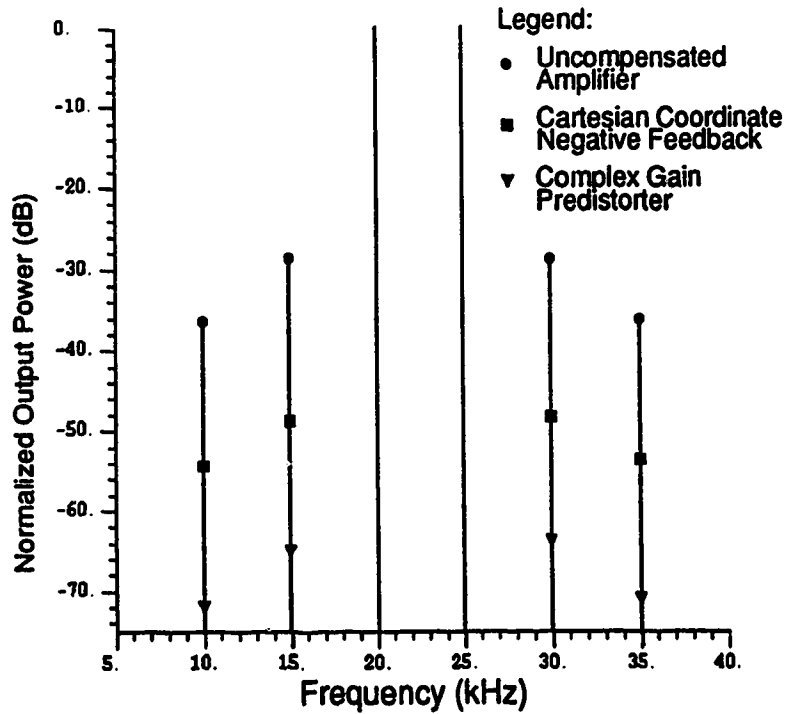


**Figure 4.24 Comparison of IM Products for the Class AB Amplifier, the Cartesian System, and the Complex Gain System**

The Cartesian system reduces the out-of-band power by approximately 22 dB in each channel for the class AB amplifier. The complex gain system reduces the out-of-band power by approximately 30 dB in channel 1, by 22 dB in channel 2, and by 10 dB in channel 3. The complex gain system reduces the  $IM_3$  and  $IM_5$  products by approximately 35 dB, while the Cartesian feedback system reduces the intermodulation products by close to 22 dB. While the complex gain system has less power close to the transmitting channel (channel 1), the Cartesian system reduces power better farther from the transmitting channel (channel 3). However, the Cartesian feedback system must be 'tuned' to each amplifier and is potentially unstable.

## **4.6 Modulation/Demodulation Distortion**

As discussed in chapter 3, both the complex gain predistorter and the Cartesian coordinate negative feedback system include quadrature modulators and demodulators. These components also add distortion to the system. This section discusses the effects of the modulator and demodulator distortion on the transmitter.

### **4.6.1 Basic Transmitter**

This part discusses the effects of the non-ideal modulator on the uncompensated system. First, a transmitter containing a quadrature modulator and a linear power amplifier is discussed, and next, a system including the class AB amplifier without linearization is considered. The modulation distortion can be described by a dc offset, and a gain imbalance and phase imbalance.

The first simulations considered each type of distortion separately for the transmitter with a linear amplifier. The simulation system is shown in Figure 4.25.

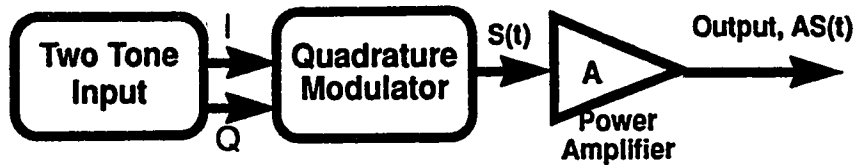


**Figure 4.25 Transmitter System with Modulator and Amplifier**

The effects of the individual distortions are:

- ❑ a relative dc offset of 2% results in a spur at dc of -27.96 dB
- ❑ a relative gain imbalance of 2% results in spurs of -40.09 dB at -20 kHz and at -25 kHz
- ❑ a phase imbalance of 2° results in spurs of -35.16 dB at -20 kHz and at -25 kHz.

This is shown in Figure 4.26.

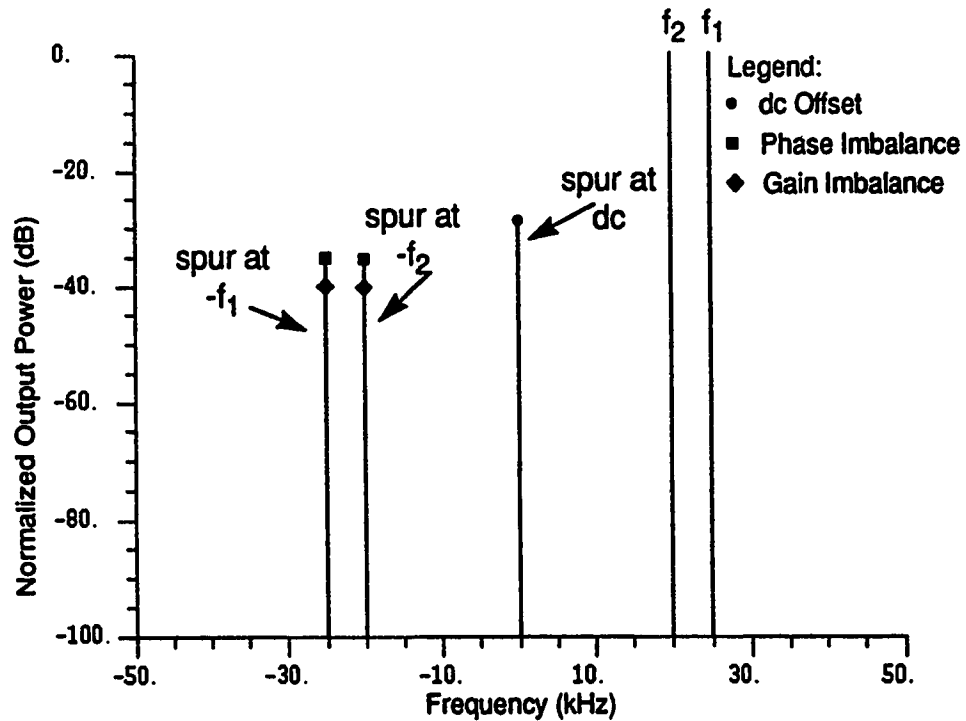


**Figure 4.26 Spurs Caused by the Modulator Distortion**

These simulation results are at baseband, however, if the signal is upconverted to a carrier frequency,  $f_c$ , the two-tone input would appear at  $f_c+f_1$  and  $f_c+f_2$ . The spurious tones would appear at  $f_c$ ,  $f_c-f_1$ , and  $f_c-f_2$ . These unequal sidebands result from the combined amplitude and phase distortion introduced by the modulator.

In the next simulations, the linear amplifier is replaced with the class AB nonlinear amplifier. This results in intermodulation distortion of the modulator spurs. The resulting spectra for the three cases are shown in Figure 4.27.

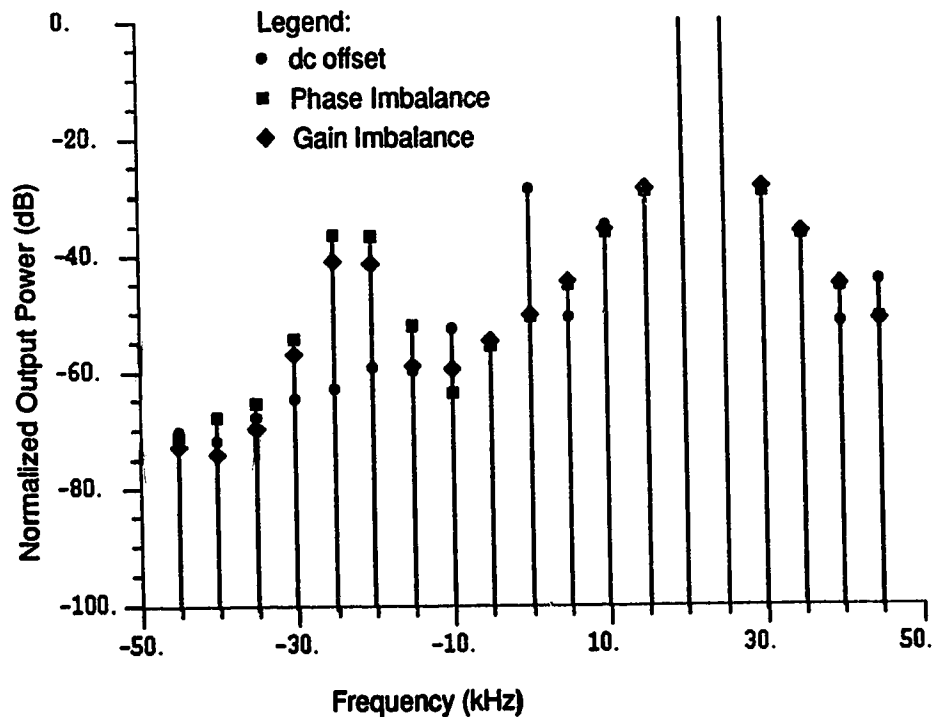


**Figure 4.27 IM Products and Spurs Resulting from Each Type of Modulator Distortion with a Nonlinear Amplifier**

Figure 4.28 shows the effect of combining the modulation distortions. The modulation distortion was represented by a relative dc offset of 2% of the signal amplitude, a relative gain imbalance of 2%, and a phase imbalance of 2°.

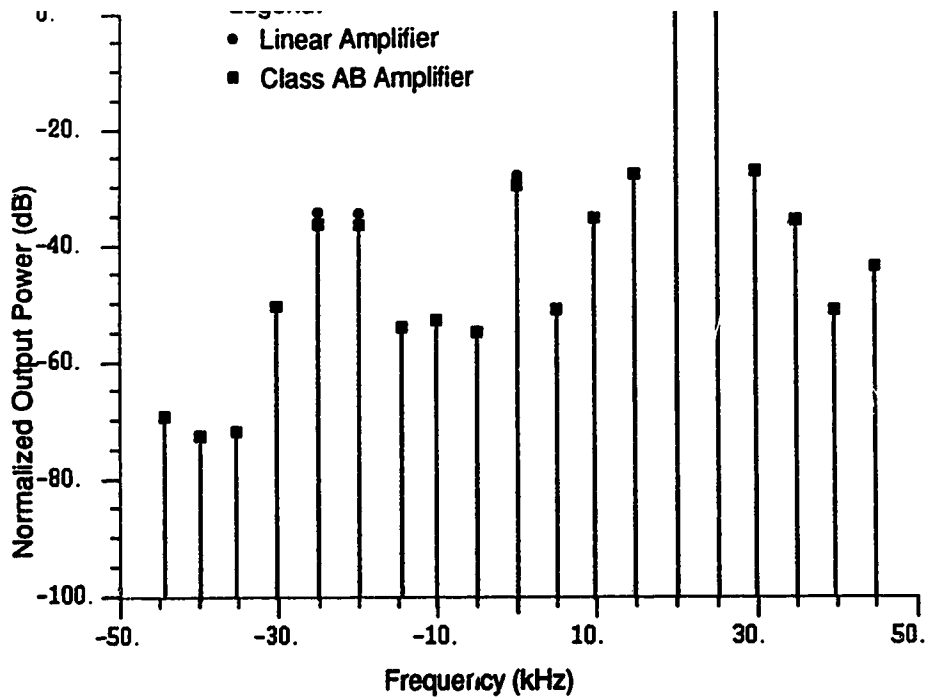


**Figure 4.28 IM Products and Spurs from Modulation Distortion for a Linear Amplifier and a Class AB Amplifier**

Figure 4.28 shows that with the class AB amplifier and a non-ideal modulator, the spurs at -20 kHz and at -25 kHz are approximately -35 dB, while the spur at dc is approximately -23 dB.  $IM_3$  is -28 dB and  $IM_5$  is -35.5 dB. Thus, the spurs at -20 kHz, at -25 kHz, and at dc have increased only slightly (1 dB to 2 dB) compared to the system with linear amplification. As well,  $IM_3$  and  $IM_5$  are similar to the system with ideal modulation.

The demodulator also adds distortion. The next set of simulations considered a system with an ideal modulator, an amplifier, and non-ideal demodulator. The demodulator has a relative dc offset of 2% of the signal amplitude, a relative gain imbalance of 2%, and a phase imbalance of  $2^\circ$ . This system is shown in Figure 4.29.

Figure 4.30 shows the output of the non-ideal demodulator with a) a linear amplifier and b) the class AB amplifier.

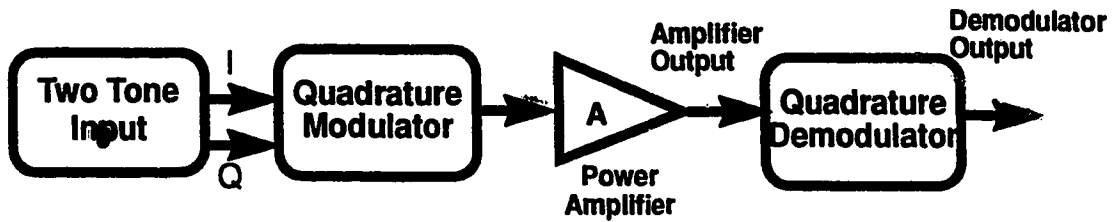


**Figure 4.29 System with Non-Ideal Demodulator**

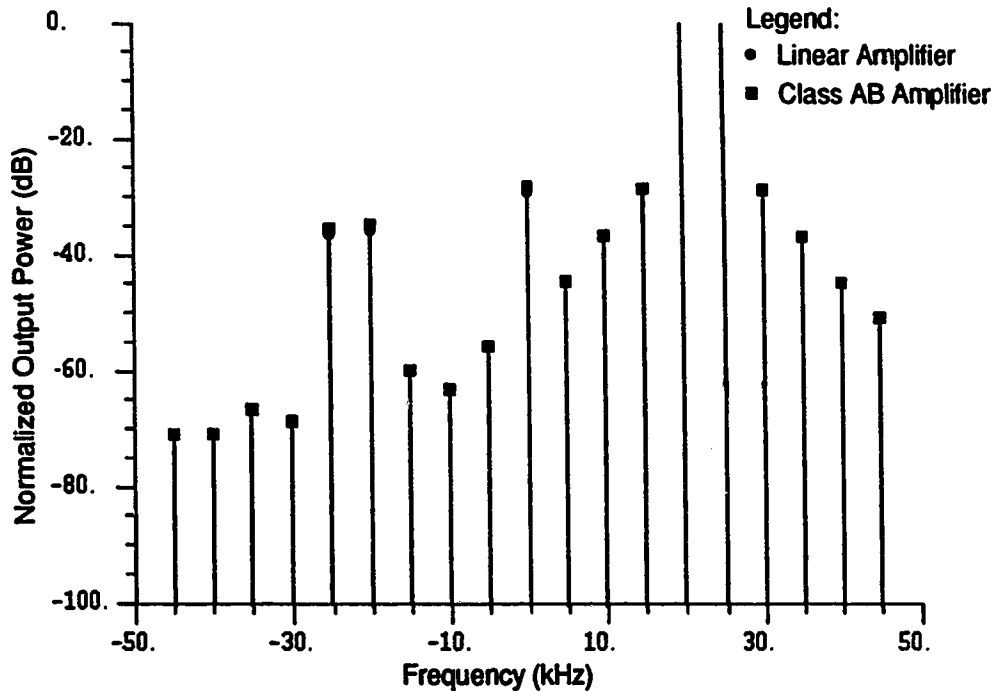


**Figure 4.30 IM Products and Spurs at the Demodulator Output Resulting from Amplifier and Demodulator Distortion**

With a linear amplifier, the demodulation distortion results in spurs at the output of the demodulator of -35.4 dB at -20 kHz and at -25 kHz (from the gain and phase imbalance) while the dc offset adds a spur of -28 dB at dc. With the class AB amplifier, the demodulator add spurs to the IM products. The resulting spurs at the output of the demodulator are: -36.6 dB at -20 kHz and at -25 kHz, and -28.8 dB at dc. The output of the amplifier is unaffected by the demodulator distortion.



This subsection discusses the effects of the modulation and demodulation distortion on the transmitter with a class AB amplifier and a complex gain predistorter.

Figure 4.31 shows the output spectrum of the class AB amplifier when the modulations errors are considered with a complex gain system.

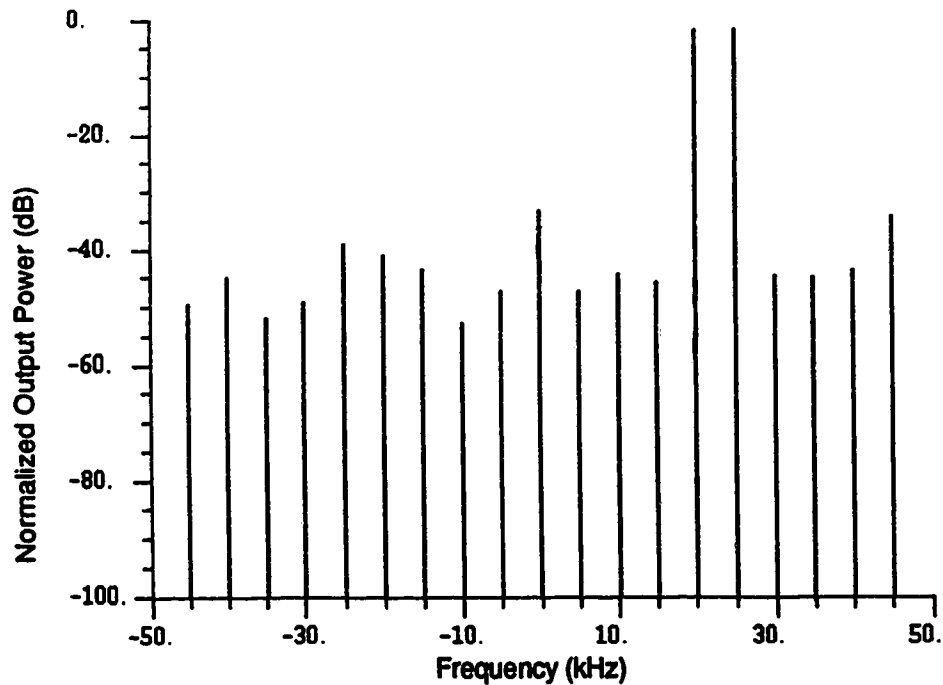


**Figure 4.31 IM Products and Spurs of the Complex Gain System with Amplifier and Modulator Distortion**

The complex gain system results in a reduction in the spurs of only 4 dB to 5 dB at -25 kHz, at -20 kHz, and at dc. The IM products are reduced by 9.5 dB for  $IM_5$  and by 17.2 dB for  $IM_3$ . A complex gain system without modulation distortion reduces both  $IM_3$  and  $IM_5$  by approximately 35 dB (see Figure 4.28).

Figure 4.32 shows the output of the system with an ideal modulator, a class AB amplifier, and a non-ideal demodulator. It is important to note that this result is

feedback introduces the distortion caused by the non-ideal demodulator at the output of the amplifier.

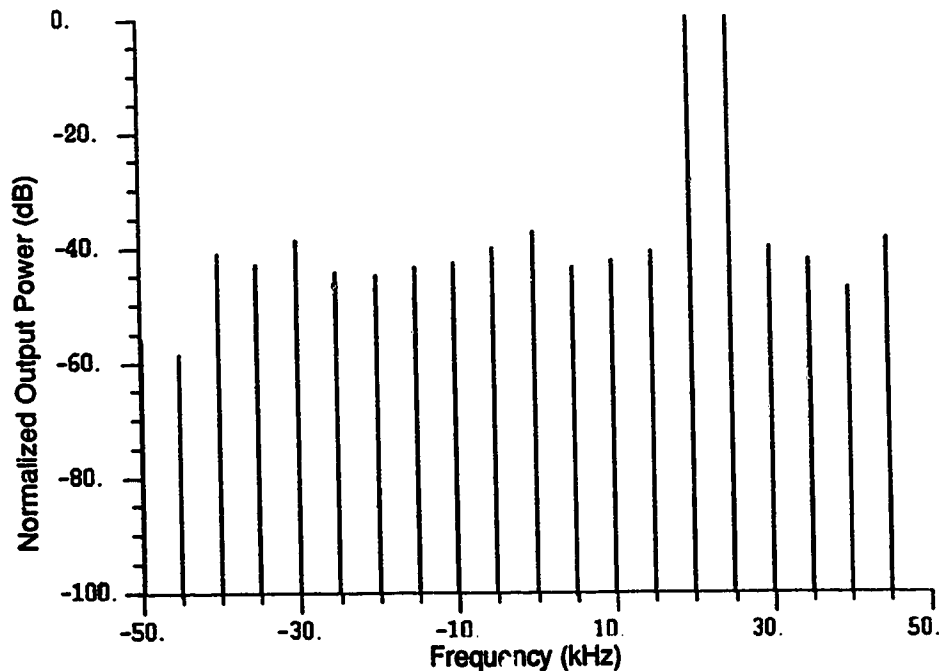


**Figure 4.32 IM Products and Spurs of the Complex Gain System with Amplifier and Demodulator Distortion (Amplifier Output)**

Figure 4.32 shows spurs at -25 kHz of -44.54 dB, at -20 kHz of -45.16 dB, and at dc of -37.96 dB.  $IM_5$  and  $IM_3$  are now -42.5 dB and -41 dB, respectively. For this case, the spurs resulting from the demodulation distortion are now introduced at the output of the amplifier and  $IM_5$  and  $IM_3$  are reduced by only 6.5 dB and 13 dB, respectively.

The next system simulated includes a non-ideal modulator, a class AB amplifier and non-ideal demodulator. Again, the output is taken after the amplifier. The resultant spectrum is shown in Figure 4.33.

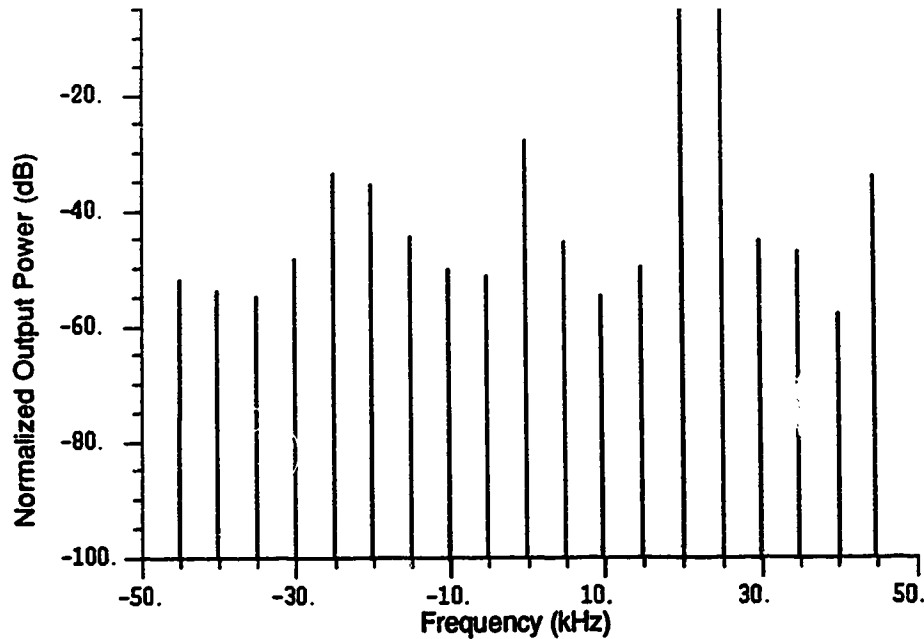


**Figure 4.33 IM Products and Spurs of the Complex Gain System with Modulator, Amplifier, and Demodulator Distortion (Amplifier Output)**

Now, the spurs at -25 kHz, at -20 kHz, and at dc are -31.6 dB, -31.1 dB, and -23.1 dB, respectively. The reduction in the spurs is only around 1 dB. The reduction in IM products is: 17 dB for  $IM_{5,lower}$ , 12 dB for  $IM_{5,upper}$ , 18 dB for  $IM_{3,lower}$ , and 17 dB for  $IM_{3,upper}$ . Thus, the spurs caused by the non-ideal modulator and demodulator have not been reduced significantly. Although the IM products have been reduced by almost 20 dB, this is still considerably less than the reduction (35 dB) obtained for the complex gain system without modulation or demodulation distortion. As well, Figure 4.33 shows that there are significantly sized (> -60 dB) intermodulation and harmonic distortion products throughout the spectrum.

The final distortion to include with the complex gain system is the phase shift,  $\theta$ , introduced by the coupling of the power amplifier output into the feedback path. The resultant spectrum of a complex gain system with a class AB amplifier,

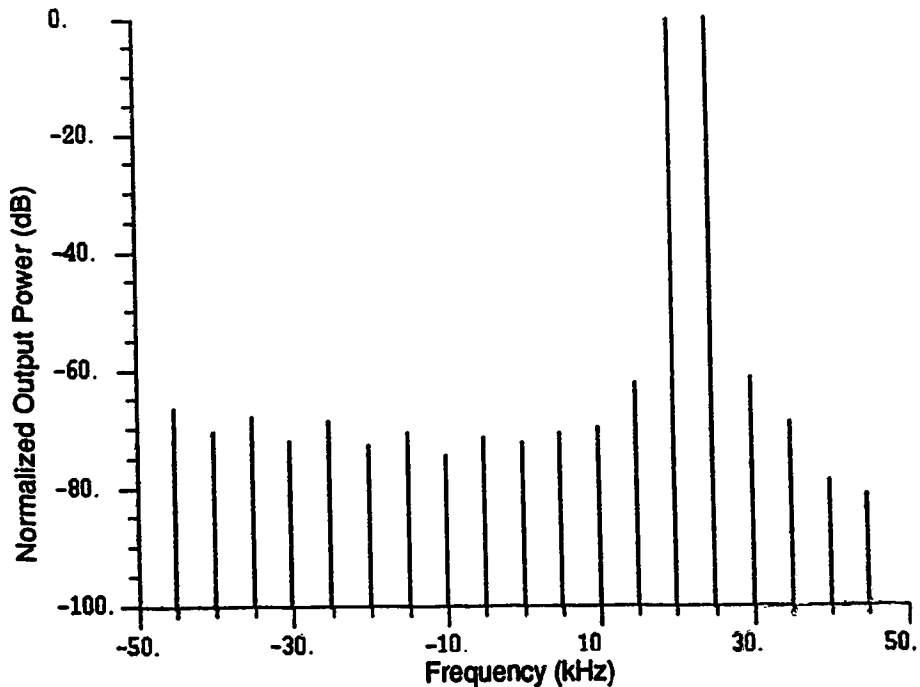


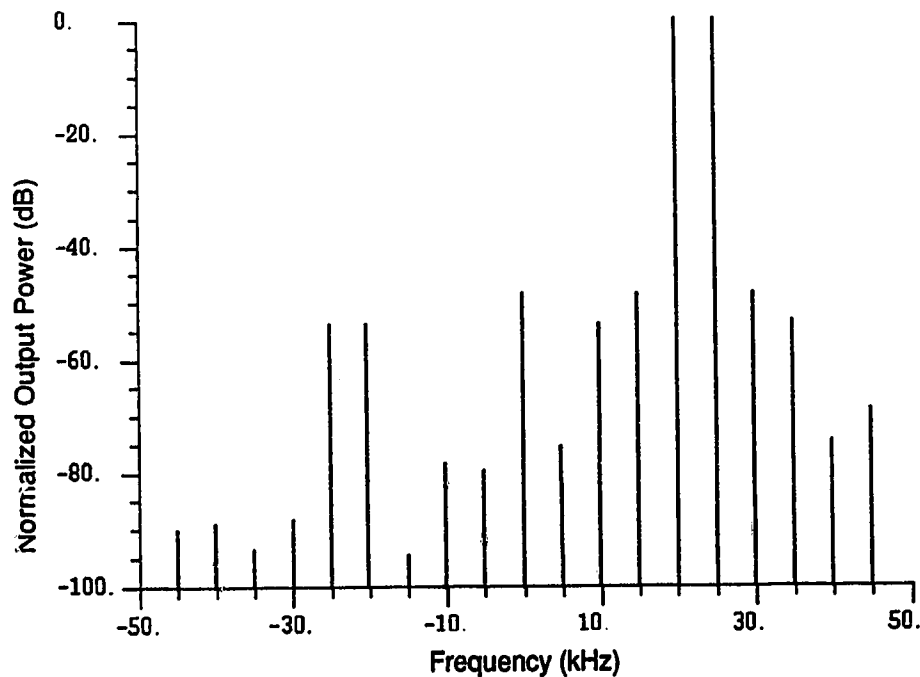
**Figure 4.34 IM products of the Complex Gain System with a Phase Shift in the Feedback Path**

This has minimal effect on the system and the additional phase shift does not cause any additional spurs.  $IM_5$  and  $IM_3$  are reduced by approximately 35 dB. The results are comparable to the complex gain system without the additional phase shift. Additional simulations to increase this phase shift were also performed. Again, there was no appreciable difference in the results. The operation of the complex gain predistorter depends only on the power of the signals and thus is unaffected by a constant phase shift.

#### **4.6.3 Cartesian Coordinate Feedback System**

This sub-section discusses the effects of the modulation and demodulation distortion on the transmitter with a class AB amplifier and a Cartesian coordinate negative feedback linearizer. This system has a loop gain of 10.

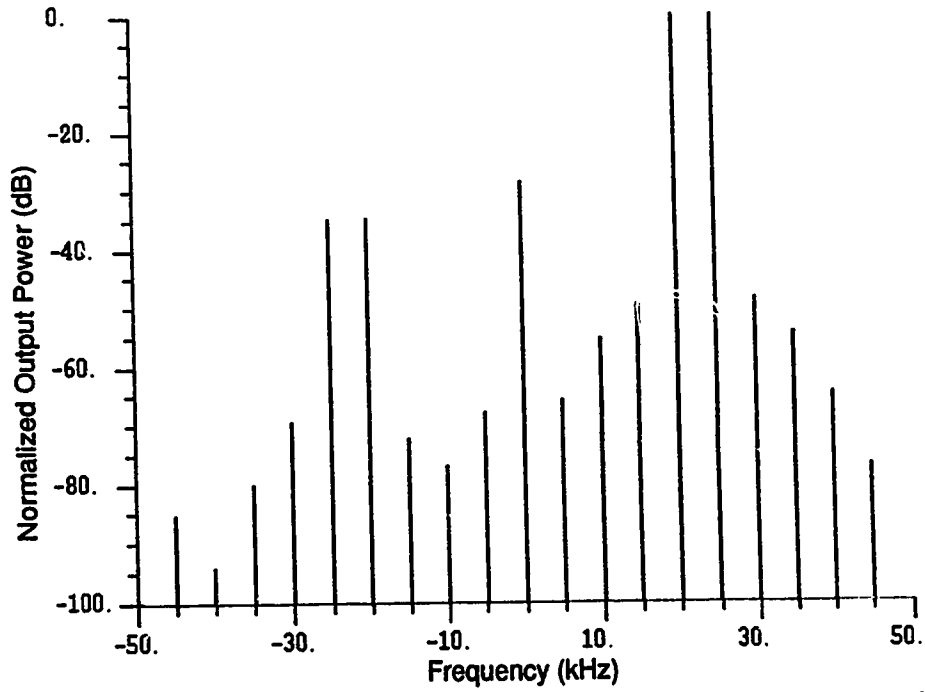
Figure 4.35 shows the output spectrum of the system with a non-ideal modulator.



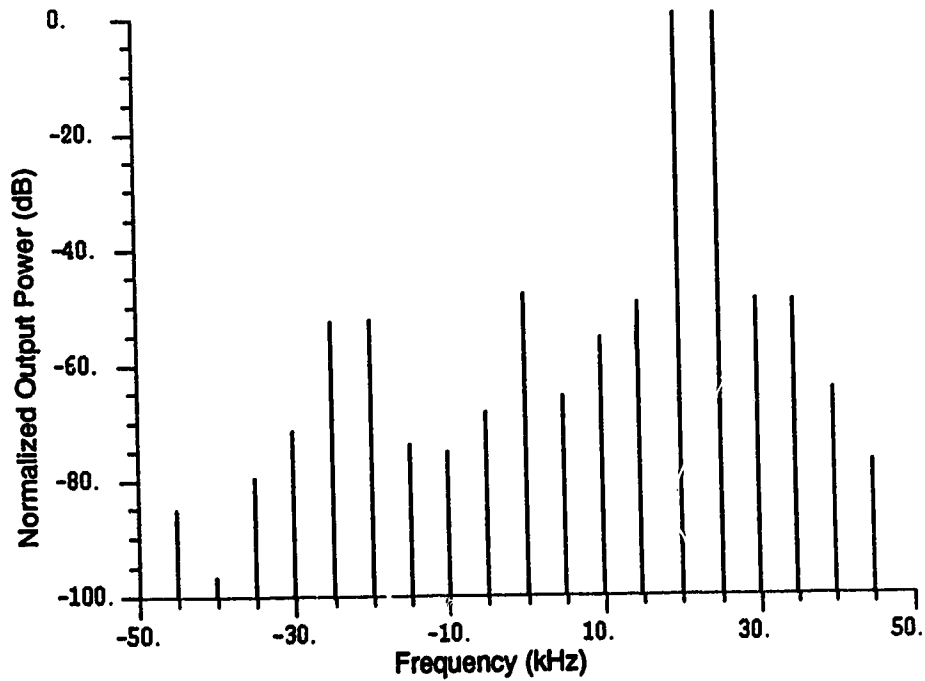
**Figure 4.35 IM Products and Spurs of the Cartesian System with Amplifier and Modulator Distortion**

Figure 4.35 shows that the modulation distortion has been reduced significantly. The spurs at -20 kHz and -25 kHz are reduced from approximately -35.5 dB to -54 dB and the spur at dc is reduced from -29.3 dB to -48.7 dB. Thus, the modulator spurs are reduced by approximately 20 dB.  $IM_5$  is reduced from -35.5 dB to -55 dB, and  $IM_3$  is reduced from -28.3 dB to -49 dB. This reduction of close to 20 dB for  $IM_5$  and  $IM_3$  compares to a reduction of close to 22 dB for the Cartesian system with an ideal modulator (see Figure 4.28).

The next results are for a simulated system including a class AB amplifier and a non-ideal demodulator. The spectrum at the output of the amplifier is shown in Figure 4.36, while Figure 4.37 shows the spectrum at the output of the demodulator.



**Figure 4.36 IM Products and Spurs of the Cartesian System with Amplifier and Demodulator Distortion (Amplifier Output)**



**Figure 4.37 IM Products and Spurs of the Cartesian System with Amplifier and Demodulator Distortion (Demodulator Output)**

Again, the demodulation distortion appears at the output of the amplifier. While  $IM_5$  and  $IM_3$  are reduced by 20 dB, the demodulation distortion results in spurs of -35 dB at both -20 kHz and -25 kHz and a spur of -30 dB at dc. However, the output of the demodulator shows close to a 20 dB reduction in these spurs. Thus, the spectrum at the output of the demodulator is reduced instead of the output of the amplifier.

The next system simulated includes a non-ideal modulator, a class AB amplifier, and a non-ideal demodulator. Figure 4.38 displays the spectrum at the output of the amplifier.

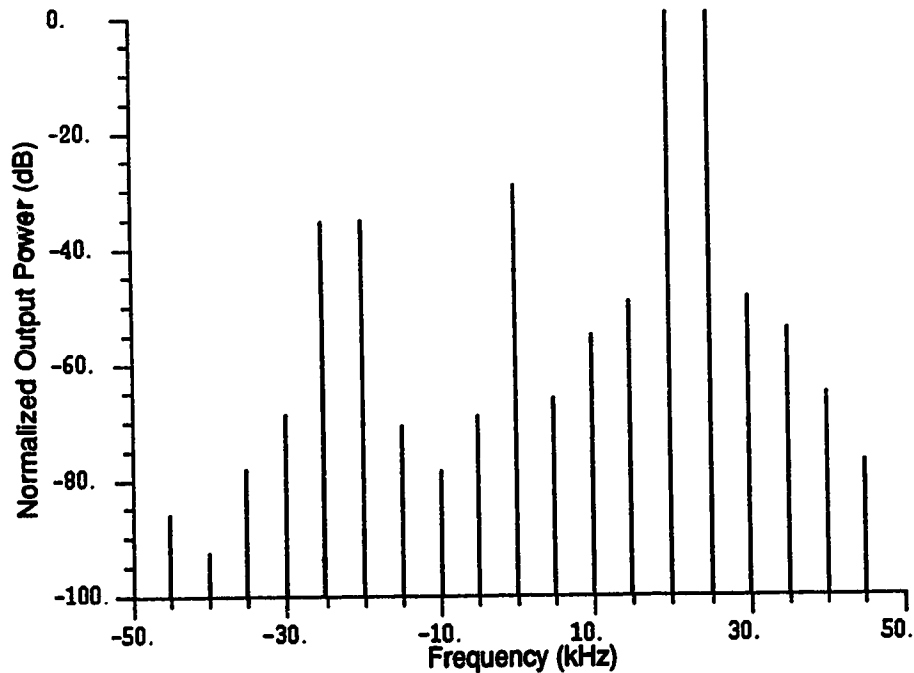


**Figure 4.38 IM Products and Spurs of the Cartesian System with Modulator, Amplifier and Demodulator Distortion (Amplifier Output)**

From Figure 4.38 the spurs at -25 kHz, at -20 kHz and at dc are not reduced significantly. However,  $IM_3$  and  $IM_5$  are reduced by about 20 dB. Although these results seem similar to the results obtained for the complex gain system, a

comparison of Figures 4.33 and 4.38 shows that the additional intermodulation and harmonic distortion spurs are reduced to below -60 dB for the Cartesian system.

#### **4.6.4 Modulation and Demodulation Distortion Summary**

The representative modulation and demodulation distortion adds spurious tones, caused by a two-tone test signal, to the spectrum at  $-f_1$  and  $-f_2$  (-32 dB) and at dc (-23 dB). The Cartesian feedback system reduces the spurious tones generated by the modulation distortion by approximately 20 dB. The spurious tones produced by the demodulation distortion are not reduced, as these are in the feedback path. The complex gain predistorter cannot adapt to the modulation distortion. It reduces the spurs from the modulation distortion by less than 5 dB. The spurious tones produced by the demodulation distortion are also not reduced. When modulation distortion is considered, the Cartesian feedback is superior in reducing the resulting output distortion, since the complex gain predistorter cannot correct for it. The demodulation distortion is critical for both systems, as neither system can reduce its effect.

### **4.7 Summary of Results**

A complex envelope simulation model has been used to compare the performance of the complex gain predistorter and of the Cartesian coordinate negative feedback system. Representative modulation distortion and demodulation distortion values were included in the model.

Using two-tone tests,  $IM_3$  and  $IM_5$  for the uncompensated class AB amplifier were found to be -28.6 dB and -36.3 dB, respectively. The complex gain system reduces  $IM_3$  and  $IM_5$  to -64.3 dB and -71 dB, respectively. This corresponds to a reduction of approximately 35 dB. The other harmonic and IM products are reduced to less than -60 dB. The Cartesian feedback system reduces  $IM_3$  and  $IM_5$



to -48.5 dB and -55.5 dB, respectively. This corresponds to a reduction in the IM products of 20 dB. Additionally, the other harmonic and IM distortion are reduced to below -60 dB.

With a  $\pi/4$  DQPSK input signal, the Cartesian system reduces the out-of-band power by approximately 22 dB in each channel for the class AB amplifier. The complex gain system reduces the out-of-band power by approximately 30 dB in channel 1, 22 dB in channel 2, and by 10 dB in channel 3.

The complex gain system reduces  $IM_3$  and  $IM_5$  products to a lower level than the Cartesian feedback system. Both systems reduce the out-of-band power to acceptable levels, however the complex gain system has less power close to the transmitting channel (channel 1) and the Cartesian system reduces power better farther from the transmitting channel (channel 3).

The representative modulation and demodulation distortion adds spurious tones, caused by a two-tone test signal, to the spectrum at  $-f_1$  and  $-f_2$ . These spurious tones generated by the modulation distortion are reduced by the Cartesian feedback system by approximately 20 dB. However, the spurious tones caused by the demodulation distortion are in the feedback path, and are not reduced. The complex gain predistorter reduces the spurs from the modulation distortion by less than 5 dB and does not reduce the spurious tones produced by the demodulator. Thus, the Cartesian feedback is superior in reducing the resulting output distortion, since the complex gain predistorter cannot correct for it. Neither system can reduce the demodulation distortion.

## 5. Summary And Conclusions

This chapter summarizes the research results produced by this project. The simulation models are discussed in Section 5.1. Next, in Section 5.2, the results obtained by comparing the two techniques are discussed. The feasibility of implementing the two linearization systems is discussed in Section 5.3. Finally, recommendations for further work in this area are presented in Section 5.4.

### 5.1 Simulation Models

In order to increase the capacity of cellular radio systems, spectrally efficient linear modulation techniques have been proposed. The EIA/TIA interim standard, IS-54, specifies  $\pi/4$  shifted differential phase shift keying ( $\pi/4$  DQPSK). Although this modulation technique is spectrally efficient, it has significant RF envelope fluctuation. Thus, if the transmitter output signal is to have low out-of-band power, highly linear RF power amplifiers are required. Such linear power amplifiers have a lower dc-to-ac conversion efficiency than less linear power amplifiers. However, nonlinear power amplifiers exhibit amplitude-to-amplitude distortion (AM-AM) and amplitude-to-phase distortion (AM-PM). To reduce these distortion effects, predistortion techniques are used so that, ideally, the output of the nonlinear amplifier is an amplified replica of the original signal. However, the amplifier is not the only source of distortion in the transmitter. The non-ideal modulator and demodulator also introduce distortion in the output signal, such as dc offset, differential gain, and differential phase. In this thesis, two prominent predistortion methods are compared: complex gain adaptive predistortion and Cartesian coordinate negative feedback.

Computer simulation offers a time-efficient method of studying complex systems. A complex envelope simulation model is used to compare the

performance of the two predistortion techniques. The simulation models were developed using a software package by COMDISCO called BOSS (Block Oriented System Simulator). It is an interactive environment for the simulation-based analysis and design of communication systems and runs on a SUN SPARC2 workstation. The simulation models for a transmitter include a random data source, a  $\pi/4$  DQPSK modulator, and a pulse shaping filter. The pulse shaping filter has a linear phase response and a square-root raised cosine frequency response. Two different nonlinear RF power amplifiers, an Avantek 6 Watt class AB amplifier and an 8 Watt, single-ended class B amplifier, were also modeled. These models were developed by measurements of the AM-AM and the AM-PM characteristics of the two nonlinear power amplifiers. Models were also developed for the complex gain predistorter and for the Cartesian coordinate negative feedback linearizer.

Although the simulation models involve the complex envelope representation of the signals, both the complex gain predistorter and the Cartesian coordinate negative feedback systems require modulators to shift the frequency to 850 MHz. Demodulators are also necessary since the output of the amplifier is demodulated and used for feedback. These system components also introduce distortion into the system such as dc offset, gain imbalance and phase imbalance.

Simulation at the carrier frequency would take an impractically long time to execute. Therefore, the simulations are carried out at baseband, with an equivalent distortion added to the system. The modulation and demodulation distortion were represented by a relative dc offset of 2% of the signal amplitude, a relative gain imbalance of 2%, and a phase imbalance of 2°.

The out-of-band power and the intermodulation distortion products are used as criteria for assessing the amplifier nonlinearity. The intermodulation products are a simple measure of the linearity of an amplifier. The IM products are found by

supplying a two-tone test input to the amplifier and measuring the power of the resultant spurious signals. The third- and fifth-order products ( $IM_3$  and  $IM_5$ ) are important, since their frequencies are close to the original tones. For these simulations, tone 1 is at 25 kHz and tone 2 is at 20 kHz. Thus  $IM_3$  is at 30 kHz (upper), and 15 kHz (lower) while  $IM_5$  is at 35 kHz (upper) and 10 kHz (lower).

The amplifier linearity can also be determined by measuring the out-of-band power of the transmitted signal. This is done by estimating the power spectral density (PSD) of the output signal. The PSD is estimated by the squared amplitude of the DFT (discrete Fourier Transform) of the signal. The FFT (fast Fourier Transform) algorithm is used to calculate the DFT. To reduce leakage, the data is windowed by a Blackman window before the calculating FFT. To reduce the variance in each frequency sample, sets of data that overlap by half are averaged together. This provides the power spectral density across the whole frequency band, for  $0 < f < f_c$  (Nyquist critical frequency). In order to find the power in each channel,  $P(f_{chan})$ , the averaged, estimated PSD is integrated over the frequency range of each channel.

The permitted power in each channel is limited by IS-54. For  $\pi/4$  DQPSK modulation, the proposed system has a channel bandwidth of 30 kHz. In the adjacent channel 1 (centered 30 kHz away), IS-54 specifies that the maximum transmitted power is 26 dB below the mean output power. In the next 30 kHz channel (adjacent channel 2), centered 60 kHz away, the allowed power is -45 dB. And, 90 kHz (adjacent channel 3) and more away from the channel center, the maximum out-of-band power is -60 dB.

## 5.2 Summary of Results

The first set of simulations examined the effect of a nonlinear amplifier on the output spectrum of a digital cellular transmitter. These simulations demonstrated that the out-of-band power increases significantly with the inclusion of the nonlinear amplifier. The nonlinear amplifiers increase the out-of-band power to approximately -40 dB in channel 1, -45 dB in channel 2, and -55 dB in channel 3.

The next simulations study the effectiveness of predistortion linearization methods. Using a class AB amplifier, the complex gain system reduces the  $IM_3$  and  $IM_5$  products by 35 dB while the Cartesian feedback system reduces them by 20 dB. Both systems reduce the out-of-band power to acceptable levels, however the complex gain system has less power close to the transmitting channel (channel 1) and the Cartesian system reduces power better farther from the transmitting channel (channel 3). The complex gain system reduces the out-of-band power by approximately 30 dB in channel 1, 22 dB in channel 2, and by 10 dB in channel 3. The Cartesian system reduces the out-of-band power by approximately 22 dB in each channel.

The representative modulation and demodulation distortion adds spurious tones, caused by a two-tone test signal, to the spectrum at  $-f_1$  and  $-f_2$ . The spurious tones generated by the modulation distortion are reduced by the Cartesian feedback system by approximately 20 dB. However, the spurious tones caused by the demodulation distortion are in the feedback path, and are not reduced. The complex gain predistorter reduces the modulation distortion by less than 5 dB and does not reduce the spurious tones produced by the demodulator. The complex gain system assumes that the distortion is dependent on the power of the input signal. However, the modulation distortion is independent of the signal strength. Thus, the Cartesian feedback is superior in reducing the resulting output distortion,

since the complex gain predistorter cannot correct for it. Neither system can compensate for the demodulation distortion since it is in the feedback path.

### **5.3 Implementation Feasibility**

The complex gain system is a DSP based system and requires complex multiplication and division to calculate the predistortion values. As well, this DSP system requires a sampling rate of close to 800 MHz.

Discussions with the Research and Development department of NovAtel Communications Ltd. (a sponsor corporation of TR Labs) indicate that they are investigating the complex gain predistortion scheme and have constructed prototypes of this system [36, 45]. Their investigations have shown that the system performs well at baseband; however, when quadrature modulators and demodulators are included, the performance is degraded. They are currently investigating solutions to the modulator and demodulator distortion. The complex gain predistortion system technology is suitable for base station operation. The high sampling rate and the complex calculations require a powerful DSP (such as a Texas Instruments TMS320C30).

The Cartesian system is an analog system and thus does not require a DSP. It is a much simpler system to implement than the complex gain predistorter. However, the adjustment of the phase must be performed automatically as it varies with carrier frequency. This is described in [14, 30]. The overall simplicity of the system makes it a suitable technique for use in mobile handsets.

## **5.4 Recommendations**

As a consequence of this project, the following topics have been identified for further research:

1. Compensation for the modulator and demodulator nonlinearities. A research project investigating methods of carrier feedthrough compensation is currently underway at TR Labs. Other projects to study either reducing or compensating for gain imbalance and phase imbalance should also be considered.
2. Investigation of different techniques to reduce the dynamic range of the  $\pi/4$  DQPSK signal. This includes investigating pulse shaping filters other than square-root raised cosine filter. One such filter is the QORC (Quadrature Overlapped Raised Cosine) filter. Alternative modulation methods such as OQPSK (offset-keyed QPSK) should also be investigated.

## References

- [1] David J. Goodman, "Trends in Cellular and Cordless Communications", *IEEE Communications Magazine*, vol. 29, no. 6, pp. 3-40, June 1991.
- [2] Arunas G. Sleky, "Exploiting The Digital Radio Wave of the 90's", *Conference Proceedings of Wireless 90*, 16-17 July 1990, Calgary, AB.
- [3] EIA/TIA Interim Standard, *Cellular System Dual-Mode Mobile Station - Base Station Compatibility Standard, IS-54*, Electronic Industries Association, May 1990.
- [4] Simon Haykin, *Communication Systems*. 2nd Edition, New York: John Wiley & Sons, 1983, pp. 465-476.
- [5] Herbert L. Krauss, Charles W. Bostian, Frederick H. Raab, *Solid State Radio Engineering*. New York: John Wiley & Sons, 1980, pp. 394-399.
- [6] B.A. Syrett, "A Feed Forward impatt Amplifier", *Ph.D. Thesis*, University of Alberta, 1976, pp. 8-30.
- [7] V.K. Bhargava, D. Haccoun, R. Matyas, P.P. Nuspl, *Digital Communications By Satellite*. New York: John Wiley & Sons, 1989, pp 96-100.
- [8] Tri T. Ha, *Solid State Microwave Amplifier Design*. New York: John Wiley & Sons, 1981, pp. 202-219.
- [9] Wolfgang J.R. Hofer, "Chapter 4 - Microwave Amplifiers", Ed. Kamilo Feher. *Digital Communications Microwave Applications*. Englewood Cliffs, NJ: Prentice-Hall, Inc., 1981.
- [10] R.D. Stewart, F.F. Tusubira, "Feedforward Linearisation of 950 MHz Amplifiers", *IEE Proceedings*, vol. 135, part H, no. 5, pp. 379-350, October 1988.
- [11] D.C. Cox, "Linear Amplification with Nonlinear Components", *IEEE Transactions on Communications*, vol. COM-22, pp. 1942-1945, December 1974.
- [12] S. Tomisato, K. Chiba, K. Murota, "Phase Error Free LINC Modulator", *Electronics Letters*, vol. 25, pp. 576-577, 27 April 1989.
- [13] Fernando Casadevall, Juan J. Olmos, "On the Behavior of the LINC Transmitter", *Proceedings of the 40th IEEE Vehicular Technology Conference*, 6-9 May 1990, Orlando, FL. New York: IEEE Press, 1990, pp. 29-34.
- [14] A. Bateman, D.M. Haines, R.J. Wilkinson, "Linear Transceiver Architectures", *Proceedings of the 38th IEEE Vehicular Technology Conference*, 15-17 June 1988, Philadelphia, PA. New York: IEEE Press, 1988, pp. 478-484.



- [15] S.A. Hetzel, A. Bateman, J.P. McGeehan, "A LINC Transmitter", *Proceedings of the 41st IEEE Vehicular Technology Conference*, 19-22 May 1991, St. Louis, MO. New York: IEEE Press, 1991, pp. 133-137.
- [16] A. Bateman, R.J. Wilkinson, J.D. Marvill, "The Application of Digital Signal Processing To Transmitter Linearisation", *8th European Conference on Electrotechnics*, 13-17 June 1988, Stockholm, Sweden. New York: IEEE Press, 1988, pp. 64-67.
- [17] F.H. Raab, "Efficiency of Outphasing RF Power-Amplifier Systems", *IEEE Transactions on Communications*, vol. COM-33, pp. 1094-1099, October 1985.
- [18] F.H. Raab, "Efficiency of Doherty RF Power-Amplifier Systems", *IEEE Transactions on Broadcasting*, vol. BC-33, pp. 77-83, September 1987.
- [19] A.A.M. Saleh, J. Salz, "Adaptive Linearization of Power Amplifiers in Digital Radio Systems", *The Bell System Technical Journal*, vol. 62, pp. 1019-1033, April 1983.
- [20] Yoshinori Nagata, "Linear Amplification Technique for Digital Mobile Communications", *Proceedings of the 39th IEEE Vehicular Technology Conference*, 1-3 May 1989, San Francisco, CA. New York: IEEE Press, 1989, pp. 159-164.
- [21] James K. Cavers, "A Linearizing Predistorter with Fast Adaptation", *Proceedings of the 40th IEEE Vehicular Technology Conference*, 6-9 May 1990, Orlando, FL. New York: IEEE Press, 1990, pp. 41-47.
- [22] James K. Cavers, "Amplifier Linearization Using a Digital Predistorter with Fast Adaption and Low Memory Requirements", *IEEE Transaction on Vehicular Technology*, vol. VT-39, no. 4, pp. 374-382, November 1990.
- [23] M. Faulkner, T. Mattsson, W. Yates, "Adaptive Linearisation using Pre-Distortion", *Proceedings of the 40th IEEE Vehicular Technology Conference*, 6-9 May 1990, Orlando, FL. New York: IEEE Press, 1990, pp. 35-39.
- [24] R.L. Johnston, *Numerical Methods: A Software Approach*. New York: John Wiley & Sons, 1982, pp. 159-177.
- [25] Y. Akaiwa, Y. Nagata, "Highly Efficient Digital Mobile Communications with a Linear Modulation Method", *IEEE Journal on Selected Areas in Communication*, vol. SAC-5, no. 5, pp. 890-895, June 1987.
- [26] A. Bateman, D. Haines, R.J. Wilkinson, "Direct Conversion Linear Transceiver Design", *Proceedings of the 5th IEE International Conference on Mobile Radio and Personal Communications*, 11-14 December 1989, Coventry, UK., pp. 53-56.

- [27] A. Bateman, D. Haines, "Direct Conversion Transceiver Design for Compact Low-Cost Portable Mobile Radio Terminals", *Proceedings of the 39th IEEE Vehicular Technology Conference*, 1-3 May 1989, San Francisco, CA. New York: IEEE Press, 1989, pp. 57-62.
- [28] M. Minowa, M. Onoda, E. Fukuda, Y. Daido, "Backoff Improvement of an 800 MHz GaAs FET Amplifier for a QPSK Transmitter using an Adaptive Nonlinear Distortion Canceller", *Proceedings of the 40th IEEE Vehicular Technology Conference*, 6-9 May 1990, Orlando, FL. New York: IEEE Press, 1990, pp. 542-546.
- [29] S. Ono, N. Kondoh, Y. Shimazaki, "Digital Cellular System with Linear Modulation", *Proceedings of the 39th IEEE Vehicular Technology Conference*, 1-3 May 1989, San Francisco, CA. New York: IEEE Press, 1989, pp. 44-49.
- [30] M. Johannsson, T. Mattsson, "Transmitter Linearization Using Cartesian Feedback For Linear TDMA Modulation", *Proceedings of the 41st IEEE Vehicular Technology Conference*, 19-21 May 1991, St. Louis, MO. New York: IEEE Press, 1991, pp. 439-444.
- [31] COMDISCO Systems, Inc., *Block Oriented Systems Simulator (BOSS) User's Guide*, COMDISCO Systems, Inc., Foster City, CA, 1989.
- [32] R. Sharma, "Forward-Error-Control Assisted Adaptive Equalization in Digital Mobile Radio", *M.Sc. Thesis*, University of Alberta, 1991, pp. 30-37.
- [33] S. Chennakeshu, G.J. Saulnier, "Differential Detection of  $\pi/4$ -Shifted-DQPSK for Digital Cellular Radio", *Proceedings of the 41st IEEE Vehicular Technology Conference*, 19-21 May 1991, St. Louis, MO. New York: IEEE Press, 1991, pp. 186-191.
- [34] C-L. Liu, K. Feher, "Noncoherent Detection of  $\pi/4$ -QPSK Systems in a CCI-AWGN Combined Interference Environment", *Proceedings of the 39th IEEE Vehicular Technology Conference*, 1-3 May 1989, San Francisco, CA. New York: IEEE Press, 1989, pp. 83-94.
- [35] S. Ariyvisitakul, T-P. Liu, "Characterizing the Effects of Nonlinear Amplifiers on Linear Modulation for Digital Portable Radio Communications", *IEEE Transactions on Vehicular Technology*, vol. VT-39, no 4, pp. 383-389, November 1990.
- [36] Correspondence with A. Wright, NovAtel, Calgary, AB, 1991, 1992.
- [37] B. Cain, "Temperature Effects on an RF Power Amplifier", *M.Sc. Thesis*, University of Alberta, 1991, pp. 99-110.
- [38] M. Faulkner, M. Johannsson, W. Yates, "Error Sensitivity of Power Amplifiers Using Pre-Distortion", *Proceedings of the 41st IEEE Vehicular Technology Conference*, 19-21 May 1991, St. Louis, MO. New York: IEEE Press, 1991, pp. 451-456.

- [39] James K. Cavers, "Adaptive Compensation for Imbalance and Offset Losses In Direct Conversion Transceivers", *Proceedings of the 41st IEEE Vehicular Technology Conference*, 19-21 May 1991, St. Louis, MO. New York: IEEE Press, 1991, pp. 578-583.
- [40] K. Anvari, M. Kaube, B. Hriskevich, "Performance of a Direct Conversion Receiver with a  $\pi/4$ -DQPSK Modulated Signal", *Proceedings of the 41st IEEE Vehicular Technology Conference*, 19-21 May 1991, St. Louis, MO. New York: IEEE Press, 1991, pp. 822-827.
- [41] William H. Press, Brian P. Flannery, Saul A. Teukolsky, William T. Vetterling, *Numerical Recipes: The Art of Scientific Computing*. Cambridge: Press Syndicate of the University of Cambridge, 1986, pp. 420-429.
- [42] Nezih C. Geckinli, Davras Yavuz, *Discrete Fourier Transformation and Its Applications to Power Spectra Estimation*. Amsterdam: Elsevier Scientific Publishing Company, 1983, pp. 93-150.
- [43] Peter D. Welch, "The Use of Fast Fourier Transform for the Estimation of Power Spectra: A Method Based on Time Averaging Over Short, Modified Periodograms." Childers, Donald G. ed., *Modern Spectrum Analysis*. New York, IEEE Press, 1978.
- [44] William D. Stanley, Gary R. Dougherty, Ray Dougherty, *Digital Signal Processing*. Reston: Reston Publishing Company, Inc., 1984, pp. 226-242, 301-309.
- [45] Andrew Wright, "Experimental Performance of an Adaptive Digital Linearized Power Amplifier", *Proceedings of the IEEE International Microwave Symposium*, 1-5 June 1992, Albuquerque, NM, Session Z.4.

## Appendix A

This Appendix gives the normalized AM-AM and AM-PM characteristics for the class AB and the class B amplifiers.

**Table A1.1 The Normalized AM-AM and AM-PM Conversion Factors for the Class AB Amplifier**

Input (dB)	Output (dB)	Phase (degrees)
-10.45757	-11.1362	-1.4177
-10.17277	-10.8118	-1.2986
-9.89700	-10.49822	-0.9026
-9.62972	-10.18631	0.1879
-9.37042	-9.87333	0.2171
-9.11864	-9.56188	0.3197
-8.87395	-9.26077	0.4832
-8.63597	-8.98124	0.531
-8.40433	-8.72045	0.6520
-8.17871	-8.46666	0.7282
-7.95880	-8.21628	0.8450
-7.74432	-7.97391	1.0429
-7.53501	-7.74200	1.2496
-7.33063	-7.51773	1.4585
-7.13095	-7.29805	1.6598
-6.93575	-7.08246	1.8540
-6.74484	-6.87164	2.0455
-6.55804	-6.66650	2.2355
-6.37517	-6.46834	2.4180
-6.19608	-6.27834	2.5864
-6.02060	-6.09450	2.7355
-5.84860	-5.91185	2.8619
-5.67993	-5.72592	2.9635

**Table A1.1 The Normalized AM-AM and AM-PM Conversion Factors for the Class AB Amplifier**

Input (dB)	Output (dB)	Phase (degrees)
-5.51448	-5.53890	3.0529
-5.35212	-5.35741	3.1531
-5.19275	-5.18765	3.2852
-5.03624	-5.02982	3.4447
-4.88250	-4.87969	3.6083
-4.73144	-4.73302	3.7523
-4.58296	-4.58793	3.8705
-4.43698	-4.44568	3.9793
-4.29340	-4.30776	4.0967
-4.15217	-4.17518	4.2351
-4.01319	-4.04680	4.3830
-3.87640	-3.92093	4.5228
-3.74173	-3.79589	4.6368
-3.60912	-3.67141	4.7166
-3.47850	-3.54917	4.7670
-3.34982	-3.43105	4.7935
-3.22302	-3.31882	4.8021
-3.09804	-3.21246	4.7997
-2.97483	-3.11031	4.7945
-2.85335	-3.01061	4.7945
-2.73354	-2.91163	4.8077
-2.61537	-2.81279	4.8339
-2.49877	-2.71473	4.8641
-2.38373	-2.61816	4.8892
-2.27019	-2.52377	4.8999
-2.15811	-2.43215	4.8912

**Table A1.1 The Normalized AM-AM and AM-PM Conversion Factors for the Class AB Amplifier**

Input (dB)	Output (dB)	Phase (degrees)
-2.04746	-2.34346	4.8687
-1.93820	-2.25785	4.8391
-1.83030	-2.17545	4.8092
-1.72372	-2.09638	4.7853
-1.61844	-2.02032	4.7641
-1.51441	-1.94666	4.7358
-1.41162	-1.87476	4.6903
-1.31003	-1.80398	4.6176
-1.20961	-1.73376	4.5093
-1.11035	-1.66425	4.3694
-1.01220	-1.59587	4.2071
-0.915150	-1.52908	4.0318
-0.819172	-1.46434	3.8527
-0.724243	-1.40208	3.6787
-0.630341	-1.34244	3.5110
-0.537443	-1.28535	3.3471
-0.445528	-1.23076	3.1841
-0.354575	-1.17861	3.0194
-0.264565	-1.12884	2.8501
-0.175478	-1.08137	2.6731
-8.72959E-02	-1.03606	2.4848
0.	-0.992751	2.2816

**Table A1.2 The Normalized AM-AM and AM-PM Conversion Factors for the Class B Amplifier**

Input (dB)	Output (dB)	Phase (degrees)
-10.45757	-10.23587	1.1364
-10.17277	-9.89631	1.4085
-9.89700	-9.57408	1.6790
-9.62972	-9.26515	1.9216
-9.37042	-8.96375	2.0990
-9.11864	-8.66448	2.1763
-8.87395	-8.36234	2.1212
-8.63597	-8.05572	1.9220
-8.40433	-7.76260	1.6864
-8.17871	-7.50415	1.5497
-7.95880	-7.27244	1.5400
-7.74432	-7.04606	1.6338
-7.53501	-6.80979	1.8116
-7.33063	-6.57164	2.0681
-7.13095	-6.34480	2.4015
-6.93575	-6.13149	2.7942
-6.74484	-5.92413	3.2149
-6.55804	-5.71631	3.6355
-6.37517	-5.50827	4.0402
-6.19608	-5.30236	4.4176
-6.02060	-5.10080	4.7572
-5.84860	-4.90569	5.0489
-5.67993	-4.71838	5.2877
-5.51448	-4.53863	5.4803
-5.35212	-4.36599	5.6342

**Table A1.2 The Normalized AM-AM and AM-PM Conversion Factors for the Class B Amplifier**

Input (dB)	Output (dB)	Phase (degrees)
-5.19275	-4.20004	5.7567
-5.03624	-4.04035	5.8550
-4.88250	-3.88655	5.9355
-4.73144	-3.73827	6.0046
-4.58296	-3.59514	6.0681
-4.43698	-3.45685	6.1317
-4.29340	-3.32306	6.2006
-4.15217	-3.19348	6.2797
-4.01319	-3.06785	6.3699
-3.87640	-2.94598	6.4691
-3.74173	-2.82766	6.5755
-3.60912	-2.71270	6.6873
-3.47850	-2.60094	6.8027
-3.34982	-2.49218	6.9203
-3.22302	-2.38627	7.0384
-3.09804	-2.28306	7.1555
-2.97483	-2.18239	7.2703
-2.85335	-2.08411	7.3814
-2.73354	-1.98809	7.4875
-2.61537	-1.89421	7.5882
-2.49877	-1.80239	7.6838
-2.38373	-1.71255	7.7750
-2.27019	-1.62460	7.8622
-2.15811	-1.53848	7.9459
-2.04746	-1.45411	8.0267
-1.93820	-1.37142	8.1050



**Table A1.2 The Normalized AM-AM and AM-PM Conversion Factors for the Class B Amplifier**

Input (dB)	Output (dB)	Phase (degrees)
-1.83030	-1.29036	8.1811
-1.72372	-1.21084	8.2557
-1.61844	-1.13281	8.3290
-1.51441	-1.05622	8.4014
-1.41162	-0.981005	8.4732
-1.31003	-0.907139	8.5445
-1.20961	-0.834591	8.6153
-1.11035	-0.763333	8.6855
-1.01220	-0.693339	8.7550
-0.915150	-0.624582	8.8239
-0.819172	-0.557036	8.8922
-0.724243	-0.490680	8.9597
-0.630341	-0.425488	9.0265
-0.537443	-0.361438	9.0925
-0.445528	-0.298506	9.1578
-0.354575	-0.236673	9.2222
-0.264565	-0.175916	9.2859
-0.175478	-0.116215	9.3487
-8.72959E-02	-5.75530E-02	9.4106
0.	9.31885E-05	9.4717

## Appendix B

The next two Appendices give the listings for the FORTRAN subroutines used to construct BOSS models which could be constructed from the BOSS library. These subroutines were written for this project. The following listing is for the BOSS primitive to perform the SECANT iteration. It calculates a new predistortion value based on the previous two calculations and their resultant errors. The calculated values are stored in the lookup table. The subroutine called each time a SECANT calculation is done. All BOSS primitives are re-entrant.

```
c ****SECANT - BOSS PRIMITIVE ****
c
c This subroutine performs the calculations for a secant iteration
c
  subroutine secant1(fk0, fk1, eg0, eg1,
+   enable, n, n1, wr_enable, finished, fk2,
+   try1, try2, max_iter, err_min, err_max )
  logical*1 enable, wr_enable , finished
  integer n, n1, max_iter
  complex fk0, fk1, eg0, eg1, fk2, try1, try2
  real err_min, err_max
  wr_enable = .FALSE.
  finished = .FALSE.

c
c If this block is not enabled, jump to the end
  IF ( .NOT. enable) THEN
    GOTO 200
  ENDIF
c if it is the first time through for this address,
c use initial guess one and skip the calculations.
  IF (n .EQ. 0) THEN
    fk2 = try1
    n1 = 1
    wr_enable = .TRUE.
    GOTO 200
  ENDIF
c if it is the second time through for this address,
c use initial guess two and skip the calculations.
c initialize the best values
  IF (n .EQ. 1) THEN
    fk2 = try2
```

```

        n1 = 2
        wr_enable = .TRUE.
        GOTO 200
    ENDIF
c    If the current error is too large, update value
    IF (cabs(eg1) .GT. err_max) THEN
        GOTO 50
    ENDIF
c    If iterations are finished, jump to the end
    IF ( n .GT. max_iter) THEN
        GOTO 200
    ENDIF
c    If at last iteration, record error value
    IF (n .EQ. max_iter) THEN
        n1 = n + 1
        finished = .TRUE.
        GOTO 200
    ENDIF
c    If error is small, don't do calculations
    IF (cabs(eg1) .LT. err_min) THEN
        n1 = n
        finished = .TRUE.
        GOTO 200
    ENDIF
50  CONTINUE
c    calculate a new value for fk.
c    check for zero divide
    IF (( eg1-eg0) .EQ. 0) THEN
        fk2 = fk1 + 0.25*eg1
    ELSE
        fk2 = (fk0*eg1 - fk1*eg0)/(eg1-eg0)
    ENDIF
    n1 = n + 1
c    set write enable so that the new values can be written to memory
    wr_enable = .TRUE.

200  CONTINUE

    RETURN
    END

```

## Appendix C

The following two listings are the BOSS FORTRAN subroutines used to calculate the out-of-band power. Figure 3.26 shows the BOSS representation of the model used to estimate the PSD and to calculate the out-of-band power. The FORTRAN subroutines listed are for the "PSD WINDOW" and the "PSD CALCULATION". The "COMPLEX FFT" subroutine was provided by BOSS and is not printed here. The algorithms for these FORTRAN subroutines are from [41].

### WINDOW.F

```
c Subroutine to apply a windowing function to the data
  subroutine window (complexinput,vector_length,complexoutput,SUMW,
+                   window_type)
c vector length is the input block length (number of complex values)
  integer vector_length, window_type, maxvector_length
  parameter (maxvector_length = 150000)
  complex complexinput(vector_length)
  complex complexoutput(vector_length)
  real SUMW
  integer J,MM
  real FACM,FACP
  real WINDOW1, WINDOW2, WINDOW3, WINDOW4, WINDOW5,
    WINDOW6
  real pi
  parameter (pi = 3.141592654)

c
c Square Window
  WINDOW1(J) = 1.
c Parzen window
  WINDOW2(J) = (1.0 - ABS(((J-1)-FACM)*FACP))
c Welch window
  WINDOW3(J) = (1. - (((J-1) - FACM)*FACP)**2)
c Hanning window
  WINDOW4(J) = .5*(1.-cos(2*pi*(J-1)/(MM-1)))
c Hamming window
  WINDOW5(J) = 0.54 - 0.46*cos(2*pi*(J-1)/(MM-1))
c Blackman window
  WINDOW6(J) = 0.42 - 0.5*cos(2*pi*(J-1)/(MM-1))
+       + 0.08*cos(4*pi*(J-1)/(MM-1))
c use J-1 in above equation as vector starts a J=1, not J=0.
  MM = vector_length
```

```

    FACM = 0.5*(MM-1.0)
    FACP = 2.0/(MM+1.0)
c Accumulate the squared sum of the weights and apply the
c window to the data
    SUMW = 0.0
    IF (window_type .EQ. 2) THEN
c use the Parzen window
        DO 11, J=1,MM
            SUMW = SUMW+WINDOW2(J)**2
            complexoutput(J)=complexinput(J)* WINDOW2(J)
11        CONTINUE
    ELSEIF (window_type .EQ. 3) THEN
c use the Welch window
        DO 12, J=1,MM
            SUMW = SUMW+WINDOW3(J)**2
            complexoutput(J)=complexinput(J)* WINDOW3(J)
12        CONTINUE
    ELSEIF (window_type .EQ. 4) THEN
c use the Hanning window
        DO 13, J=1,MM
            SUMW = SUMW+WINDOW4(J)**2
            complexoutput(J)=complexinput(J)* WINDOW4(J)
13        CONTINUE
    ELSEIF (window_type .EQ. 5) THEN
c use the Hamming window
        DO 14, J=1,MM
            SUMW = SUMW+WINDOW5(J)**2
            complexoutput(J)=complexinput(J)* WINDOW5(J)
14        CONTINUE
    ELSEIF (window_type .EQ. 6) THEN
c use the Blackman window
        DO 15, J=1,MM
            SUMW = SUMW+WINDOW6(J)**2
            complexoutput(J)=complexinput(J)* WINDOW6(J)
15        CONTINUE
    ELSE
c use a square window
        DO 16, J=1,MM
            SUMW = SUMW+WINDOW1(J)**2
            complexoutput(J)=complexinput(J)* WINDOW1(J)
16        CONTINUE
    ENDIF
    return
    end

```

```

c Subroutine to calculate the PSD of a set of data
  subroutine psd (compin,vector_lengthin,vector_lengthout,compout,SUMW)
c vector_lengthin is the input block length (number of complex values)
c if a window isn't used before the FFT, set SUMW = 1
  integer vector_lengthin,max_vector_length,vector_length_out
  parameter (max_vector_length = 150000)
  complex compin(max_vector_length)
  real compout(max_vector_length)
  real SUMW
  integer J,M,MM,MM2

c
  M = vector_lengthin/2
  MM = vector_lengthin
  MM2 = MM + 2
  SUMW = SUMW*MM
c Calculate PSD for 1st element
  compout(1) = (cabs(compin(1))**2)/SUMW
c Calculate the PSD
  DO 16 J=2,M
    compout(J)=(cabs(compin(J))**2+cabs(compin(MM2-J))**2 )/SUMW
16 CONTINUE
  compout(M+1) = (cabs(compin(M+1))**2)/SUMW
  return
  end

```